Fall 11-13-2017

CONSTRUCTION OF SYNTHETIC SIGNAL PATHWAYS IN MAMMALIAN CELLS VIA INDUCED PROTEIN PROXIMITY

Guihua Zeng
University of New Mexico - Main Campus

Guihua Zeng

Candidate

Chemistry and Chemical Biology

Department

This dissertation is approved, and it is acceptable in quality and form for publication:

Approved by the Dissertation Committee:

Prof. Fu-Sen Liang, Chairperson

Prof. Changjian Feng

Prof. Lina Cui

Prof. Wei Wang

CONSTRUCTION OF SYNTHETIC SIGNAL PATHWAYS IN MAMMALIAN CELLS VIA INDUCED PROTEIN PROXIMITY

BY
GUIHUA ZENG

B.S. Applied Chemistry, Shantou University, China, 2011

DISSERTATION

Submitted in Partial Fulfillment of the
Requirements for the Degree of

Doctor of Philosophy
Chemistry

The University of New Mexico
Albuquerque, New Mexico

December 2017

ACKNOWLEDGEMENTS

First and foremost, I want to thank my advisor Dr. Fu-Sen Liang for his guidance and assistance on my research projects during the past five years. Dr. Liang could always use his knowledge and experience to guide me to tackle the problems in my projects and to push them forward. I really appreciate his patience and individual hands-on training, which helped me gain extensive experimental skills. More importantly, he taught me the way of scientific thinking and how to do research step by step. Without his help, it would be impossible to have this dissertation in press. Anyway, I believe the skills, knowledge and research experience that I gained from him will benefit me in the future.

Secondly, I would like to express my gratitude to my committee members, Dr. Wang, Dr. Feng, Dr. Cui and Dr. Melancon (for research proposal) for their precious time spent in reading this dissertation and valuable suggestions on finalizing this draft. In addition, I want to thank them for their advices during my research proposal, which really expedited the progress of this project.

Thirdly, all our lab collaborators are also acknowledged for their effort to facilitate this project. Dr. Wei Wang and his students Weimin Xuan, Yongyi Wei, Jin Zhang and visiting professor Huanqiu Li gave me a lot of good ideas and helped to synthesize most of compounds for my project, also all students from Dr. Wang's group to provide the assistance in find some chemicals and the use of some specific

instruments; Dr. Marcel P. Bruchez (Carnegie Mellon University) and his student Yi Wang synthesized the molecules and generated good ideas for manuscript preparation. Besides, my thanks also go to Dr. Debra Dunaway-Mariano, Dr. Lina Cui, and Dr. Charles E. Melancon, Dr. Yang Qin for their generosity to allow me to access the instruments in their lab conveniently during the past years.

Fourthly, I am grateful to all my current and former lab members. They gave me a lot of assistance and good suggestions for my research experiments and for daily life. I am really appreciated the wonderful working atmosphere they make, and it is my honor to be one member of this group.

Moreover, I want to thank my parents for their understanding and support on my PhD study in the USA. Especially, their significant help on taking care of my son during the busy research times. At the same time, many thanks to my local friends James and Priscilla Duncan, for their significant help on guiding me adapt to the lifestyle in Albuquerque and arranging the impressive wedding ceremony for my husband and me.

At last, I also want to appreciate my husband, who was a PhD student in our department and graduated last December. Thanks for what he did to build our little family in US; thanks for his preparation of our meaningful wedding; thanks for his encouragement on my research; thanks for his care on our daily life; and thanks for him to bring me enter into a new world.

CONSTRUCTION OF SYNTHETIC SIGNAL PATHWAYS IN MAMMALIAN CELLS VIA INDUCED PROTEIN PROXIMITY

BY

GUIHUA ZENG

B.S. Applied Chemistry, Shantou University, China, 2011

Ph.D. Chemistry, University of New Mexico, USA, 2017

ABSTRACT

Cell signaling translates extracellular signals into intracellular processes that carry out cellular functions. The introduction of artificial signaling networks using synthetic biology methods has facilitated the investigation of signaling mechanisms and the generation of novel cell functions. Several synthetic biology methods that are based on chemical controls have been developed to provide precise temporal regulation. In my dissertation, we constructed new synthetic biology engineering strategies to control tailored cellular events.

Described in Chapter 2, we developed a new chemical strategy to generate de novo signaling pathways that link a signaling molecule, H_2O_2, to different downstream cellular events in mammalian cells. This approach combines the reactivity-based H_2O_2 sensing with the chemically induced proximity (CIP) technology. By chemically modifying a CIP inducer, abscisic acid (ABA), with an H_2O_2-sensitive boronate ester probe, novel H_2O_2 signaling pathways were engineered to induce transcription, protein translocation and membrane ruffle formation upon exogenous or endogenous H_2O_2 stimulation. This strategy has also been successfully applied to gibberellic acid (GA)-based CIP system, which provides the potential to build signaling networks based on orthogonal cell stimuli.

Encouraged from development of the H_2O_2-based strategy, described in chapter 3,

we developed another new synthetic biology strategy which integrated chemical reactivity sensing and CIP methods to generate artificial Fe^{2+} signaling circuitry to control tailored cellular events in mammalian cells. A new probe **ABA-FE18** (Fe^{2+}-sensing and protein dimerization) derived from **ABA** was developed and used to control gene activation, signal transduction, and cytoskeletal remodeling in response to Fe^{2+}. Combining Fe^{2+} and H_2O_2 sensing with ABA and GA CIP systems, signal circuitries were designed to implement "AND" and "OR" biologic gates that enables mammalian cells to convert different combinations of Fe^{2+} and H_2O_2 signals into pre-defined biological outputs.

Described in the last chapter, we engineered a unique CIP method based on mutant antibody VL domain using a fluorogenic malachite green derivative as the inducer, which gives fluorescent signals upon VL domain dimerization while simultaneously inducing downstream biological effects.

TABLE OF CONTENTS

List of figures

List of abbreviations

ABA	Abscisic acid
ABI	ABA insensitive
AD	Alzheimer's disease
CID	Chemically induced dimerization
CIP	Chemically induced dimerization
DAPI	4',6-diamidino-2-phenylindole
DMEM	Dulbecco's modified eagle medium
DMSO	Dimethyl sulfoxide
EDTA	Ethylene Diamine Tetraacetic Acid
EGFP	Enhanced green fluorescent protein
EYFP	Enhanced Yellow Fluorescent Protein
FAP	Fluorogen activating protein
FBS	Fetal Bovine Serum
FKBP12	FK506 binding protein 12
FRB	FKBP-rapamycin binding
GA	Gibberellic acid
GA-AM	Acetoxy methoxy ester modified Gibberellic acid
GAI	Giberellin insensitive
Gal4DBD	Gal4 DNA binding domain
GID1	Giberellin insensitive dwarf 1
hEGF	Human Epidermal Growth Factor
HEPES	2-[4-(2-hydroxyethyl) piperazin-1-yl]ethane sulfonic acid
HPLC	High Performance Liquid Chromatography
IRES	Internal ribosome entry site
L5**	V_L domain of an antibody
MG	Malachite Green
mTOR	Mammalian target of rapamycin
NES	Nuclear export sequence
NLS	Nuclear localization signal
NMR	Nuclear magnetic resonance
PBS	Phosphate buffer
PCR	Polymerase Chain Reaction
PD	Parkinson's diseases
PEI	Polyethyleneimine
PFA	paraformaldehyde

POIs	Protein(s) of interest
PYL	Pyrabactin-like regulatory component
Rap	Rapamycin
ROS	Reactive oxygen species
scFv	Single-chain variable fragment
TLC	Thin-Layer Chromatography
TOF-HRMS	Time-of-flight high resolution mass spectrometry
UAS	Upstream activation sequence
VP16AD	VP16 transactivation domain

Chapter 1

Introduction

1.1 Synthetic signaling pathways and cellular functions

Synthetic biology aims to engineer and assemble predictable biological "parts" to create tailored cells that transmission information and generate novel functions.[1] One of the focus in mammalian synthetic biology is to engineer signal transduction, which allows cells to convert (and amplify) external stimuli in cellular environment into proper cellular responses (Figure 1.1).[3,4]

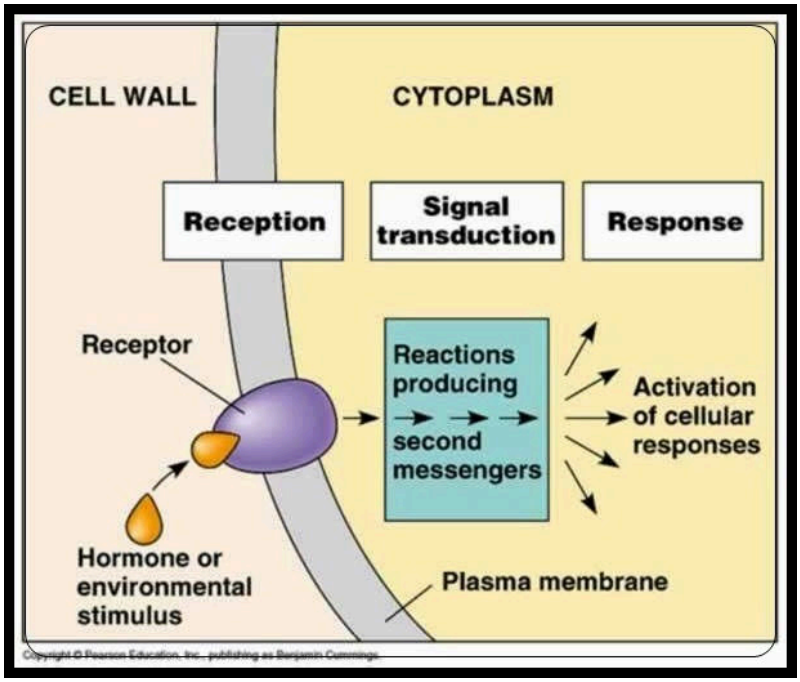

Figure 1.1 Principles of signal transduction pathway[2]

The signal transduction processes typically are constituted of 3 major steps: sensing, processing and actuation. The sensing step employs various mechanisms to perceive environmental signals, such as surrounding chemicals, light, heat, nucleic acids, antigens or pH. In the processing step, these detected signals are integrated and combinatorically processed via internal logic circuits to reach decisions that are coupled to the production of different biological outputs in the actuation step (Figure 1.2).[5-7]

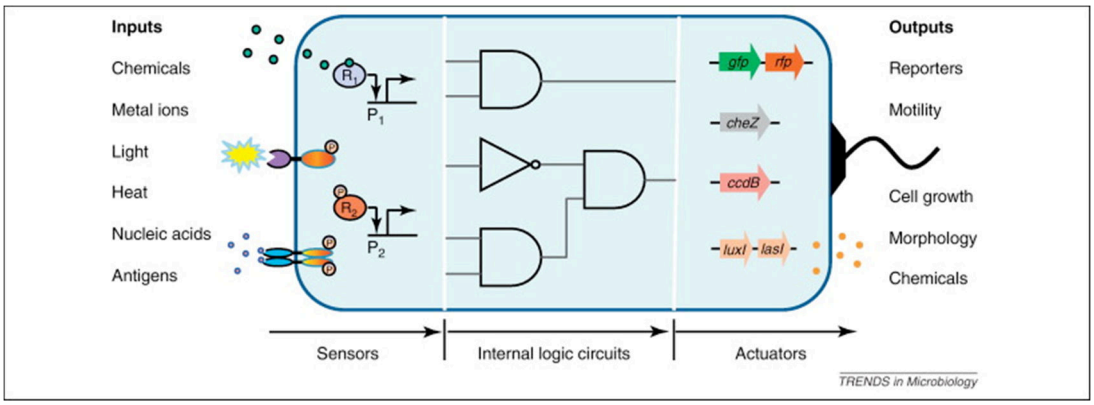

Figure 1.2 Designing customized cell signaling responses by harnessing the inherent modularity of cell signaling and gene regulatory networks[7]

Various efforts in synthetic biology research have been dedicated to engineer predictable and tailored cellular functions in response to detected stimuli by rewiring or creating synthetic signal transduction pathways.[8-10] To create a synthetic signaling pathway, one needs to consider how to create sensing units that can recognize only the chosen signals, how to transmit and process the detected signals, and how to link a processed decision to desired functional outputs. Most of the current methods to

engineer synthetic signaling pathways rely on either rewiring nature-evolved pathways or creating de novo synthetic pathways by evolving and selecting novel signaling parts.[6] The first approach requires extensive knowledge of native cell signaling pathways and is limited to existing pathways in nature. The second approach can potentially provide unlimited possibility in constructing new signaling pathways. However, it requires substantial efforts and may still not obtain functional products as desired. The engineering information that is gained is also less likely to be transferable to the design of a new signaling component. In my thesis, I developed an alternative chemistry-integrated synthetic biology strategy combining chemically induced proximity (CIP) and reactivity-based signal sensing methods to engineering novel signaling pathways.

1.2 Chemically induced proximity

The CIP methods, or chemically induced dimerization (CID), use small molecule-inducers to control the homo- or hetero-dimerization of two proteins (Figure 1.3). The small molecule dimerizers either bind to both corresponding proteins simultaneously or bind one of the proteins to induce a conformational change that leads to the binding of the second protein. Each CIP inducer triggers the association between two unique inducer-binding adaptor proteins that are typically fused individually to two other proteins of interest (POIs). Depending on the choice of POIs, various downstream biological events can be linked to the stimulation of these exogenous inducers,[11-13] which provide a rapid and modular way to create novel CIP inducer-responsive

synthetic cellular functions and signaling pathways (Figure 1.4).

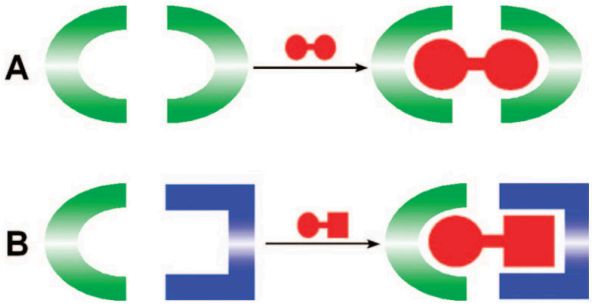

Figure 1.3 General principle of chemically induced dimerization (CID). In the presence of a symmetrical ligand, two proteins can be brought together to form a homodimer (A). With a nonsymmetrical ligand, two different proteins can be brought together to form a heterodimer (B)[11].

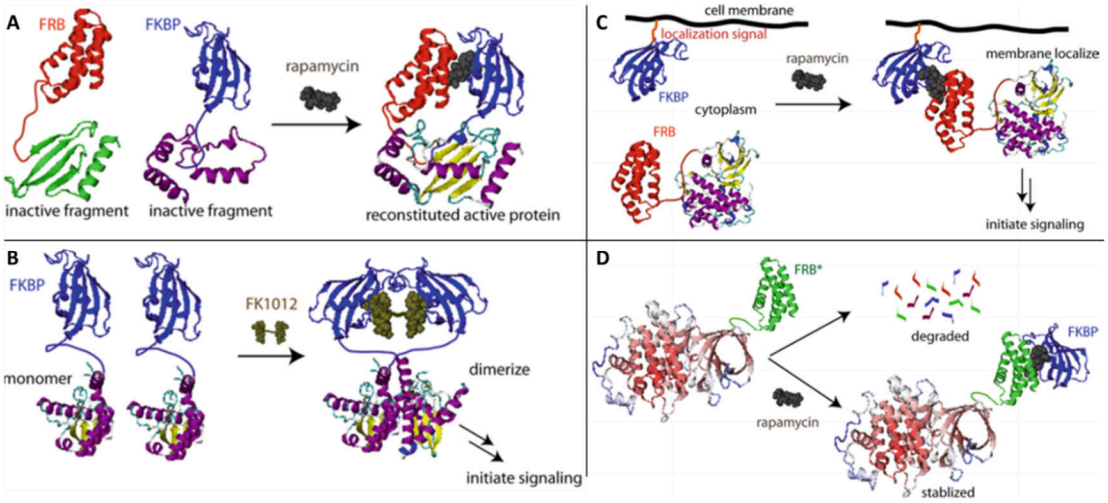

Figure 1.4 Strategies used in CIP: reconstitution of functional proteins/domains (A), inducing proximity between proteins (B), controlling protein localization (C),

modulation of protein or small molecule activities by recruiting endogenous protein (D).[14]

The CIP systems have been proven to be useful and versatile tools for biological research and biomedical applications. The concept of CIP was inspired from the discovery that the immunosuppressive activity of FK506 stem from the FK506-induced dimerization between FKBP12 and calcineurin. A homo-dimerization system using FK1012 (that links 2 FK506) to dimerize two FKBP12-fusion proteins was introduced by Schreiber, Crabtree and coworkers.[15] In this study, FK1012 was used to activate the endogenous signal transduction cascade by fusing FKBP12 to the proximity regulated ζ-chain of the T-cell receptor (Figure 1.5).

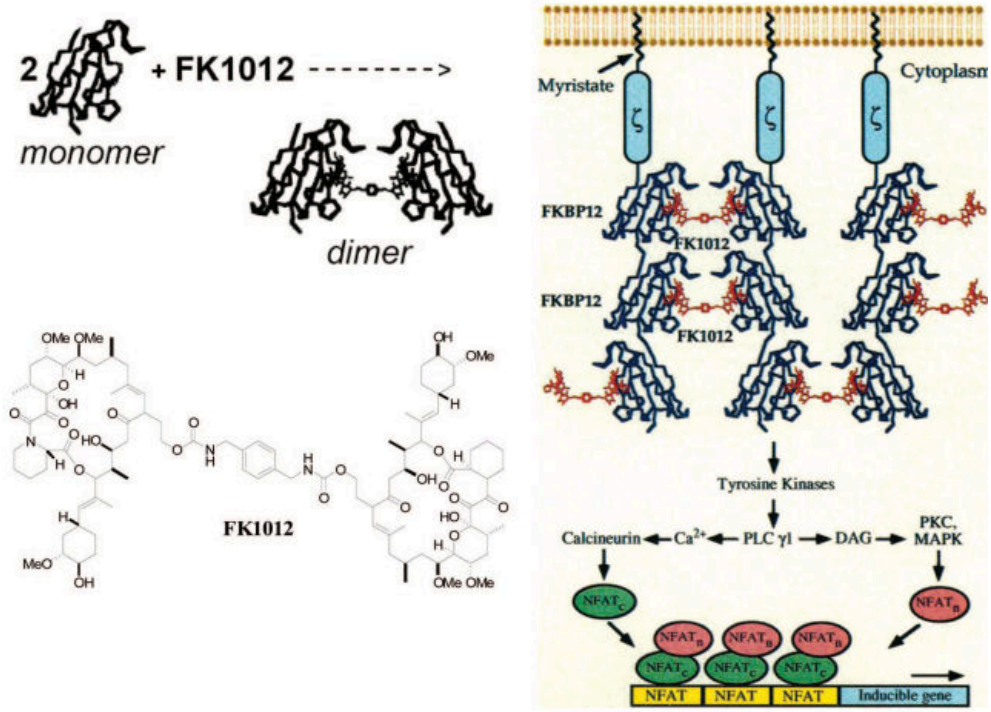

Figure 1.5 Initial demonstration of the CID concept. On the left, two FKBP monomers bind the bivalent drug FK1012. On the right, FKBP-TCR fusion proteins are dimerized by FK1012, initiating intracellular signaling.[15]

In the following years, multiple orthogonal CIP systems using different chemical inducers, including rapamycin, abscisic acid (**ABA**), gibberellic acid (GA) and other synthetic ligands [11, 14, 16] have been developed and applied in broad biological applications. Several dimerization systems have been derived from plant signaling systems. Plant hormones involved in these systems are readily available, inexpensive and often nontoxic as they do not have homologous partner in mammalian cells.

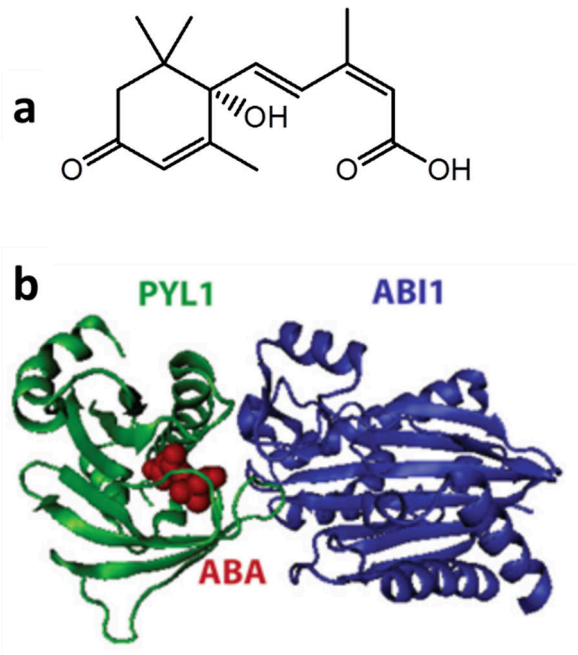

Figure 1.6 The structure of **ABA** (a) and the X-ray crystal structure of PYL1-**ABA**-ABI1(b).[14]

One of the plant hormone-based CIP systems is engineered from the **ABA** signaling pathway.[17] **ABA** (Figure 1.6a) is a small molecule plant hormone that controls the stress responses when plants face drought or extreme temperature and regulate plant growth and development such as leaf abscission. Figure 1.6b shows the X-ray structures of PYL1-**ABA**-ABI1: The PYL protein contains two flexible loops that are open in the absence of **ABA**. In the presence of **ABA**, PYL binds to **ABA** with these two loops closed to totally enclose **ABA**, which creates an extensive complementary surface that can bind another protein ABI1.

Another example of the plant hormone-based CIP is engineered based on the GA signaling pathway.[13] As shows in Figure 1.7, a modified GA, GA3-AM, can cross the cell membrane and be processed by cytosolic esterase to release free GA3. GA3 then binds GID1 (blue), which induces formation of a complex between GID1 and GAI (red).

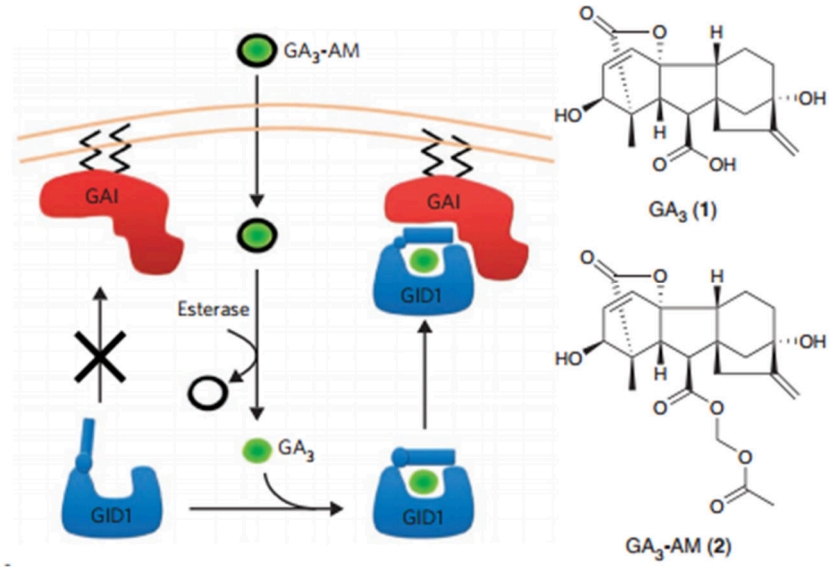

Figure 1.7 General scheme of gibberellin-induced CID used in this study.[13]

1.3 Reaction-based small-molecule probes

Many reaction-based small-molecule fluorescent probes have been developed to report the existence or levels of specific cellular species in living cells with minimal perturbation.[18-19] These probes have unique "signal-sensing" units conjugated to the fluorophores and remain non-fluorescent until they are exposed to specific signals, for example, endogenous cellular signaling molecules (e.g. H_2O_2, H_2S, O_3), metal ions (e.g. Hg^{2+}, Cu^{+}, Co^{2+}, Fe^{2+}) [19] or specific pH value (Figure 1.8). These tools not only help decipher the roles of these probed molecules in cells, they also find applications in diagnostics for human diseases that differentiate between the normal and disease tissues by probing molecules that are signature of pathological conditions.[20-21] It is possible to conjugate the "signal sensing" chemical moieties with therapeutic molecules to achieve the selective release of drugs in or around diseased tissues. We expect that these signal sensing units can be used to cage CIP inducers that allows the control of protein dimerization and associated downstream cellular effects to be regulated by specific cellular signals.

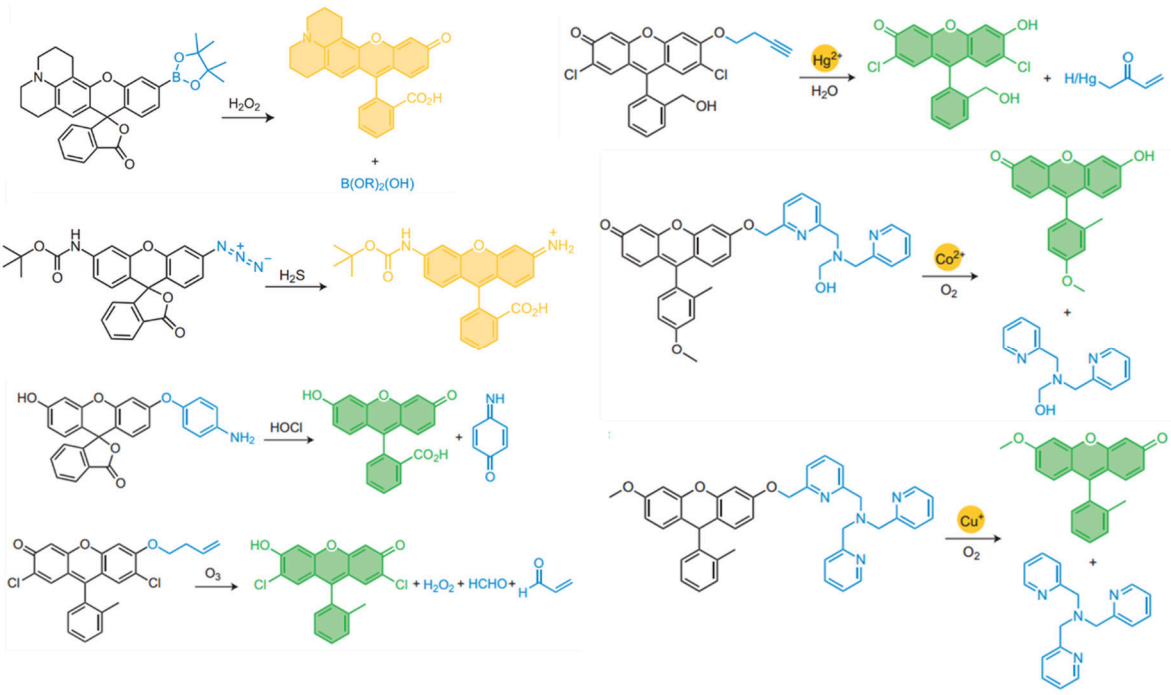

Figure 1.8 Some examples for reaction-based small-molecule fluorescent probes.[19]

1.4 My thesis project

My PhD research aims to develop alternative synthetic biology strategies that are chemistry-based and allow rapid and modular construction of new signaling pathways with unique signal responding specificity and giving tailored biological outputs. It integrated the CIP technology and reactivity-based signal sensing methods. My goal is to combine CIP system with existing and new reactivity-based chemical probes to enable the controls of biological processes by user-chosen cell signals (eg., H_2O_2 and Fe^{2+}) in living cells. This approach should be versatile in generating new signaling pathways and controlling biological systems by changing the signal sensing probes or the CIP protein components according to specific needs. This strategy can be used to

create biological computing systems in mammalian cells which can translate different combinations of cell signals into pre-defined biological outputs. These works will be described in detail in Chapter 2 and Chapter 3. To expand the available CIP toolbox and create a new "self-reporting" CIP method, we developed a new CIP system based on fluorogenic Malachite Green derivatives, where the dimerization process can be monitored through the fluorescence changes, and different downstream biological processes can be induced through protein dimerization. This work will be described in Chapter 4.

1.5 References

1. Berg, J. M.; Tymoczko, J. L.; Stryer, L., Biochemistry. *New York* **2002**.

2. Siuti, P.; Yazbek, J.; Lu, T. K., Synthetic circuits integrating logic and memory in living cells. *Nature biotechnology* **2013,** *31* (5), 448-452.

3. Campbell, N. A.; Reece, J. B., Biology. 6th. San Francisco: Benjamin Cummings: 2002.

4. Tymoczko, J. L.; Berg, J. M.; Stryer, L., *Biochemistry: a short course*. Macmillan: 2011.

5. Kobayashi, H.; Kaern, M.; Araki, M.; Chung, K.; Gardner, T. S.; Cantor, C. R.; Collins, J. J., Programmable cells: Interfacing natural and engineered gene networks.

Proceedings of the National Academy of Sciences of the United States of America **2004,** *101* (22), 8414-8419.

6. Lim, W. A., Designing customized cell signalling circuits. *Nat Rev Mol Cell Bio* **2010,** *11* (6), 393-403.

7. Wang, B. J.; Buck, M., Customizing cell signaling using engineered genetic logic circuits. *Trends Microbiol* **2012,** *20* (8), 376-384.

8. Bashor, C. J.; Horwitz, A. A.; Peisajovich, S. G.; Lim, W. A., Rewiring cells: synthetic biology as a tool to interrogate the organizational principles of living systems. *Annual review of biophysics* **2010,** *39*, 515-37.

9. Purnick, P. E.; Weiss, R., The second wave of synthetic biology: from modules to systems. *Nature reviews. Molecular cell biology* **2009,** *10* (6), 410-22.

10. Haynes, K. A.; Silver, P. A., Eukaryotic systems broaden the scope of synthetic biology. *The Journal of cell biology* **2009,** *187* (5), 589-96.

11. Fegan, A.; White, B.; Carlson, J. C.; Wagner, C. R., Chemically controlled protein assembly: techniques and applications. *Chemical reviews* **2010,** *110* (6), 3315-36.

12. Gestwicki, J. E.; Marinec, P. S., Chemical control over protein-protein interactions: beyond inhibitors. *Combinatorial chemistry & high throughput screening* **2007,** *10* (8), 667-75.

13. DeRose, R.; Miyamoto, T.; Inoue, T., Manipulating signaling at will: chemically-inducible dimerization (CID) techniques resolve problems in cell biology. *Pflugers Archiv : European journal of physiology* **2013,** *465* (3), 409-17.

14. Liang, F.-S.; Crabtree, G. R., Small Molecule-Induced Proximity. In *Chembiomolecular Science: At the Frontier of Chemistry and Biology*, Shibasaki, M.; Iino, M.; Osada, H., Eds. Springer Japan: Tokyo, 2013; pp 115-126.

15. Spencer, D. M.; Wandless, T. J.; Schreiber, S. L.; Crabtree, G. R., Controlling signal transduction with synthetic ligands. *Science* **1993,** *262* (5136), 1019-24.

16. Miyamoto, T.; DeRose, R.; Suarez, A.; Ueno, T.; Chen, M.; Sun, T. P.; Wolfgang, M. J.; Mukherjee, C.; Meyers, D. J.; Inoue, T., Rapid and orthogonal logic gating with a gibberellin-induced dimerization system. *Nature chemical biology* **2012,** *8* (5), 465-70.

17. Cutler, S. R.; Rodriguez, P. L.; Finkelstein, R. R.; Abrams, S. R., Abscisic acid: emergence of a core signaling network. *Annual review of plant biology* **2010,** *61*, 651-79.

18. Chen, X. Q.; Tian, X. Z.; Shin, I.; Yoon, J., Fluorescent and luminescent probes for detection of reactive oxygen and nitrogen species. *Chem Soc Rev* **2011,** *40* (9), 4783-4804.

19. Chan, J.; Dodani, S. C.; Chang, C. J., Reaction-based small-molecule fluorescent probes for chemoselective bioimaging. *Nat Chem* **2012,** *4* (12), 973-984.

20. Connor, J. R.; Snyder, B. S.; Beard, J. L.; Fine, R. E.; Mufson, E. J., Regional distribution of iron and iron-regulatory proteins in the brain in aging and Alzheimer's disease. *Journal of neuroscience research* **1992,** *31* (2), 327-35.

21. Prousek, J., Fenton chemistry in biology and medicine. *Pure Appl Chem* **2007,** *79* (12), 2325-2338.

Chapter 2

Constructing de novo H_2O_2 Signaling via Induced Protein Proximity

(Reproduced with permission from

ACS Chemical Biology 2015, 10(6), 1404−1410

The other authors, Roushu Zhang, Weimin Xuan, are acknowledged.

Supporting information of the publication is incorporated in this chapter)

2.1 Introduction

Nature evolves sophisticated cell signaling circuits that convert perceived environmental signals into proper cellular responses to maintain normal function of cells. Recent efforts have been dedicated to engineer predictable and tailored cellular functions in response to detected stimuli by rewiring or creating synthetic signal transduction pathways.[1-3] These efforts contribute to the understanding of how sophisticated cellular functions and behaviors are built and hold great promise for biological computing[4-5] and novel therapeutic applications.[6-7]

To create a synthetic signaling pathway, one needs to consider how to create a sensing unit that can recognize only the chosen signal, how to transmit and process the detected signal, and how to link a processed decision to a desired functional output. Most of the current methods to engineer synthetic pathways that respond to cellular signals rely on either rewiring nature-evolved pathways or creating de novo synthetic pathways by evolving and selecting novel signaling parts.[8] The first approach requires extensive knowledge of native cell signaling pathways and is limited to existing pathways in nature. The second approach can potentially provide unlimited possibility in constructing new signaling pathways. However, it requires substantial efforts and may still not obtain functional products as desired. The engineering information that is gained is also less likely to be transferable to the design of a new signaling component.

The chemically induced proximity (CIP), or chemically induced dimerization (CID), technology has been developed to regulate biological processes using exogenous chemical inducers.[9] Each CIP inducer triggers the association between two unique inducer-binding adaptor proteins that are fused individually to two other proteins of interest (POIs). Depending on the choice of POIs, various downstream biological events can be linked to the stimulation of these exogenous inducers,[10-12] which provide a rapid and modular way to create novel CIP inducer-responsive synthetic signaling pathways. This technology provides a rapid and modular way to create novel CIP inducer-responsive synthetic signaling pathways. Several orthogonal CIP systems using

different chemical inducers, including rapamycin, abscisic acid (**ABA**), gibberellic acid (GA), and other synthetic ligands,[10, 13-14] have been developed for broad biological applications.

H_2O_2 is a member of the reactive oxygen species (ROS) and an important diffusible secondary messenger in biological systems.[15] It plays critical roles in several biological processes (e.g., signal transduction, cell differentiation, and apoptosis) and human diseases (e.g., cancer and neurodegenerative diseases).[16-20] Here, we report a novel chemical strategy to create de novo H_2O_2 signaling pathways that can be tailored to give desired downstream biological outcomes by integrating the CIP methods and the H_2O_2 sensing technology. We showed that new signaling pathways can be engineered to link the H_2O_2 signal to otherwise unrelated cellular processes, including expression of chosen genes, translocation of chosen proteins, and remodeling of cytoskeleton through activating endogenous Rac1 signaling.

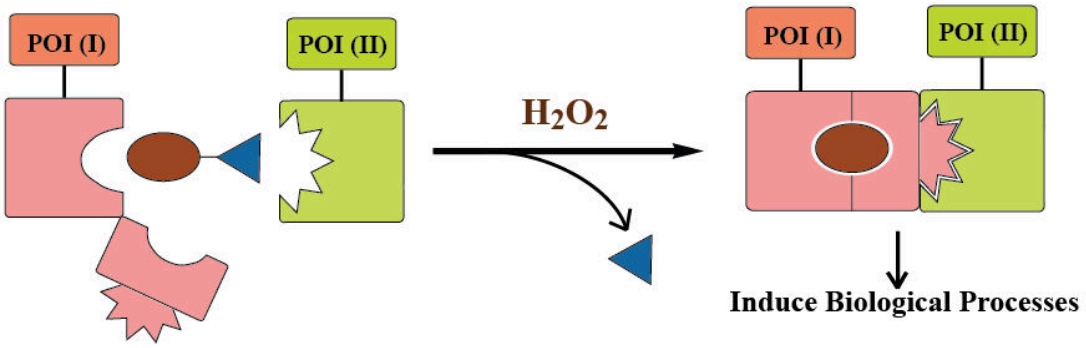

Figure 2.1 General process for H_2O_2-induced proximity to control biological processes.

In the design of an H_2O_2-signaling inducer, an H_2O_2 responsive masking group is incorporated into a CIP inducer to abolish the protein dimerization ability of the inducer. It is expected that the modified inducer remains inactive until being exposed to H_2O_2. H_2O_2 then promotes the chemical cleavage of the masking group to regenerate the original CIP inducer that triggers the predesigned biological effects (Figure 2.1).

2.2 Design and application of ABA-HP

To explore the feasibility of this strategy, we first focused on the **ABA** CIP system that we developed.[13] **ABA** binds selectively to the PYL protein and causes a conformational change of PYL to create a surface that can subsequently bind the ABI protein. On the basis of the crystal structure, **ABA** is totally embedded within the PYL pocket where it makes extensive contacts.[21] We hypothesize that any chemical modification of **ABA** will likely disrupt its binding to PYL and therefore abolish the induced association between PYL and ABI. By modifying **ABA** with a chemical moiety that can be removed by H_2O_2, the **ABA**-based CIP activity should then be controlled by H_2O_2. We have recently shown that modifications at the carboxylic acid group on **ABA**, which engages in critical hydrogen bonding to PYL,[21] disrupted the CIP activity of the caged **ABA**.[22] We expect that a similar strategy can be used to install an H_2O_2-sensing unit onto **ABA** to mask its CIP activity. Several H_2O_2-responsive fluorescent probes have been developed.[23] H_2O_2-inducible systems that control transcription or cellular targeting were also reported.[24-25] In these studies, a boronate ester moiety was used as

the H_2O_2-sensing unit. We reason that when **ABA** is equipped with the same boronate ester moiety, the **ABA** inducible CIP should then be controlled by H_2O_2.

2.2.1 Synthesis and HPLC test of ABA-HP

To examine the feasibility of this strategy, we synthesized an H_2O_2-responsive boronate-conjugated **ABA**, referred to as **ABA**-HP (Figure 2.2), which is expected to convert back to **ABA** upon the exposure to H_2O_2 based on a reported oxidative cleavage mechanism (Figure 2.3).[23]

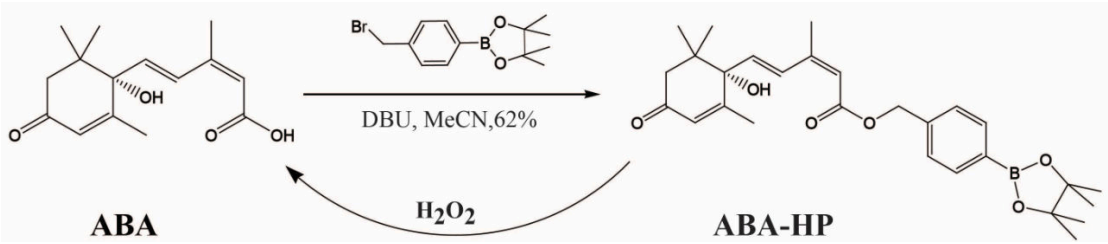

Figure 2.2 Synthesis of **ABA**-HP and its conversion to **ABA** in the presence of H_2O_2.

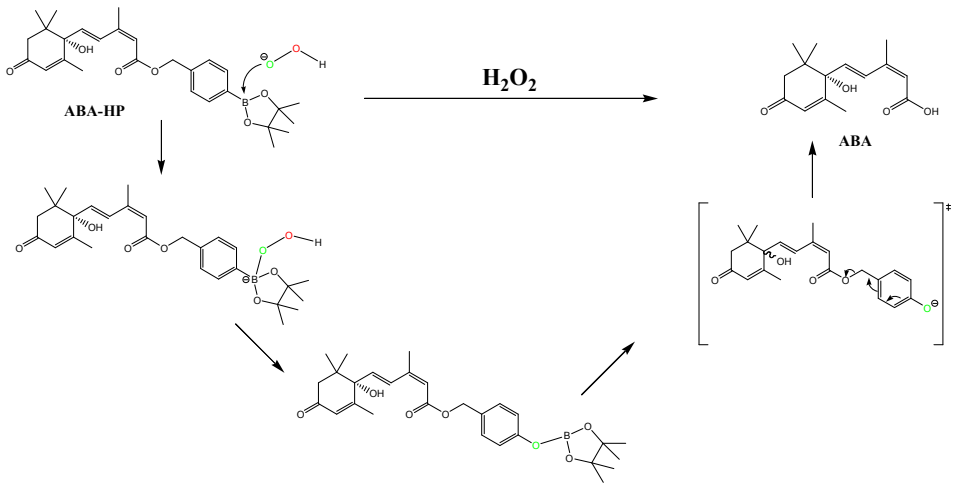

Figure 2.3 A proposed mechanism of **ABA**-HP cleavage to form **ABA** in the present of H_2O_2 based on the reported oxidative cleavage mechanism of boronate ester.[23]

Monitored by HPLC, we observed that, without H_2O_2, **ABA**-HP was not hydrolyzed to give **ABA** in HEPES buffer at 37 °C throughout the 24 h observation period (Figure 2.4). A dimer was observed (based on mass spectrometry analysis, Figures 2.4 and 2.5) during this incubation period, which was likely formed through the coordination between the electron deficient boron on **ABA**-HP with an oxygen lone pair on another molecule of **ABA**-HP. Upon the addition of H_2O_2, **ABA**-HP started to convert back to **ABA** within minutes, and the transformation was completed in 4 h (Figures 2.4 and 2.5). Following the cleavage process using HPLC, we observed that besides the regenerated **ABA** and the dimeric **ABA**-HP, another peak appeared, which was converted to **ABA** at later time points and was likely an intermediate of the conversion (Figure 2.3).

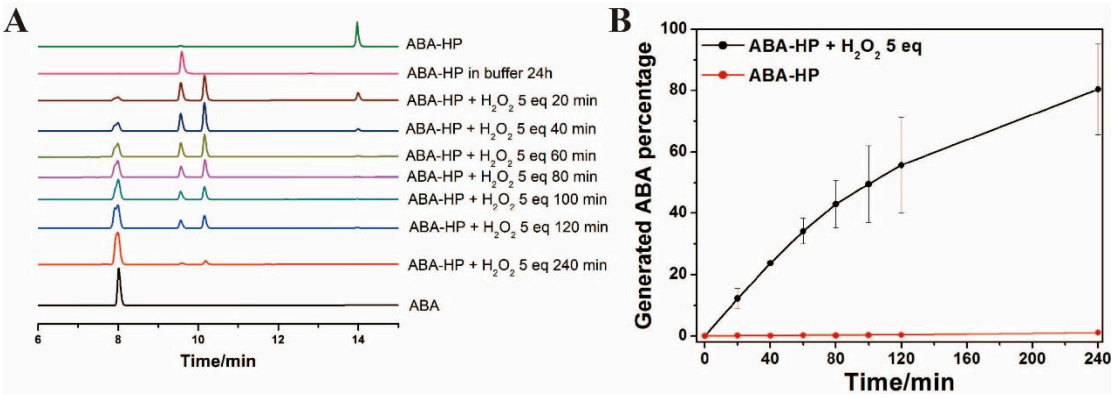

Figure 2.4 Time dependent cleavage of **ABA**-HP by H_2O_2 detected by HPLC. 1 mM **ABA**-HP was treated with 5 mM H_2O_2 in 50% HEPES/DMSO (10 mM HEPES, pH 7.4) from 0 to 240 min at 37℃. (**A**) The representative HPLC chromatograms from 3 independent experiments. (**B**) The quantitative analysis of generated **ABA** from **ABA**-HP in the presence of H_2O_2. The results were quantified by integrating the peak area corresponding to the **ABA** peak over the total areas of all peaks to give the generated **ABA** %. The shown result was the average from 3 independent experiments. Error bars are SD (N=3).

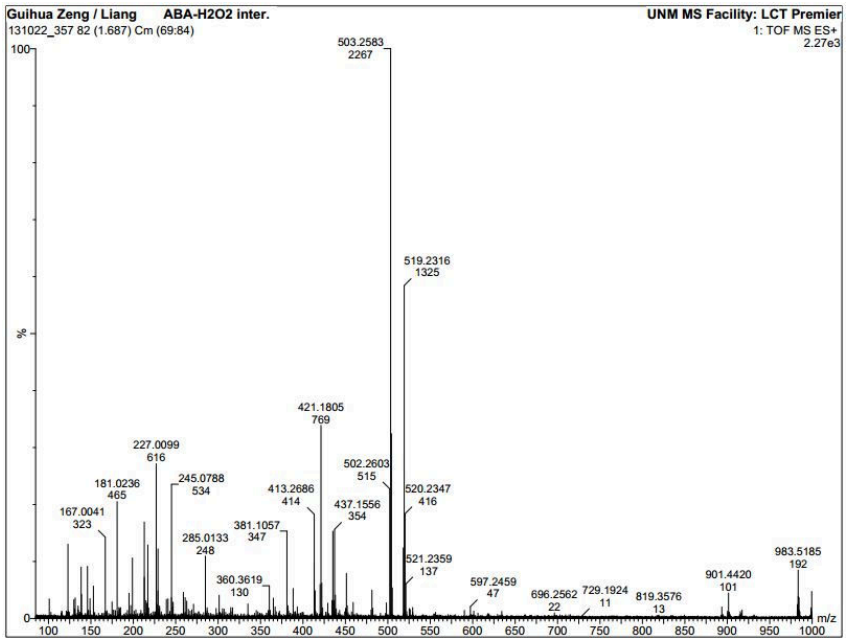

Figure 2.5 MS of **ABA**-HP and **ABA**-HP dimer. TOF-HRMS (m/z) found (calcd.) for $C_{28}H_{37}O_6B$ (M): $[M+Na]^+$, 503.2583 (503.2581) and [2M+Na]+, 983.5185 (983.5264).

To confirm that the dimeric **ABA**-HP can be converted to **ABA**, we preincubated

ABA-HP in HEPES buffer to form the dimer and then treated it with H_2O_2. We found that **ABA** can indeed be generated from this dimer (Figure 2.6).

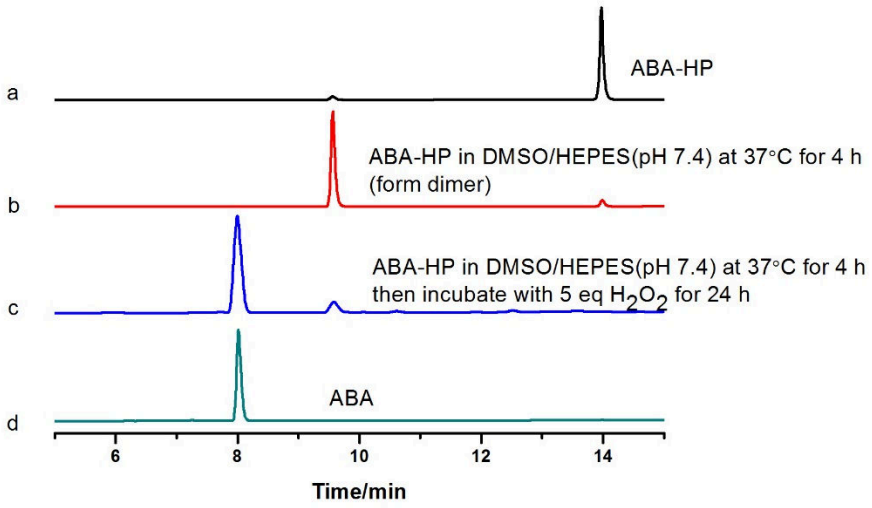

Figure 2.6 Formation of **ABA**-HP dimer and its cleavage in the presence of H_2O_2. 1 mM **ABA**-HP was incubated in 50% DMSO/HEPES (10 mM HEPES, pH 7.4) for 4 h (**b**), and then treated with 5 mM H_2O_2 for 24 h (**c**). The chromatograms are representative results from 3 independent experiments.

Next, we tested the selectivity of **ABA**-HP toward H_2O_2 over other ROS, metal ions, and signaling molecules. **ABA**-HP was incubated with different molecules as indicated in Figure 2.7 for 4 h, and the products were analyzed using HPLC. **ABA**-HP was found to be unreactive to all molecules tested at 100 μM (Figure 2.7,), except Cu^{+} and Cu^{2+}, which produced a minimal amount of cleavage but were later shown to have no effects at the more physiologically relevant concentration of 10 μM (Figure 2.7).

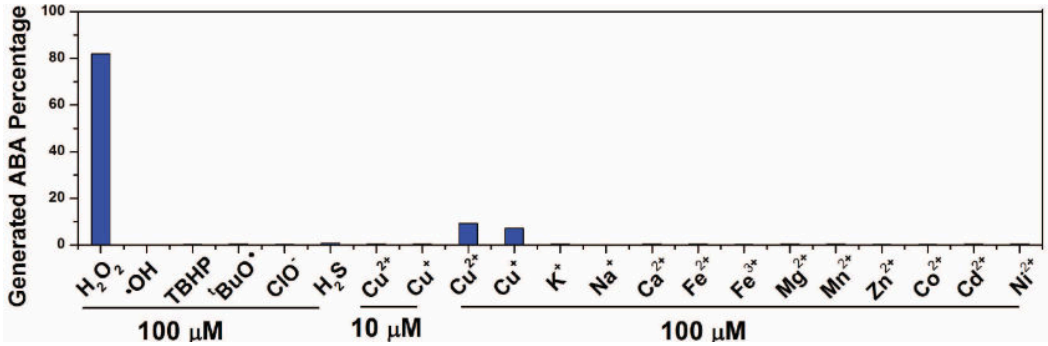

Figure 2.7 Stability test of **ABA**-HP upon different molecules detecting by HPLC. **ABA**-HP (100 μM) was incubated with 10uM or 100 μM of indicated molecules for 4 h at 37°C. Error bars are SD (N = 3). The results were quantified by integrating the peak area corresponding to the **ABA** peak over the total areas of all peaks to give the generated **ABA** %. The shown result was the average from 3 independent experiments. Error bars are SD (N=3).

2.2.2 H_2O_2 induced transcription activation in living cells

To test if this strategy works in cells, we first investigated whether the H_2O_2 signal can be linked to activate transcription since most cell signaling events eventually lead to gene expression. We used an HEK293T stable cell line, in which enhanced GFP (EGFP) expression occurs only in the presence of functional **ABA**.[22] This cell line has both the **ABA**-responsive split transcriptional activator DNA fragment (VP-PYL and GAL4DBD-ABI linked by IRES)[13] and an inducible EGFP DNA fragment (with 5xUAS) inserted into the genome (Figure 2.8).

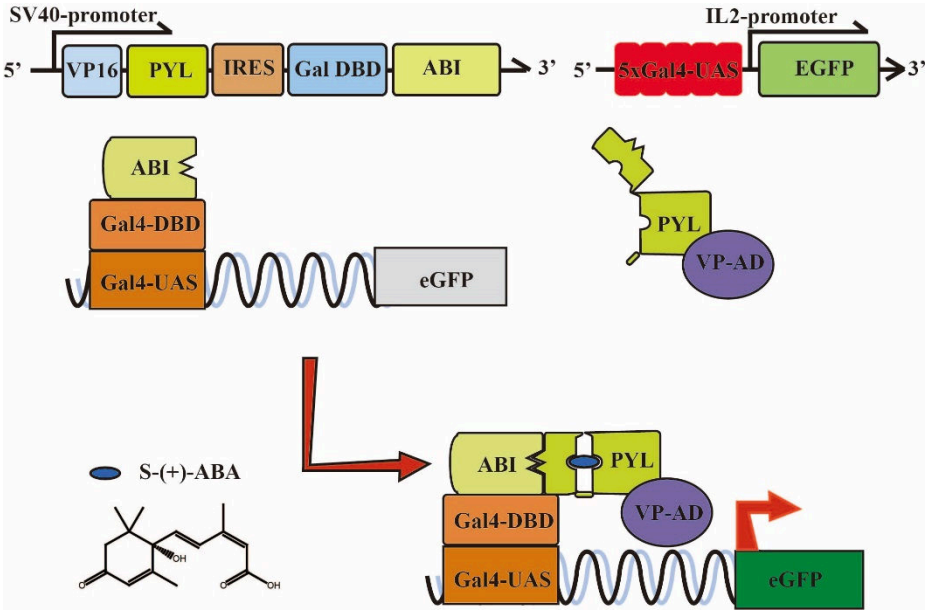

Figure 2.8 DNA constructs for **ABA**-inducible EGFP expression

To determine if the **ABA** generated from the H_2O_2-induced cleavage of **ABA**-HP is biologically active, we tested its ability to induce EGFP expression in this HEK293T reporter cell line. We pre-cleaved **ABA**-HP with H_2O_2 and added the resulting products to the HEK293T cells. After incubation for 7 h, EGFP production was observed under a fluorescence microscope (Figure 2.9). This result indicates that the regenerated **ABA** is indeed biologically active. On the contrary, uncleaved **ABA**-HP failed to induce EGFP expression, which confirmed that the boronate modification blocked the activity of **ABA** as expected.

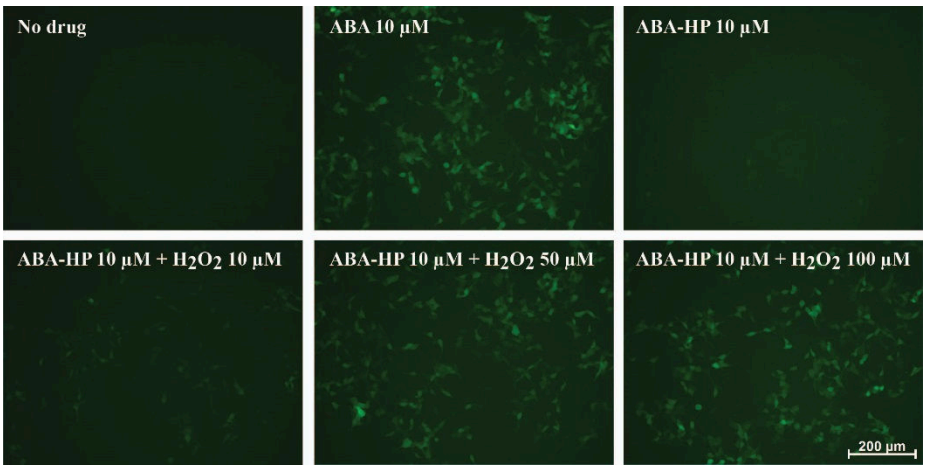

Figure 2.9 EGFP expression in HEK 293T EGFP reporter cells with **ABA**, **ABA**-HP or **ABA**-HP pre-cleaved by H_2O_2. Cells were treated with indicated molecules and the EGFP expression was observed under a fluorescence microscope after 7 h. Images shown are the representative results from 3 independent experiments.

We next tested whether **ABA**-HP can respond to H_2O_2 in cell culture conditions and cause the gene expression to be activated by H_2O_2 in cells. It has been reported that the endogenous H_2O_2 concentrations of tissue samples vary from 10 to 100 μM range and that the pathologic tissues usually have even higher levels of H_2O_2.[26-30] We therefore tested the response of our system to H_2O_2 at micromolar concentrations in living cells. The HEK293T reporter cells were treated with no drug, 10 μM **ABA**, **ABA**-HP, or **ABA**-HP plus 10, 50, or 100 μM H_2O_2 for 5 to 24 h. The expression of EGFP was monitored at indicated time points using a fluorescence microscope. The EGFP expression was detected only when **ABA**, or **ABA**-HP plus H_2O_2, were added (Figure 2.10). These results confirm that the H_2O_2-induced cleavage of **ABA**-HP generates

functional **ABA** in situ. Notably, we observed differential levels of EGFP production when different amounts of H_2O_2 were added. The **ABA** CIP system is known to give a wide-range of dosage response.[13] These results indicate that this dosage response can be reproduced in the **ABA**-based H_2O_2-inducible system. This property can be useful for converting differential levels of H_2O_2 signals into different levels of transcription activity.

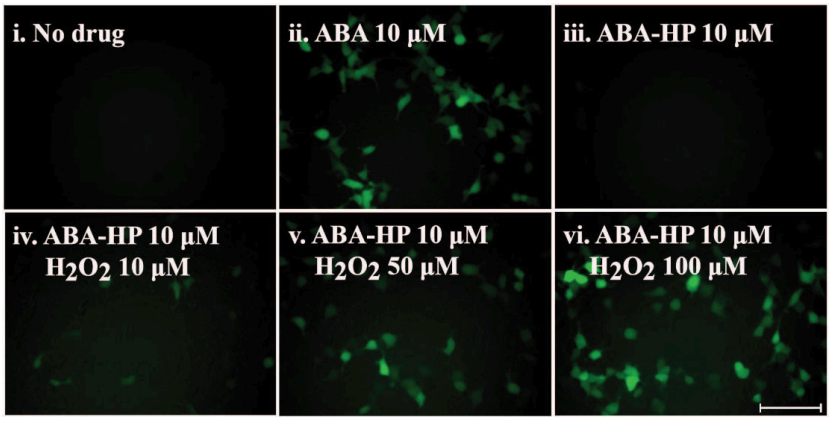

Figure 2.10 EGFP expression in HEK293T cells under different treating conditions (10 h). Scale bar is 100 μm.

One concern for the stability of **ABA**-HP in cells is the existence of an ester linkage in the molecule, which may be susceptible to the hydrolysis by cellular esterases. In the above experiments, only a minimal level of the EGFP expression was observed within a 10 h period following the addition of **ABA**-HP in the absence of H_2O_2 (Figure 2.10). This result suggests that the rate of **ABA** built up from the esterase cleavage of **ABA**-HP may be much slower than the H_2O_2-promoted cleavage. We suspect that the bulky

benzyl boronate moiety may contribute to the enhanced stability when compared to simple ester structures commonly used in pro-drugs. With an extended incubation period (24 h), the EGFP expression was indeed observed (Figure 2.11).

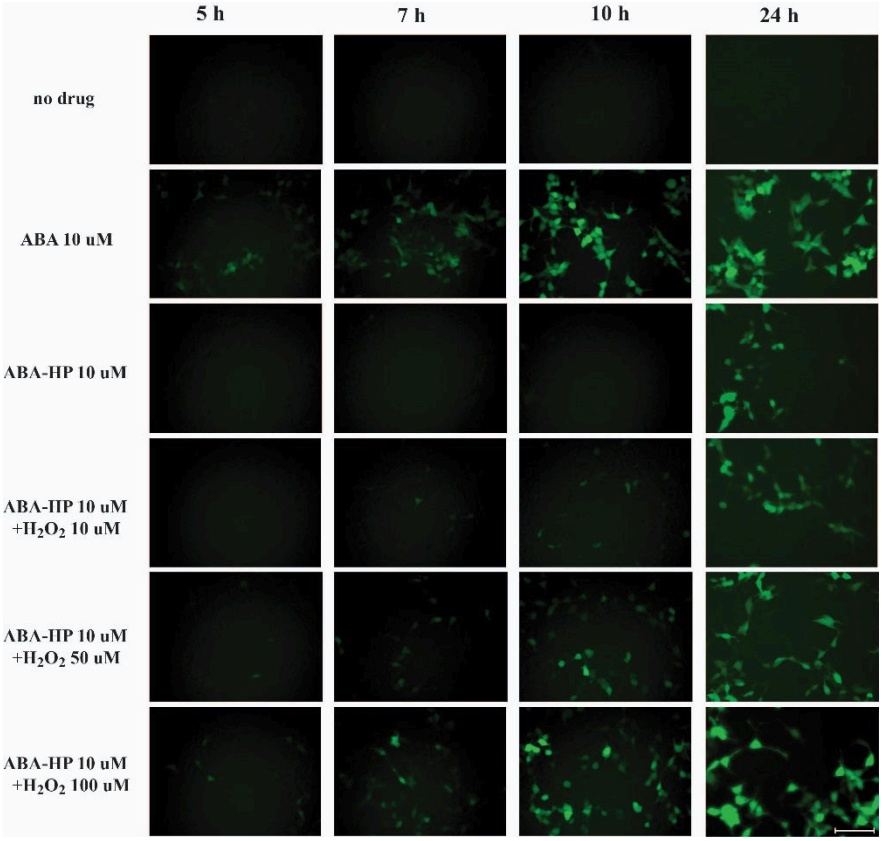

Figure 2.11 Dose and time dependent EGFP expression controlled by H_2O_2 in HEK 293T eGFP reporter cells. Cells were treated with indicated molecules and the EGFP expression was observed under a fluorescence microscope after indicated times. The scale bar is 100 μm. Images shown are the representative results from 3 independent experiments.

When using a more sensitive **ABA** inducible luciferase reporter assay,[16] **ABA**-HP

alone indeed induced observable luciferase expression in a shorter time (within 6 h), although free **ABA** induced a much higher expression of luciferase (Figure 2.12). These results indicate that further structural modifications of the boronate probe (e.g., increasing structural bulkiness near the ester linkage)[31] will be required to increase the cellular stability of **ABA**-HP for applications requiring extended incubation periods.

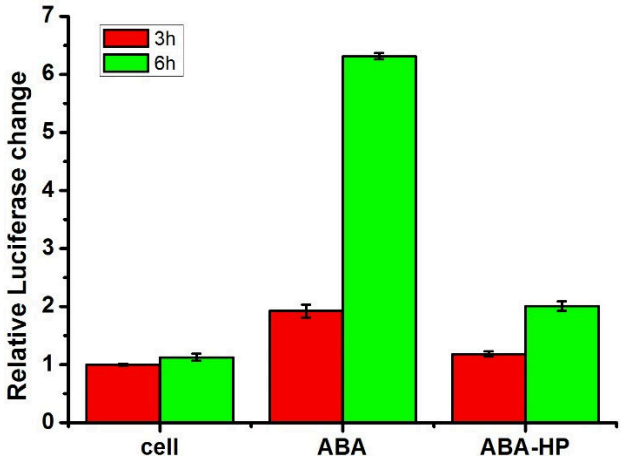

Figure 2.12 Stability assay of **ABA**-HP in CHO cells analyzed by the luciferase assay. CHO cells were transfected with **ABA**-inducible luciferase reporter constructs. Drugs were added for 3 or 6 h and then the cells were lysed for luciferase assays. Error bars are SD (N = 4).

2.2.3 H_2O_2 induced protein translocation in living cells

Many signaling events are regulated through the dynamic subcellular translocation of proteins. To test if we can redirect the H_2O_2 signal to control protein translocation, we used a reported **ABA**-inducible EGFP nuclear export system consisting of NES-

ABI and EGFP-PYL DNA constructs (Figure 2.13).[13]

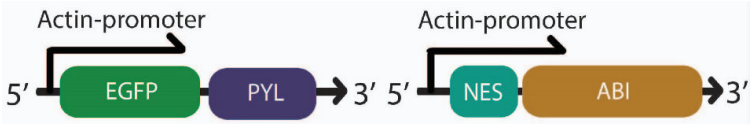

Figure 2.13 DNA constructs for **ABA**-inducible nuclear export of EGFP

CHO cells were transfected with both plasmids for 24 h and then incubated without additive, or with 10 μM **ABA**, **ABA**-HP, or **ABA**-HP plus 100 μM H_2O_2 for 30 min. The subcellular localization of the EGFP-PYL fusion protein was monitored under a fluorescence microscope, and the percentage of cells showing nuclear export in each condition was quantified (Figure 2.14). EGFP-PYL showed pan-cellular distribution in the absence of **ABA** and was localized outside of the nucleus when **ABA** was added. **ABA**-HP alone did not change the subcellular location of EGFP-PYL. However, the addition of **ABA**-HP plus H_2O_2 caused rapid nuclear export of EGFP-PYL similar to the case when **ABA** was added. When different concentrations of H_2O_2 were added, dosage-dependent responses were also observed based on the percentage of cells showing nuclear export (Figure 2.14). The lowest detection limit for H_2O_2 was observed to be around 1 μM.

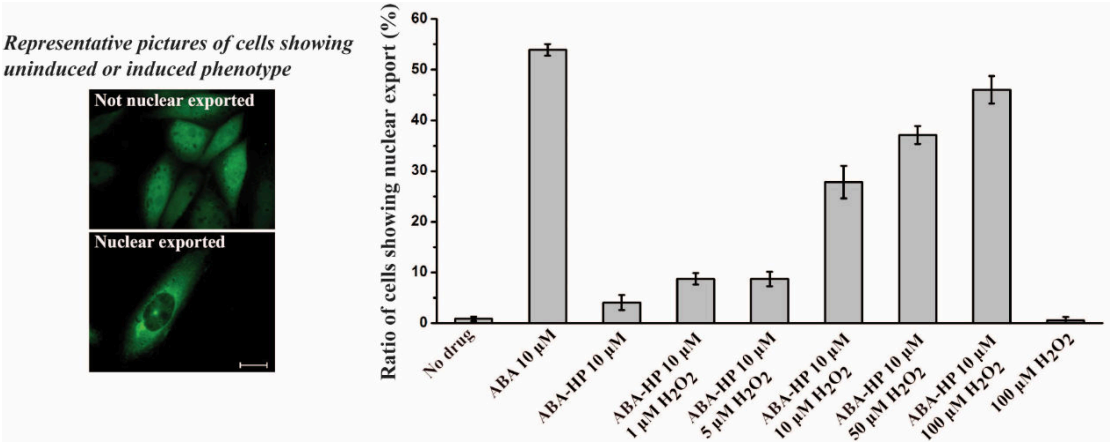

Figure 2.14 Nuclear export of EGFP in CHO cells under different treating conditions (30 min). The statistical data was obtained by counting cells to give the percentage of cells showing nuclear export or ruffling over the total EGFP positive cells. Cells were counted from three separate experiments each with five different areas chosen randomly, and over 700 cells were counted for each sample. Scale bar is 20 μm. Error bars are SD (N = 3).

To characterize and correlate the kinetics of H_2O_2-promoted **ABA**-HP cleavage and H_2O_2-induced protein translocation, the **ABA**-HP cleavage and the EGFP-PYL nuclear export were monitored immediately after **ABA**-HP and H_2O_2 addition (from 5 to 30 min, Supplementary Figure 2.15). Followed by HPLC, we observed that **ABA** was rapidly generated in 5 min, and the amount was increased with longer incubation periods. It correlated well with the observation that the EGFP nuclear export occurred at around 5 min, and the percentage of cells showing EGFP-PYL translocation also increased with longer incubation periods. These results indicate fast kinetics of **ABA**

induced dimerization between PYL and ABI.

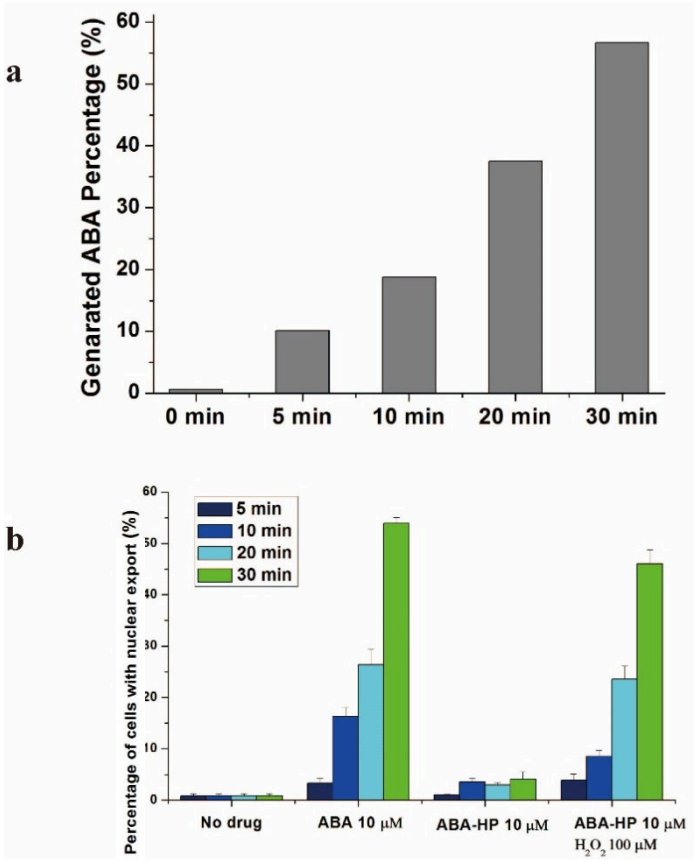

Figure 2.15 Time dependent cleavage of **ABA**-HP *in vitro* and in cells. (**a**) 10 μM **ABA**-HP was incubated with 100 μM H_2O_2 in 50% DMSO/HEPES (10mM, pH 7.4) at 37℃ for 5, 10, 20 and 30 min, and then analyzed using HPLC to give the generation of **ABA** percentage. The results were quantified by integrating the peak area corresponding to the **ABA** peak over the total areas of all peaks to give the generated **ABA** %. (**b**) CHO cells were transfected with NES-ABI & PYL-EGFP plasmids for 24 h. Cells were then treated with no drug, 10 μM **ABA**, 10 μM **ABA**-HP or 10 μM **ABA**-HP plus 100 μM H_2O_2 for 30 min. Cells were counted to obtain the percentage of the

cells showing unclear export over the total cell number (> 700 cells for each sample). The shown results were from 3 independent experiments. Error bars are SD (N = 5).

To determine changes at the single cell level, we performed live-cell imaging using a confocal microscope and quantified the fluorescence intensity inside and outside the nucleus of a cell at different time points after **ABA** or **ABA**-HP plus H_2O_2 was added to the transfected cells (Figure 2.16). Consistent with previous observations, cells started to show decreased fluorescence intensity in the nucleus at around 5 min and continuing to decrease thereafter. These results demonstrate that we can link the H_2O_2 signal to the translocation of a protein to a chosen subcellular location. Several localization signal peptides have been reported,[32] which can be used in our system to transport chosen proteins to different subcellular locations upon the stimulation of H_2O_2.

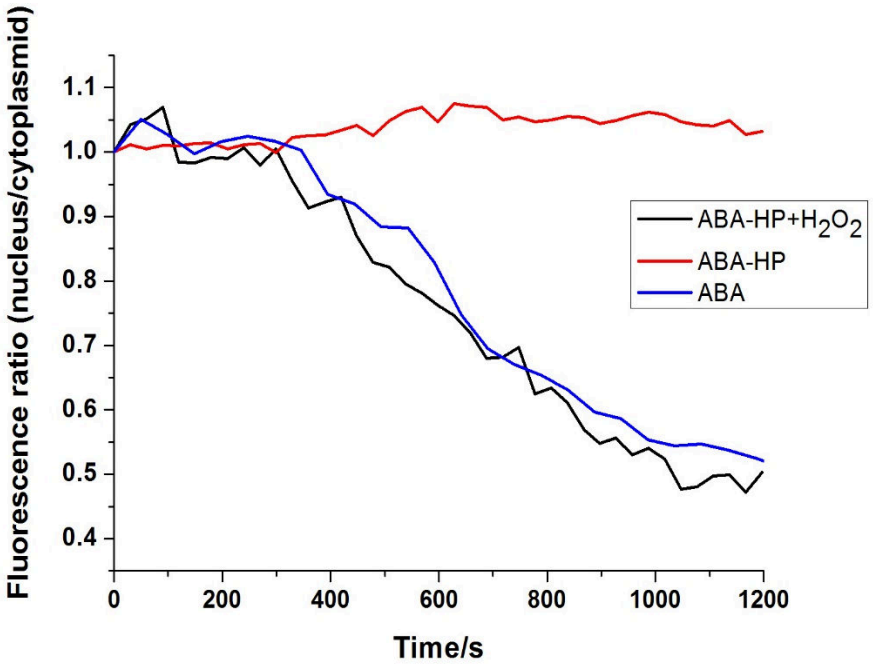

Figure 2.16 Live cell analysis of EGFP nuclear export in CHO cells. Cells were transfected with NES-ABI & PYL-EGFP plasmids for 24 h and then were treated with 10 μM **ABA**, 10 μM **ABA**-HP, or 10 μM **ABA**-HP plus 100 μM H_2O_2 and the chosen cells were followed under a confocal microscope in real time. The fluorescence intensity was quantified using Slide Book v.6 software as described in methods. The results were the average of fluorescence intensity ratio of nuclear/cytoplasm from 3 cells in 3 independent experiments.

With this rapidly responsive protein translocation assay at hand, were-evaluated the stability of **ABA**-HP against esterases in biological environments (both in cells and in the serum). CHO cells were transfected with the inducible nuclear export DNA constructs for 24 h and then incubated either with **ABA**-HP for 30 min to 4 h or with **ABA**-HP that was preincubated (for 30 min to 4 h at 37 °C) with non-heat-inactivated fetal bovine serum (FBS) for 30 min in cells (Figure 2.17). The nuclear export of EGFP-PYL was used as an indication of the **ABA**-HP hydrolysis. It was found that **ABA**-HP was relatively stable in cells within 30 min as only a minimal percentage of cells showed nuclear export. To rule out the possibility that there may be endogenous H_2O_2 that could also cleave **ABA**-HP to give **ABA**, control experiments were conducted in which cells were pretreated with catalase, an enzyme that has been used to quench H_2O_2 in cellular experiments,[33] for 1 h before adding **ABA**-HP. No difference in the percentages of cells showing nuclear export was observed with or without catalase

pretreatment. These results suggest that the observed **ABA**-HP hydrolysis is likely caused by esterases. To our surprise, **ABA**-HP that was preincubated with FBS up to 4 h did not lead to obvious nuclear export when incubated in cells for 30 min. If any cleavage of **ABA**-HP caused by FBS occurred before adding to cells, a much higher ratio of cells showing nuclear export would be expected. This observation suggests that **ABA**-HP is stable in FBS for at least 4 h. The difference in results between the incubation in cells and in FBS may likely be due to the different level of esterases in each condition.

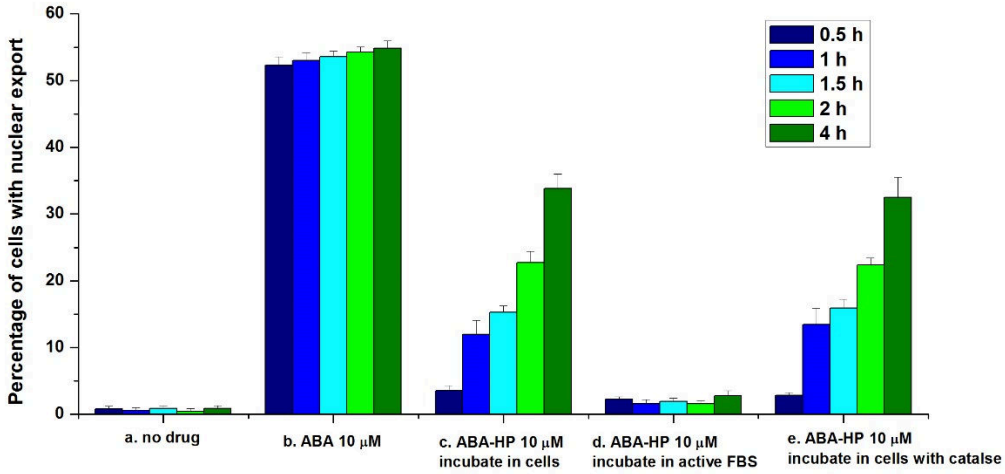

Figure 2.17 Stability of **ABA**-HP in cells and in FBS. CHO cells were transfected with NES-ABI & PYL-EGFP plasmids for 24 h before the drugs. Cells were treated with **(a)** no drug; (**b**) **ABA** for 0.5, 1, 1.5, 2 and 4 h; (**c**) **ABA**-HP for 0.5, 1, 1.5, 2 and 4 h; (**d**) FBS pre-incubated **ABA**-HP (at 37 ℃ for 0.5, 1, 1.5, 2 and 4 h) for 30 min; (**e**) 1 mg/mL of catalase for 1 h and then **ABA**-HP for 0.5, 1, 1.5, 2 and 4 h. The results were

analyzed by counting the cells showing EGFP unclear export over the total cell number (> 700 cells for each sample). The shown results were from 3 independent experiments. Error bars are SD (N = 5).

2.2.4 H_2O_2 induced cytoskeletal remodeling in living cells

To further investigate whether we can integrate the de novo H_2O_2 signal components into an endogenous signaling network, we examined the possibility of routing the H_2O_2 signal to induce membrane ruffling through the activation of the endogenous Rac1 signaling pathway. Tiam1 is a guanine exchange factor for Rac1, which is a member of Rho GTPase. The membrane translocation of Tiam1 activates Rac1 signaling and induces ruffle formation.[34] We constructed an **ABA**-inducible Tiam1 membrane localization system, which consists of DNA plasmids encoding the membrane-localized ABI (myr-ABI)[13] and the cytoplasmic EGFP/PYL-fused Tiam1 (PYL-EGFP-Tiam1) (Figure 2.18).

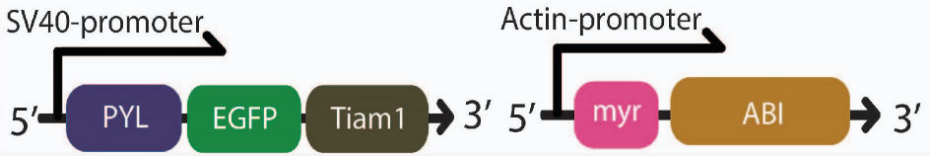

Figure 2.18 DNA constructs for **ABA**-inducible Rac1 signaling/ruffle formation.

CHO cells were transfected with these plasmids for 24 h and then incubated for 30 min without additive, or with 10 μM **ABA**, **ABA**-HP, or **ABA**-HP plus 100 μM

H_2O_2.The ruffle formation was analyzed by counting the number of cells showing morphological changes among all EGFP positive cells using a confocal microscope. As expected, only when cells were treated with **ABA**, or **ABA**-HP plus H_2O_2, did they show increased ruffle formation (Figure 2.19). Either **ABA**-HP or H_2O_2 alone gave background levels of ruffling similar to those without drug addition. These results indicate that the ruffling was caused by the presence of free **ABA** instead of by H_2O_2 alone.

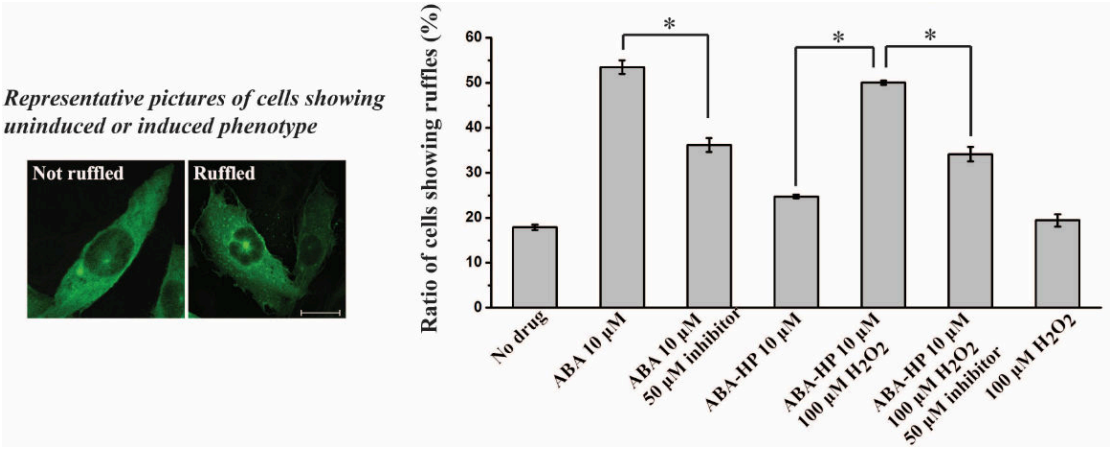

Figure 2.19 Ruffle formation of CHO cells under different treating conditions (30 min). The statistical data was obtained by counting cells to give the percentage of cells showing nuclear export or ruffling over the total EGFP positive cells. Cells were counted from three separate experiments each with five different areas chosen randomly, and over 700 cells were counted for each sample. Scale bar is 20 μm. Error bars are SD (N = 3). *P-value < 0.001.

To further confirm that the observed ruffling was induced through activating the

endogenous Rac1 signaling, the transfected cells were treated with a Rac1 inhibitor, NSC23766 (50 μM), for 1 h before adding **ABA** or **ABA**-HP plus H_2O_2. NSC 23766 is known to block the binding between Tiam1 and Rac1 and inhibit the activation of Rac1 signaling.[35] The NSC 23766 treatment lead to decreases in the percentage of cells showing ruffling in both cases of **ABA** and **ABA**-HP plus H_2O_2 addition (Figure 2.19), which indicated that the Tiam1-activated Rac1 signaling was indeed involved in the observed H_2O_2-induced ruffling. To examine whether the degree of ruffling can be reduced to the background level, we used higher concentrations of NSC 23766, which, however, led to severe cell death. Alternatively, when we treated cells with lower concentrations of **ABA**-HP (5 μM) and H_2O_2 (50 μM), the ruffling was indeed reduced to the background level with the NSC 23766 (50 μM) treatment (Figure 2.20). Overall, the above results demonstrate that our approach enabled an endogenous signaling pathway to become responsive to a new signal (i.e., H_2O_2), which is not normally associated with the pathway in the tested cell type.

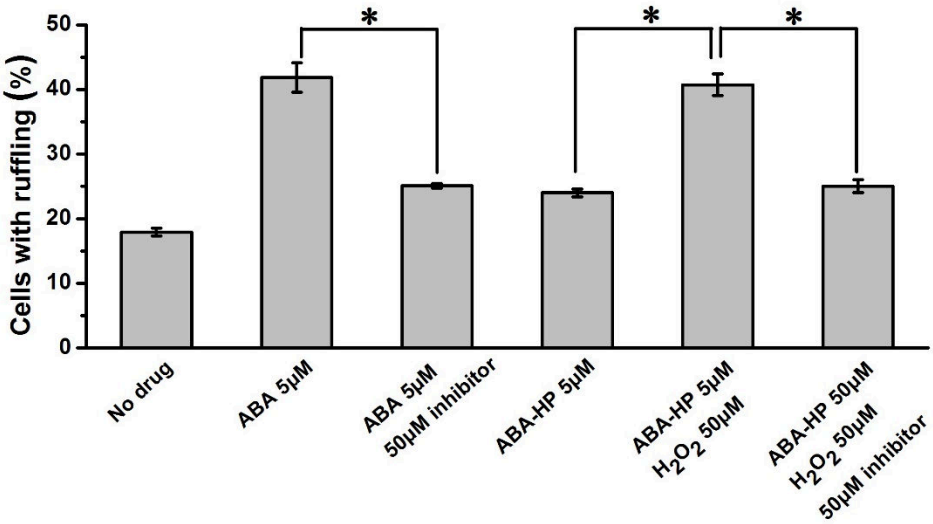

Figure 2.20 Ruffle formation of CHO cells in 30 min. The statistical data were obtained by counting the cells to give the percentage of the cells with ruffling over the total cell number. Cells were counted from three separate experiments with 5 different areas by random and > 700 cells for each sample. Error bars are SD (N=3). *P-value < 0.001.

2.2.5 Response to endogenous H_2O_2 in living cells

We next tested whether the created H_2O_2 signaling system can respond to endogenously generated H_2O_2 instead of exogenously applied H_2O_2 as in previous experiments. It has been reported that A431 cells can be stimulated by epidermal growth factor (EGF) to produce H_2O_2 in micromolar concentrations.[36-37] A431 cells were transfected with the inducible EGFP nuclear export DNA constructs for 24 h and then treated with no drug, **ABA**-HP alone, 10 μM **ABA**-HP plus 100 μM H_2O_2, or 10 μM **ABA**-HP plus 500 or 1000 ng/mL of EGF. The percentage of cells showing EGFP-PYL nuclear export in each condition was then quantified using a fluorescence microscope. The EGFP nuclear export was readily detected within 30 min after EGF stimulation, which was similar to the case when cells were stimulated by exogenous H_2O_2 (Figure 2.21). No obvious EGFP nuclear export was observed without EGF stimulation. To confirm that H_2O_2 was indeed generated by the EGF stimulation to give the observed EGFP-PYL translocation, the EGF stimulated cells were treated with catalase for 1 h before adding **ABA**-HP. The level of EGFP nuclear export was found to reduce to a level similar to the case when cells were treated with **ABA**-HP only (without H_2O_2 or

EGF) (Figure 2.21). These results clearly demonstrate that the engineered H_2O_2 signaling system can respond to the H_2O_2 generated endogenously in cells.

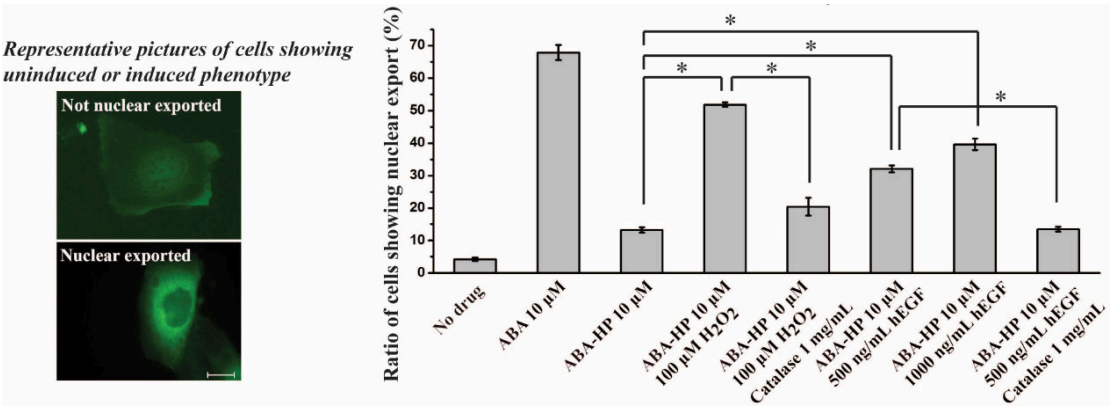

Figure 2.21 Nuclear export of EGFP in A431 cells under different treating conditions. The statistical data was obtained by counting cells to give the percentage of cells showing nuclear export or ruffling over the total EGFP positive cells. Cells were counted from three separate experiments each with five different areas chosen randomly, and over 700 cells were counted for each sample. Scale bar is 20 μm. Error bars are SD (N = 3). *P-value < 0.001.

2.3 Design and application of GA-HP

We expect that the same strategy can be expanded to other CIP inducers, which will allow us to build orthogonal signaling pathways in the same cell and potentially to construct cross talking pathways. To test this possibility, we applied this strategy to the GA-based CIP system. GA induces the binding between GAI and GID1 proteins in a similar way as **ABA** does.[38] GA has been developed as an orthogonal CIP system that

was used to perform cellular computing.[14] GA is not cell permeable. It was modified as the acetoxy methoxy ester (GA-AM) to cross the cell membrane and subsequently be cleaved by esterases to generate functional GA.[14] It has been shown that the carboxylate group on GA is critical for its biological functions. A minor modification that converts the carboxylate into a nonhydrolyzable hydroxamate abolishes its CIP activity.[14]

2.3.1 Synthesis and HPLC test of GA-HP

A recent report also showed that photolabile groups can be linked to the carboxylate group on GA to cage its activity.[39] We expect that modifying this carboxylate group of GA with the H_2O_2-sensitive boronate probe will give an H_2O_2-responsive GA system. We synthesized GA-HP by coupling the boronate group to GA (Figures 2.22 and 2.23).

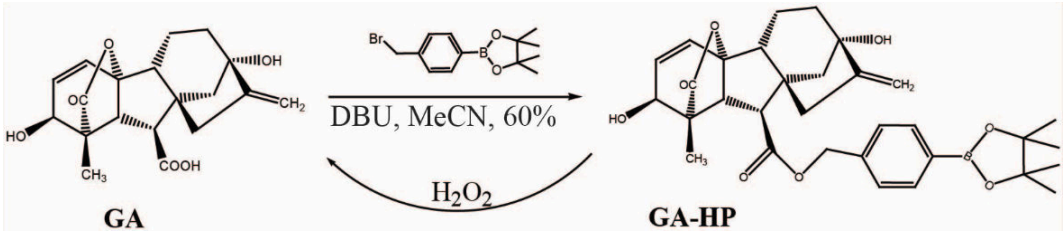

Figure 2.22 Synthesis of GA-HP and its conversion to GA in the presence of H_2O_2.

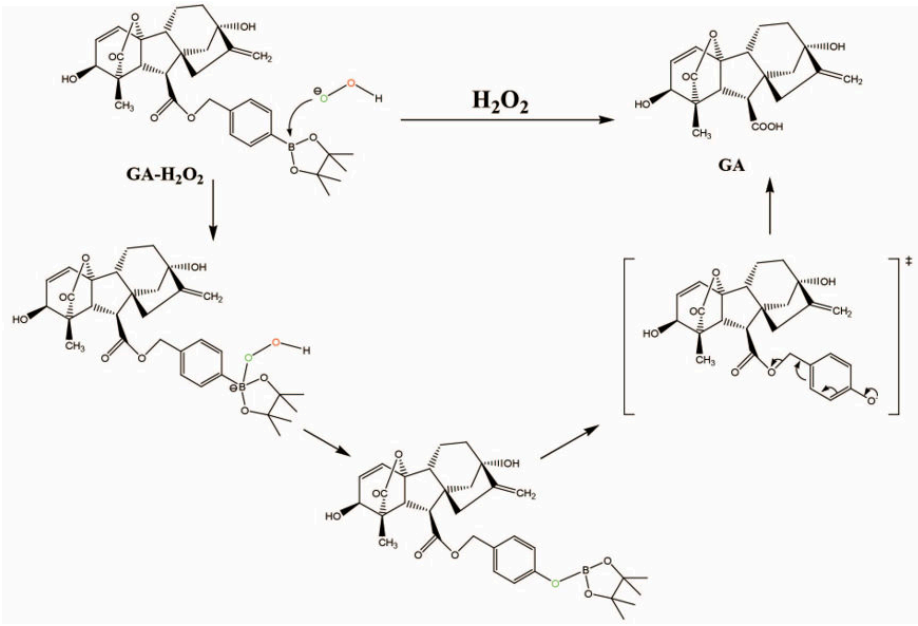

Figure 2.23 A proposed mechanism of GA-HP cleavage to form GA in the present of H_2O_2 based on the reported oxidative cleavage mechanism of boronate ester.

We analyzed the chemical stability of GA-HP and its conversion back to GA upon H_2O_2 addition using HPLC. In the presence of H_2O_2, GA was rapidly regenerated from GA-HP within 2 h (Figures 2.24 and 2.25).

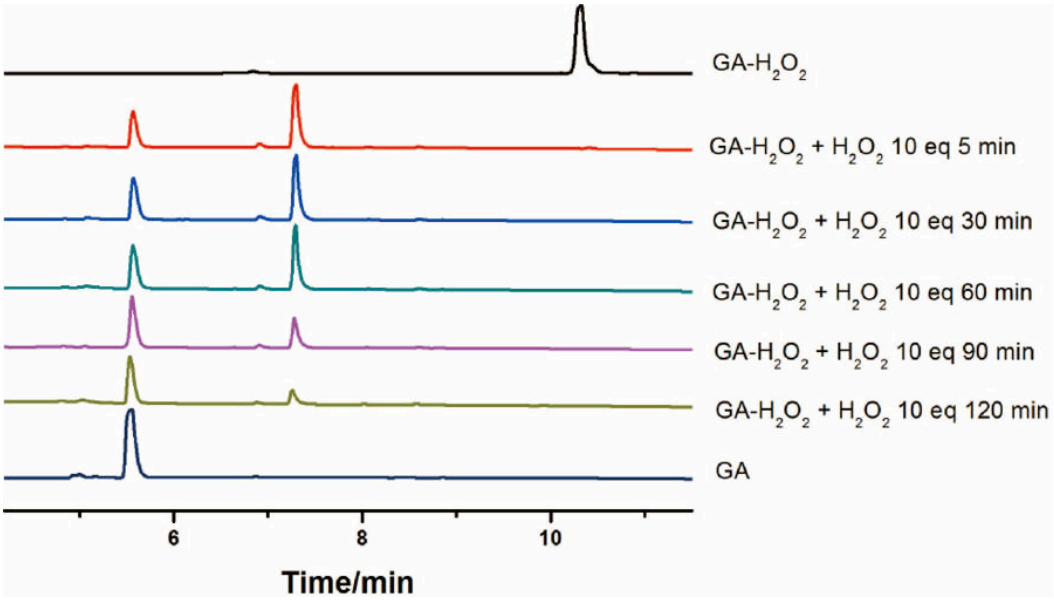

Figure 2.24 Time dependent cleavage of GA-HP by H_2O_2 detected by HPLC. 5 mM GA-HP was treated with 50 mM H_2O_2 in 50% HEPES/DMSO (10 mM HEPES, pH 7.4) from 0 to 120 min at 37℃. The HPLC chromatograms shown are representative from 3 independent experiments.

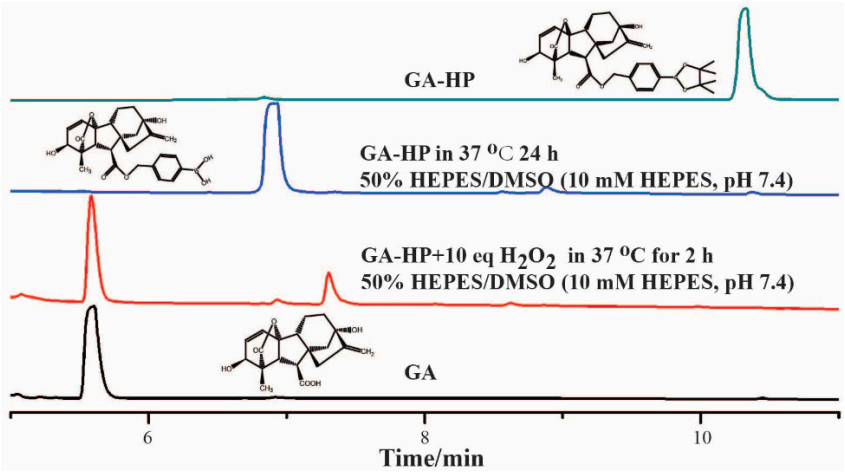

Figure 2.25 GA-HP (5 mM) was treated with or without 50 mM of H_2O_2 for indicated time periods. The results shown are representative from 3 independent experiments.

It was observed that, without H_2O_2, GA-HP did not release GA when incubated in HEPES buffer for 24 h, although the boronate group was partially hydrolyzed as reported in a similar case to give an inert but convertible product (Figures 2.26).[40]

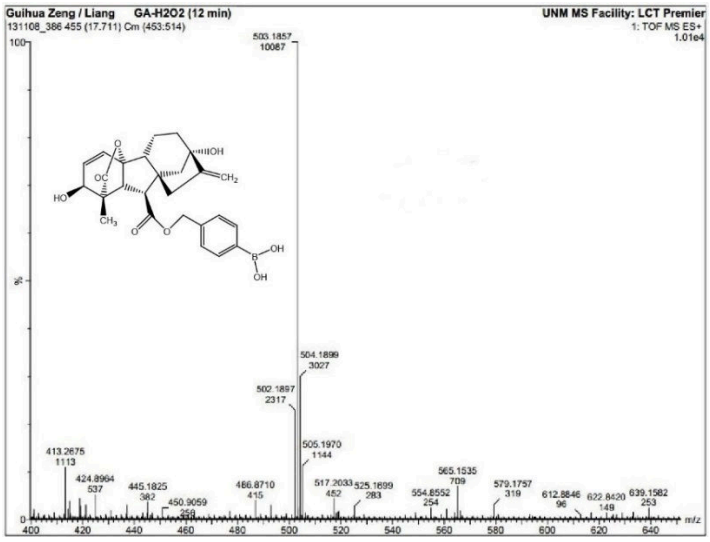

Figure 2.26 MS of partial hydrolyzed GA-HP. TOF-HRMS (m/z) found (calcd.) for $C_{26}H_{29}O_8B$ (M): $[M+Na]^+$, 503.1857 (503.1853).

We also tested the selectivity of GA-HP against different ROS and cellular metals and found that GA-HP was selective for H_2O_2 among tested molecules (Figures 2.27 and 2.28).

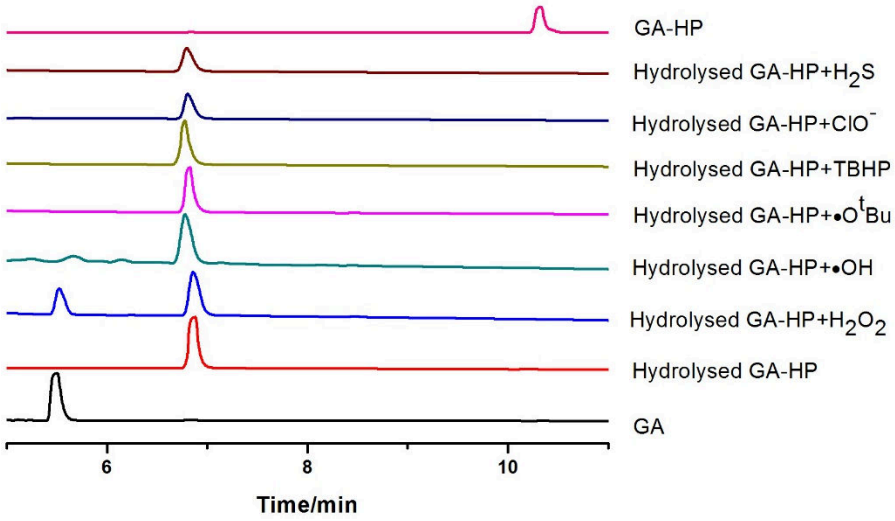

Figure 2.27 Reaction selectivity of GA-HP (1 mM) against H_2S and different ROS (1 mM) in 50% DMSO/HEPES at 37℃ for 4 h. The results were analyzed by HPLC. H_2S was generated by Na_2S in HEPES buffer (pH 7.4). •OH and •O^tBu were generated by reaction of Fe^{2+} with H_2O_2 or tert-butyl hydroperoxide (TBHP), respectively. The HPLC chromatograms shown are representative from 3 independent experiments.

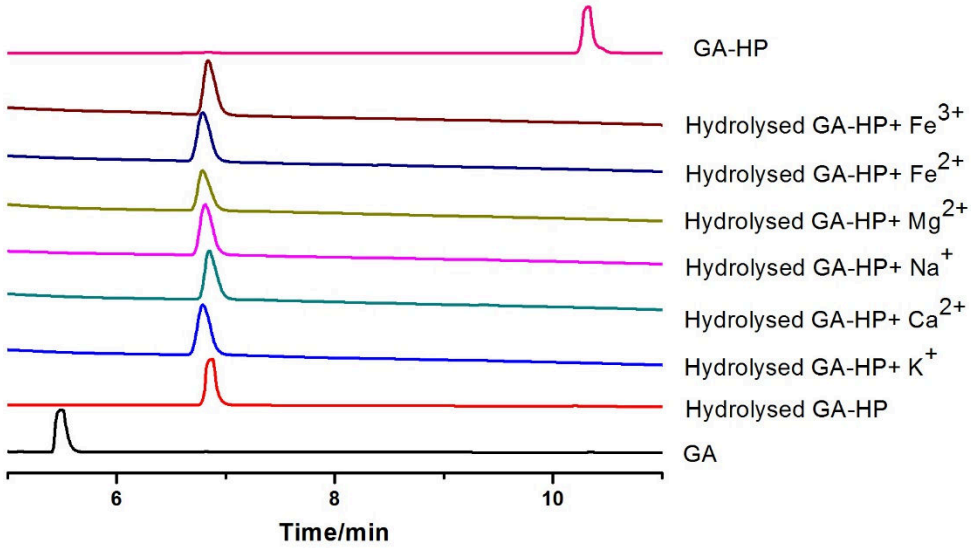

Figure 2.28 Reaction selectivity of GA-HP (1 mM) against common cellular metal ions (1 mM) in 50% HEPES/DMSO. The results were analyzed by HPLC after 4-h incubation in 37 ℃. Shown HPLC chromatograms are representative from 3 independent experiments.

2.3.2 H_2O_2 induced protein translocation in living cells based on GA-CIP system

To examine if we can produce biologically active GA from GAHP in the presence of H_2O_2 in cells, we made DNA constructs to encode a nuclear exported GID1 (NES-GID1) and a pan-cellular distributed EGFP-tagged GAI (EGFP-GAI) (Figure 2.29).

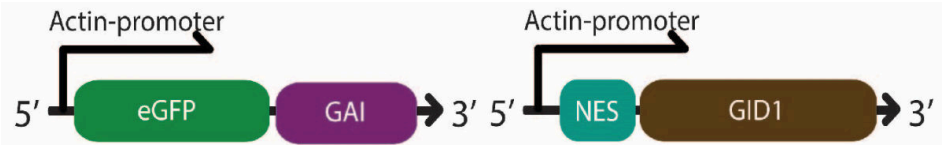

Figure 2.29 DNA constructs for GA-inducible EGFP nuclear export

CHO cells were transfected with these plasmids for 24 h and then incubated without additive or with 100 μM GA-AM, GA-HP, or GA-HP plus 100 μM H_2O_2 for 30 min. The percentage of cells showing EGFP-GAI nuclear export was quantified in each condition using a fluorescence microscope (Figure 2.30). Only cells treated with GA-AM or GA-HP plus H_2O_2 showed nuclear export, which indicated that functional GA was generated from GA-HP upon H_2O_2 addition. Given that GA cannot cross the cell membrane, the observed intracellular effects suggested that the H_2O_2-induced cleavage

of GA-HP occurred inside the cells. The successful implementation of this strategy using GA demonstrates the potential generality of our strategy.

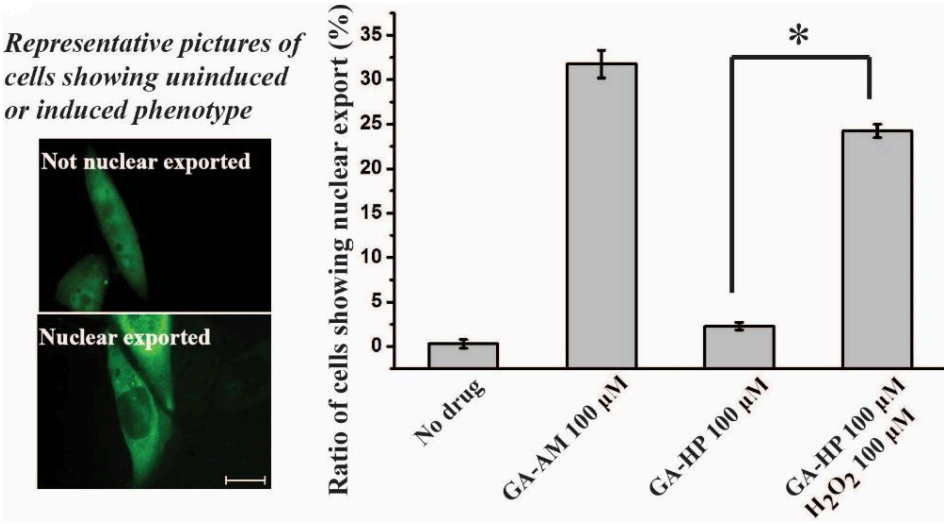

Figure 2.30 Nuclear export of EGFP in CHO cells under different treating conditions (30 min). CHO cells were transfected with these plasmids in Figure 2.29, and then treated with different conditions. The statistical data was obtained by counting cells to give the percentage of cells showing nuclear export over the total EGFP positive cells. Cells were counted from three separate experiments each with five different areas chosen randomly, and over 700 cells were counted for each sample. Scale bar is 20 μm. Error bars are SD (N = 3). *P-value < 0.001.

2.4 Conclusion

In conclusion, we have developed a novel strategy integrating CIP methods and H_2O_2-sensing to construct de novo cell signaling pathways that redirected H_2O_2 to control different cellular processes (i.e., transcription and protein translocation) or to

interface with an existing endogenous signaling circuit (i.e., the Rac1 signaling). We have showed that **ABA** can be converted to become responsive to exogenous or endogenous H_2O_2 stimulation rapidly and specifically at physiologically relevant concentrations. Moreover, this strategy can be generally applied to different CIP inducers (i.e., **ABA** and GA). It provides the potential to expand this strategy in building signaling networks when each orthogonal CIP inducer is designed to become activated by a unique signal. We expect that sensing units for different cell signals can be used to replace the H_2O_2 sensing unit used in this study to switch the responding specificity.[41-42] We believe that our novel strategy to engineer de novo cell signaling circuits will have wide applications in the fields of cell signaling research, biocomputing, and synthetic biology and contribute to the future development of gene and cell therapies for human diseases.

2.5 Methods

2.5.1 Chemical synthesis

General. ^{1}H (300 MHz) and ^{13}C (75 MHz) NMR were recorded on a Bruker Avance 500. All commercially available reagents were used without further purification. The progress on the reactions was monitored by analytical thin-layer chromatography (TLC) on Whatman silica gel plates with UV indicator. And Merk 60 silica gel was used for chromatography.

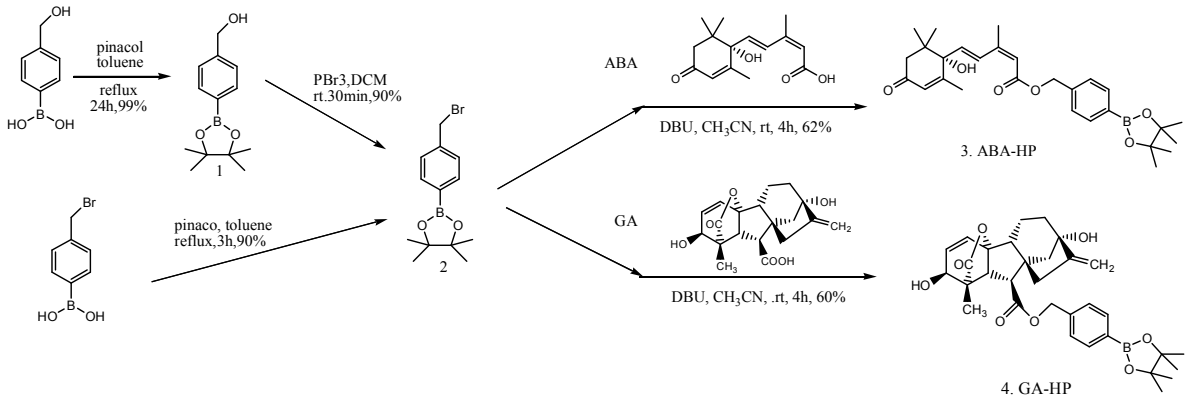

Figure 2.31 Synthesis of **ABA**-HP and GA-HP

Synthesis of 2-[4-(Bromomethyl)phenyl]-4,4,5,5-tetramethyl-1,3,2-dioxaborolane (2). To 4-(bromomethyl)phenylboronic acid (200 mg, 0.93 mmol, Sigma Aldrich) in 1 mL toluene was added pinacol (165 mg, 1.40 mmol, Sigma Aldrich), then heated to reflux with Dean-Stark trap and stirred for 3 h. The solvent was removed by rotavapor, and the product was purified through column chromatography (EA : Hex = 1:3) and obtained as white solid (250 mg, 91%). Also compound 2 was synthesized through compound 1. ^{1}H-NMR (300 MHz, CDCl3), δ (ppm): 1.340 (12H, s), 4.488 (2H, s), 7.378-7.404 (2H, d, J = 7.8Hz), 7.772-7.798 (2H, d, J = 7.8Hz).

*Synthesis of **ABA**-HP (3).* To **ABA** (44 mg, 0.17 mmol, Gold Biotechnology, USA) in 10 mL CH_3CN was added compound 2 (55 mg, 0.19 mmol) and DBU (55 μL, 0.37 mmol, Sigma Aldrich), then stirred at RT for 4 h. The solvent was removed by rotavapor, then the product was purified by column chromatography (EA : Hex = 1:3) to give white solid (50 mg, 62%). The compound was characterized by ^{1}H and ^{13}C NMR and

high-resolution mass spectrometry with > 95% purity based ^{1}H NMR. HPLC was used for further purification before biological activity test. ^{1}H-NMR (300 MHz, $CDCl_3$), δ (ppm): 0.997 (3H, s), 1.097 (3H, s), 1.334 (12H, s), 1.896 (3H, s), 2.004 (3H, s), 2.165 (1H, s), 2.254-2.311 (1H, d, J = 17.1Hz), 2.443-2.500 (1H, d, J = 17.1Hz), 5.155 (2H, s), 5.802 (1H, s), 5.917 (1H, s), 6.130-6.183 (1H, d, J = 15.9Hz), 7.345-7.372 (2H, d, J = 8.1Hz), 7.785-7.812 (2H, d, J = 8.1Hz), 7.855-7.910 (1H, d, J = 16.5Hz). ^{13}C-NMR (75 MHz, $CDCl_3$), δ (ppm): 18.9, 21.3, 23.1, 24.3, 24.8, 41.5, 49.8, 65.7, 79.6, 83.8, 118.3, 127.0, 127.2, 128.1, 135.0, 136.5, 139.1, 149.7, 162.4, 165.6, 197.7. TOF-HRMS (m/z) found (calcd.) for $C_{28}H_{37}O_6B$ (M): $[M+Na]^+$, 503.2583 (503.2581) and [2M+Na]+, 983.5185 (983.5264).

Synthesis of GA-HP (4). To GA (100 mg, 0.29 mmol, Alfa Aesar) in 20 mL CH_3CN was added compound 2 (102.9 mg, 0.35 mmol) and 1,8-Diazabicyclo[5.4.0]undec-7-ene (DBU, 52 μL, 0.35 mmol, Sigma Aldrich), then stirred at RT for 4 h. The solvent was removed by rotavapor, and the product was purified by column chromatography (EA : Hex = 1:1) and obtained as white solid (97 mg, 60%). The compound was characterized by ^{1}H and ^{13}C NMR and high-resolution mass spectrometry with > 95% purity based ^{1}H NMR. HPLC was used for further purification before biological activity test. ^{1}H-NMR (300 MHz, $CDCl_3$), δ (ppm): 1.198 (3H, s), 1.338 (12H, s), 1.632-2.172 (9H, m), 2.795-2.831 (1H, d, J = 10.8Hz), 3.200-3.236 (1H, d, J = 10.8Hz), 4.127 (1H, s), 4.876 (1H, s), 5.117-5.231 (3H, m), 5.867-5.910 (1H, dd,

J = 3.6, 9.3Hz), 6.280-6.313 (1H, d, J = 9.9Hz), 7.318-7.345 (2H, d, J = 8.1Hz), 7.778-7.805 (2H, d, J = 8.1Hz). ^{13}C-NMR (75 MHz, $CDCl_3$), δ (ppm): 14.8, 17.3, 25.1, 38.4, 43.1, 45.1, 50.8, 51.0, 51.4, 53.1, 53.7, 67.1, 69.9, 75.4, 78.3, 84.2, 90.8, 107.8, 127.7, 132.7,133.0, 135.3, 138.5, 157.0, 172.3, 179.0. TOF-HRMS (m/z) found (calcd.) for $C_{32}H_{39}O_8B$ (M): $[M+Na]^+$, 585.2653 (585.2636).

2.5.2 Reverse-phase HPLC analysis

*Chemical stability and reactivity of **ABA**-HP towards H_2O_2.* **ABA**-HP chemical stability: 1 mM **ABA**-HP (in DMSO) was incubated in 50% HEPES/DMSO (10 mM HEPES, pH 7.4) for 24 h at 37 ℃. HPLC results were detected at 0 min, 20 min, 40 min, 60 min, 80 min, 100 min, 120 min, 240 min, and 24 hrs. **ABA**-HP reactivity towards H_2O_2: 1 mM **ABA**-HP was incubated with 5 mM (5 eq) H_2O_2 in 50% HEPES/DMSO (10 mM HEPES, pH 7.4) at 37 ℃. The cleavage products were detected at 0, 20, 40, 80, 100, 120 and 240 min by HPLC. 100 mM H_2O_2 was diluted with 11 µL of 30% (10 M) stock H_2O_2 (VWR) and 989 µL of ddH_2O. All concentrations shown were the final concentration. HPLC chromatograms were acquired using Dionex-UltiMate 3000 LC System with Acclaim 120 Å, C18, 3 µm analytical (4.6 x 100 mm) column. Chromatographic conditions: eluent A: 0.1% v/v TFA in water; eluent B: 0.1% v/v TFA in acetonitrile. **ABA** in ethanol or **ABA**-HP in DMSO was eluted at a flow rate of 0.750 ml/min monitored at a wavelength of 260 nm. 0-12 min (linear): 95% A, 5% B to 5% A, 95% B; 12-15 min: 5% A, 95% B; 15-17 min (linear): 5% A, 95% B

to 95% A, 5% B. Generation of **ABA** was quantified by the peak area of **ABA** out of the total peak area.

Reaction selectivity versus different molecules. 100 μM **ABA**-HP was incubated with 100 μM (1 eq) of different molecules as indicated in 50% HEPES/DMSO (pH 7.4) at 37℃ for 4 h and the cleavage products were detected by HPLC. H_2S was generated by 100 μM Na_2S solution in HEPES buffer, which can slowly release H_2S. •OH and •O^{t}Bu were generated by reaction of Fe^{2+} with H_2O_2 or tert-butyl hydroperoxide (TBHP), respectively. HPLC condition was the same as the stability and reactivity test of **ABA**-HP.

Chemical stability and reactivity of GA-HP towards H_2O_2. GA-HP chemical stability: 5 mM GA-HP (in DMSO) was incubated in 50% HEPES/DMSO (10 mM HEPES, pH 7.4) for 24 h at 37 ℃ and the products were analyzed by HPLC. GA-HP reactivity towards H_2O_2: 5 mM GA-HP was incubated with 50 mM (10 eq) H_2O_2 in 50% HEPES/DMSO (10 mM HEPES, pH 7.4) at 37 ℃. The products were analyzed at 5, 30, 60, 90 and 120 min using HPLC. HPLC chromatograms were acquired using Dionex-UltiMate 3000 LC System with Acclaim 120 Å, C18, 3 μm analytical (4.6 x 100 mm) column. Chromatographic conditions: eluent A: 0.1% v/v TFA in water; eluent B: 0.1% v/v TFA in acetonitrile. Solutions in DMSO were eluted at a flow rate of 1.000 ml/min monitored at a wavelength of 206 nm. 0-12 min (linear): 95% A, 5% B to 5% A, 95% B; 12-16 min: 5% A, 95% B; 16-18 min (linear): 5% A, 95% B to 95% A, 5%

B.

2.5.3 Cloning and plasmid construction

All DNA fragments were amplified by PCR (Polymerase chain reaction) from other intermediate constructs with the enzyme of Phusion DNA Polymerase (New England Biolabs), or PfuUltra II Fusion HotStart DNA Polymerase (Agilent Technologies) under S1000 thermal cycler with Dual 48/48 Fast Reaction Module (Bio-Rad). All the restriction enzymes used below are purchased from New England Biolabs. PYL-EGFP-Tiam1 construct was derived from pSV40-VP16-PYL-IRES-Gal4DBD-ABI[12] by inserting codon optimized PYL fragment (PCR amplified by primers CCGACA GAATTCGCCACCAT-GACCCAGGACGAGTTTACCCAG and CCGACAGGC GCGCCGCTGCCGCCGTTCATAGCCTCAGTAATGCT) using EcoRI and AscI sites, Tiam1-SG linker fragment (amplified by primers GCTATGAACGGCGCGCCA AGTGCTGGTGGTAGTGCTGGT and CTAGAGTCGCGGCCGCTCAGATCTCA GTGTTCAGTTTC) using AscI and NotI sites, and eGFP-SG-linker fragment (amplified by primers CCGACAGGCGCGCCAGGTGGATCTGGAGGTTCAGG TGGATCTGGAGGTGTGAGCAAGGGCGAGGAGCTG and CCGACAGGCGCG CCCTTGTACAGCTCGTCCATGCC) using AscI site. NES-GID1 construct was generated from NES-ABI[25] by inserting GID1 fragment (amplified by primers CCGACAACGCGTGGATCTGGTGGAGCTGCGAGCGATGAGTTAAT and CCGACAGCGGCCGCTCAACATTCCGCGTTTACAAACGC) using MluI and NotI

sites. EGFP-GAI construct was generated from eGFP-PYL.[12] GAI fragment (amplified by primers CCGACAGGCGCGCCAGGATCTGGTGGAAAGAGAGATCATC-ATCATCAT and CCGACAGGATCCTCAAGGATTAAGGTCGGTGAGCAT) was inserted by AscI and blunt end ligation into AscI and blunted NotI sites on the vector.

2.5.4 Mammalian cell culture and transfection

All cells were cultured in DMEM medium (Gibco) supplemented with 10% FBS, 2 mM GlutaMAX (life technologies), 100 U/ml penicillin (life technologies) and 100 μg/ml streptomycin (life technologies) at 37℃ in a humidified atmosphere containing 5% CO_2.

EGFP expression experiments. HEK 293T EGFP reporter cells were seeded 24 h prior to treatment in 24-well plates at 100,000/well. 10 μM **ABA**-HP was added to the cells 10 min prior to the addition of 10 μM **ABA** and 10, 50, or 100 μM of H_2O_2. Images were taken for living cells at 5, 7, 10 and 24 h.

NES localization experiments in CHO cells. CHO cells were seeded over glass coverslips in 24-well plates at 50,000/well for 24 h. 0.4 μg NES-ABI and 0.2 μg EGFP-PYL DNA plasmids were mixed with 30 μL of Opti-MEM (life technologies) and 1.8 μL of PEI (Polysciences). After incubation at RT for 15 min, the mixture was added to the cells and cultured for 24 h. Then, 10 μM **ABA** or 10 μM **ABA**-HP plus 100 μM of H_2O_2 (**ABA**-HP added 10 min prior to H_2O_2), or 100 μM GA or 100 μM GA-HP plus

100 μM of H_2O_2 (GA-HP added 10 min prior to H_2O_2) was added to the cells. 30 min after adding compounds, the coverslips were washed with phosphate-buffered saline (PBS) and fixed with 300 μL of 4% paraformaldehyde (PFA, prepared in PBS) at room temperature for 20 min. The cells were then washed twice with PBS and incubated with 1x DAPI in the dark at the room temperature for 5 min. After a final wash with PBS, the coverslips were mounted on a glass slide with Vectashield (VWR) mounting media and images of cells were then taken using a fluorescence microscope.

Live cells imaging experiment for CHO cells with nuclear export experiments and its analysis. CHO cells were seeded in 8 Chamber coverglass plate at 25,000/well for 24 h. 0.2 μg NES-ABI and 0.1 μg EGFP-PYL DNA plasmids were mixed with 15 μL of Opti-MEM (life technologies) and 0.9 μL of PEI (Polysciences). After incubation at RT for 15 min, the mixture was added to the cells and cultured for 24 h. Medium was changed 1 h before the addition of 10 μM **ABA**, 10 μM **ABA**-HP with and without 100 μM H_2O_2. Images were taken every 30 secs for duration of 20 min for the same area. Images generated were analyzed for fluorescent intensity using Slide Book v.6 software. Equal sized regions of interest were analyzed to get the EGFP fluorescent intensity ratio of the nucleus over cytoplasm. Three cells for each condition were analyzed to get the average ratio and normalized.

NES localization experiments in A431 cells. A431 cells were seeded over glass coverslips in 24-well plates at 100,000/well for 24 h. 0.4 μg NES-ABI and 0.2 μg

EGFP-PYL DNA plasmids were mixed with 30 μL of Opti-MEM and 1.8 μL of PEI. After incubation at RT for 15 min, the mixture was added to the cells and cultured for 24 h. Then, 10 μM **ABA** or 10 μM **ABA**-HP plus 100 μM of H_2O_2 or plus 500 ng/mL hEGF (Sigma-Aldrich) (**ABA**-HP added 10 min prior to H_2O_2 or hEGF) was added to the cells. Slides were prepared 30 min after adding compounds and images were then taken using a fluorescence microscope.

NES localization experiments in A431 and CHO cells treated with catalase. Cells were seeded over glass coverslips in 24-well plates at 100,000/well for A431 cells and 50,000/well for CHO cells 24 h before the transfections. 0.4 μg NES-ABI and 0.2 μg EGFP-PYL DNA plasmids were mixed with 30 μL of Opti-MEM and 1.8 μL of PEI. After incubation at RT for 15 min, the mixture was added to the cells and cultured for 24 h. Then, cells were treated with 1mg/mL of catalase (Sigma-Aldrich, C1345) by changing the medium with catalase for 1 h incubation, followed by the addition of other drugs.

Ruffle generation experiment. CHO were seeded over glass coverslips in 24-well plates at 50,000/well for 24 h. 0.1 μg PYL-EGFP-Tiam1 and 0.1 μg myr-ABI DNA plasmids were mixed with 30 μL of Opti-MEM and 1.8 μL PEI. After incubation at room temperature for 15 min, the mixture was added to the cells and cultured for 24 h. Then, 10 μM **ABA** or 10 μM **ABA**-HP plus 100 μM of H_2O_2 (**ABA**-HP added 10 min prior to H_2O_2) (or 5 μM **ABA** or 5 μM **ABA**-HP plus 50 μM of H_2O_2) was added to the

cells. For the cells treated with rac1 inhibitor NSC 23766, 50μM of NSC 23766 was added to the medium 1h prior to drug addition. Slides were prepared 30 min after adding compounds and images were then taken using a Zeiss LSM 510 META Confocal Microscopy the next day.

Luciferase reporter assay with CHO cells. CHO were seeded over glass coverslips in 24-well plates at 50,000/well for 24 h. 0.1 μg 5 × FL and 0.5 μg SV-VP-PYL-ires-Gal-ABI DNA plasmids were mixed with 30 μL of Opti-MEM and 1.8 μL PEI. After incubation at RT for 15 min, the mixture was added to the cells and cultured for 24 h. 10 μM **ABA**-HP or **ABA** was added to the cells. After 6 h, cells were washed with PBS and lysed with 100 μL of Reporter Lysis Buffer (Promega) by incubating and gently shaken at room temperature for 10 min. Cell lysates were centrifuged at 15,000 rpm in an Eppendorf Centrifuge 5424 and 10 μL of lysate was used for luciferase assay. 100 μL of luciferase assay reagent (5 mg luciferin (GoldBio) and 7 mg coenzyme A (Sigma) in 33 mL of Luciferase Assay Buffer [20 mM tricine, 1.07 mM $(MgCO_3)_4Mg(OH)2•5H_2O$, 2.67 mM $MgSO_4$, 0.1 mM EDTA, 33.3 mM dithiothreitol, and 0.53 mM ATP in water) was added to lysates. Luciferase assay reagent was added through the auto-injector of GLOMAX-Multi Detection System (Promega), and the signal was detected by the instrument with a 1.5 s delay and 0.5 s integration time. All experiments were conducted in triplicate.

Fluorescence microscopy. Zeiss Axio Observer. D1 outfitted with HBO 100

microscopy illumination system (GFP: excitation 470/40 and emission 525/50) and Zeiss LSM 510 META Confocal Microscopy outfitted with GFP/Alexa Fluor 488 (491 laser excitation, 528/38 emission) were used. *EGFP expression experiment:* Zeiss Axio Observer. D1 was used with the 20× objective and image areas were chosen randomly. *NES localization:* Zeiss Axio Observer. D1 was used with the 63× oil-immersion objective. *Ruffle formation*: Zeiss LSM 510 META Confocal Microscopy with 40× and 63× oil-immersion objectives. Fluorescent channels in all experiments were adjusted to the same intensity ranges. Acquisition times ranged from 100 to 1000 ms.

Statistical Analysis of Cell Population. Cell were categorized as displaying nuclear export of EGFP when the fluorescent intensity of the nucleus was less than 60% of the intensity over the cytoplasm. Cells were categorized as Ruffled when they displayed broad extensions identifiable as lemellopodia or fillopodia from the GFP fluorescence from membrane localized EGFP-PYL-Tiam1. Cells were counted from three separate experiments with 5 different areas by random and > 700 cells for each sample. P values were obtained by using EXCEL with the function “CHISQ.TEST”.

2.6 reference

1. Bashor, C. J.; Horwitz, A. A.; Peisajovich, S. G.; Lim, W. A., Rewiring cells: synthetic biology as a tool to interrogate the organizational principles of living systems. *Annual review of biophysics* **2010,** *39*, 515-37.

2. Purnick, P. E.; Weiss, R., The second wave of synthetic biology: from modules to systems. *Nature reviews. Molecular cell biology* **2009,** *10* (6), 410-22.

3. Haynes, K. A.; Silver, P. A., Eukaryotic systems broaden the scope of synthetic biology. *The Journal of cell biology* **2009,** *187* (5), 589-96.

4. Auslander, S.; Auslander, D.; Muller, M.; Wieland, M.; Fussenegger, M., Programmable single-cell mammalian biocomputers. *Nature* **2012,** *487* (7405), 123-7.

5. Miyamoto, T.; Razavi, S.; DeRose, R.; Inoue, T., Synthesizing biomolecule-based Boolean logic gates. *ACS synthetic biology* **2013,** *2* (2), 72-82.

6. Tigges, M.; Fussenegger, M., Recent advances in mammalian synthetic biology-design of synthetic transgene control networks. *Current opinion in biotechnology* **2009,** *20* (4), 449-60.

7. Ruder, W. C.; Lu, T.; Collins, J. J., Synthetic biology moving into the clinic. *Science* **2011,** *333* (6047), 1248-52.

8. Lim, W. A., Designing customized cell signalling circuits. *Nat Rev Mol Cell Bio* **2010,** *11* (6), 393-403.

9. Fegan, A.; White, B.; Carlson, J. C. T.; Wagner, C. R., Chemically Controlled Protein Assembly: Techniques and Applications. *Chemical reviews* **2010,** *110* (6), 3315-3336.

10. Fegan, A.; White, B.; Carlson, J. C.; Wagner, C. R., Chemically controlled protein assembly: techniques and applications. *Chemical reviews* **2010,** *110* (6), 3315-36.

11. Gestwicki, J. E.; Marinec, P. S., Chemical control over protein-protein interactions: beyond inhibitors. *Combinatorial chemistry & high throughput screening* **2007,** *10* (8), 667-75.

12. DeRose, R.; Miyamoto, T.; Inoue, T., Manipulating signaling at will: chemically-inducible dimerization (CID) techniques resolve problems in cell biology. *Pflugers Archiv : European journal of physiology* **2013,** *465* (3), 409-17.

13. Liang, F. S.; Ho, W. Q.; Crabtree, G. R., Engineering the **ABA** plant stress pathway for regulation of induced proximity. *Science signaling* **2011,** *4* (164), rs2.

14. Miyamoto, T.; DeRose, R.; Suarez, A.; Ueno, T.; Chen, M.; Sun, T. P.; Wolfgang, M. J.; Mukherjee, C.; Meyers, D. J.; Inoue, T., Rapid and orthogonal logic gating with a gibberellin-induced dimerization system. *Nature chemical biology* **2012,** *8* (5), 465-70.

15. Stone, J. R.; Yang, S., Hydrogen peroxide: a signaling messenger. *Antioxidants & redox signaling* **2006,** *8* (3-4), 243-70.

16. Rice, M. E., H2O2: a dynamic neuromodulator. *The Neuroscientist : a review journal bringing neurobiology, neurology and psychiatry* **2011,** *17* (4), 389-406.

17. Xiao, Q. Z.; Luo, Z. L.; Pepe, A. E.; Margariti, A.; Zeng, L. F.; Xu, Q. B., Embryonic stem cell differentiation into smooth muscle cells is mediated by Nox4-produced H2O2. *Am J Physiol-Cell Ph* **2009,** *296* (4), C711-C723.

18. Nindl, G.; Peterson, N. R.; Hughes, E. F.; Waite, L. R.; Johnson, M. T., Effect of hydrogen peroxide on proliferation, apoptosis and interleukin-2 production of jurkat T cells. *Tech Papers Isa* **2004,** *449*, 123-128.

19. Lopez-Lazaro, M., Dual role of hydrogen peroxide in cancer: Possible relevance to cancer chemoprevention and therapy. *Cancer Lett* **2007,** *252* (1), 1-8.

20. Lee, J.; Giordano, S.; Zhang, J. H., Autophagy, mitochondria and oxidative stress: cross-talk and redox signalling. *Biochem J* **2012,** *441*, 523-540.

21. Miyazono, K.; Miyakawa, T.; Sawano, Y.; Kubota, K.; Kang, H. J.; Asano, A.; Miyauchi, Y.; Takahashi, M.; Zhi, Y. H.; Fujita, Y.; Yoshida, T.; Kodaira, K. S.; Yamaguchi-Shinozaki, K.; Tanokura, M., Structural basis of abscisic acid signalling. *Nature* **2009,** *462* (7273), 609-U79.

22. Wright, C. W.; Guo, Z. F.; Liang, F. S., Light Control of Cellular Processes by Using Photocaged Abscisic Acid. *Chembiochem : a European journal of chemical biology* **2015,** *16* (2), 254-261.

23. Lippert, A. R.; De Bittner, G. C. V.; Chang, C. J., Boronate Oxidation as a

Bioorthogonal Reaction Approach for Studying the Chemistry of Hydrogen Peroxide in Living Systems. *Accounts Chem Res* **2011,** *44* (9), 793-804.

24. Govan, J. M.; McIver, A. L.; Riggsbee, C.; Deiters, A., Hydrogen Peroxide Induced Activation of Gene Expression in Mammalian Cells using Boronate Estrone Derivatives. *Angew Chem Int Edit* **2012,** *51* (36), 9066-9070.

25. Weinstain, R.; Sayariar, E. N.; Felsen, C. N.; Tsien, R. Y., In Vivo Targeting of Hydrogen Peroxide by Activatable Cell-Penetrating Peptides. *Journal of the American Chemical Society* **2014,** *136* (3), 874-877.

26. Spanos, M.; Gras-Najjar, J.; Letchworth, J. M.; Sanford, A. L.; Toups, J. V.; Sombers, L. A., Quantitation of hydrogen peroxide fluctuations and their modulation of dopamine dynamics in the rat dorsal striatum using fast-scan cyclic voltammetry. *ACS chemical neuroscience* **2013,** *4* (5), 782-9.

27. Hyslop, P. A.; Zhang, Z.; Pearson, D. V.; Phebus, L. A., Measurement of striatal H2O2 by microdialysis following global forebrain ischemia and reperfusion in the rat: correlation with the cytotoxic potential of H2O2 in vitro. *Brain research* **1995,** *671* (2), 181-6.

28. Gill, R. S.; Lee, T. F.; Liu, J. Q.; Chaudhary, H.; Brocks, D. R.; Bigam, D. L.; Cheung, P. Y., Cyclosporine treatment reduces oxygen free radical generation and

oxidative stress in the brain of hypoxia-reoxygenated newborn piglets. *PloS one* **2012,** *7* (7), e40471.

29. Mueller, S.; Riedel, H. D.; Stremmel, W., Determination of catalase activity at physiological hydrogen peroxide concentrations. *Analytical biochemistry* **1997,** *245* (1), 55-60.

30. Imlay, J. A., Cellular defenses against superoxide and hydrogen peroxide. *Annual review of biochemistry* **2008,** *77*, 755-76.

31. Kusaka, N.; Maisch, J.; Nick, P.; Hayashi, K.; Nozaki, H., Manipulation of Intracellular Auxin in a Single Cell by Light with Esterase-Resistant Caged Auxins. *Chembiochem : a European journal of chemical biology* **2009,** *10* (13), 2195-2202.

32. von Heijne, G., Signal Peptides. In *eLS*, John Wiley & Sons, Ltd: 2001.

33. Martinez-Outschoorn, U. E.; Lin, Z.; Trimmer, C.; Flomenberg, N.; Wang, C.; Pavlides, S.; Pestell, R. G.; Howell, A.; Sotgia, F.; Lisanti, M. P., Cancer cells metabolically "fertilize" the tumor microenvironment with hydrogen peroxide, driving the Warburg effect: implications for PET imaging of human tumors. *Cell Cycle* **2011,** *10* (15), 2504-20.

34. Michiels, F.; Habets, G. G. M.; Stam, J. C.; Vanderkammen, R. A.; Collard, J. G., A Role for Rac in Tiam1-Induced Membrane Ruffling and Invasion. *Nature* **1995,** *375*

(6529), 338-340.

35. Sharma, A.; Muresanu, D. F.; Patnaik, R.; Lafuente, J. V.; Sharma, H. S., Engineered nanoparticles Ag, Cu and Al (50-60nm) induce oxidative stress, neuronal nitric oxide synthase upregulation and brain pathology. Neuroprotection by Insulin-like growth factor1. *Eur J Neurol* **2012,** *19*, 441-441.

36. Jin, H.; Heller, D. A.; Kalbacova, M.; Kim, J. H.; Zhang, J. Q.; Boghossian, A. A.; Maheshri, N.; Strano, M. S., Detection of single-molecule H2O2 signalling from epidermal growth factor receptor using fluorescent single-walled carbon nanotubes. *Nature nanotechnology* **2010,** *5* (4), 302-U81.

37. Bae, Y. S.; Kang, S. W.; Seo, M. S.; Baines, I. C.; Tekle, E.; Chock, P. B.; Rhee, S. G., Epidermal growth factor (EGF)-induced generation of hydrogen peroxide - Role in EGF receptor-mediated tyrosine phosphorylation. *Journal of Biological Chemistry* **1997,** *272* (1), 217-221.

38. Shimada, A.; Ueguchi-Tanaka, M.; Nakatsu, T.; Nakajima, M.; Naoe, Y.; Ohmiya, H.; Kato, H.; Matsuoka, M., Structural basis for gibberellin recognition by its receptor GID1. *Nature* **2008,** *456* (7221), 520-U44.

39. Schelkle, K. M.; Griesbaum, T.; Ollech, D.; Becht, S.; Buckup, T.; Hamburger, M.; Wombacher, R., Light-induced protein dimerization by one- and two-photon activation

of gibberellic acid derivatives in living cells. *Angew Chem Int Ed Engl* **2015,** *54* (9), 2825-9.

40. Song, C. C.; Ji, R.; Du, F. S.; Liang, D. H.; Li, Z. C., Oxidation-Accelerated Hydrolysis of the Ortho Ester-Containing Acid-Labile Polymers. *Acs Macro Lett* **2013,** *2* (3), 273-277.

41. Chan, J.; Dodani, S. C.; Chang, C. J., Reaction-based small-molecule fluorescent probes for chemoselective bioimaging. *Nat Chem* **2012,** *4* (12), 973-984.

42. Choi, K. Y.; Swierczewska, M.; Lee, S.; Chen, X. Y., Protease-Activated Drug Development. *Theranostics* **2012,** *2* (2), 156-178.

Chapter 3

Engineering Iron Responses in Mammalian Cells by Signal-Induced Protein Proximity

(Reproduced with permission from

ACS Synthetic Biology, 2017, 6 (6), 921–927

The other authors, Huanqiu Li, Yongyi Wei, Weimin Xuan, Roushu Zhang, Larisa E. Breden, are acknowledged.

Supporting information of the publication is incorporated in this chapter)

3.1 Introduction

The aim of synthetic biology research is to rewire biological systems in order to understand and control the functions of cellular systems that ultimately lead to novel therapies.[1-6] Cell signaling translates extracellular signals into intracellular processes that carry out cellular functions. The introduction of artificial signaling networks using synthetic biology methods has facilitated the investigation of signaling mechanisms and

the identification of essential components in signaling pathways. [7-10] Several synthetic biology methods that are based on chemical controls have been developed to provide precise temporal regulation.[1, 11] We recently reported a new strategy to engineer custom signaling pathways in mammalian cells that integrates the chemically induced proximity (CIP) technology [12-13] and reactivity-based signal sensing.[14] The approach enables cells to link H_2O_2 or light with different cellular responses including gene activation, protein translocation, and cytoskeleton remodeling.[15-16] The method uses caged CIP inducers (e.g., abscisic acid (**ABA**)[17]) that are inactive until being stimulated by a specific signal (e.g., H_2O_2) that removes the caging group and activates an inducer to promote the heterodimerization of selected PYL/ABI fusion proteins. Induced protein dimerization then triggers predesigned biological outputs. Our continuing investigations in this are aimed at testing the generality of this strategy for creating new signaling pathways for other important stimuli and exploring the possibility of constructing cross-talking pathways. In the study described below, we have developed a method to engineer artificial Fe^{2+} signaling that responds to elevated Fe^{2+} levels and to build "AND" and "OR" Boolean logic-based signaling circuitries that respond to a combination of H_2O_2 and Fe^{2+} in a predefined manner.

Iron is the most abundant transition metal in humans and its redox chemistry interconverting Fe^{2+} and Fe^{3+} plays numerous biological roles.[18] Although most iron ions exist in complexes with proteins, free Fe^{2+} is present in cellular environments

where it is believed to participate in critical physiological functions.[19] An increased level of Fe^{2+} has been observed in brains of patients with neurodegenerative diseases (e.g., Alzheimer's disease (AD) and Parkinson's diseases (PD)).[20] It is proposed that the combination of elevated levels of Fe^{2+} and H_2O_2 (under oxidative stress) leads to the production of free radicals which promote neuron death in AD and PD.[21-23] The availability of an engineered system that enables cells to detect elevated levels of H_2O_2 and Fe^{2+} in local environments and respond with specific therapeutic outputs would contribute to the development of novel therapies for AD and PD.

3.2 Design, synthesis and screening of ABA-FEs

Several fluorescent probes have been developed to assess the level of Fe^{2+} in living cells.[24-28] Included in this group is the new reactivity-based "off-on" fluorescent reporter we recently developed, which is based on unique Fe^{2+}-mediated cleavage of N-aryl-O-acylhydroxyalamine.[29] We envisioned that the chemistry involved in the Fe^{2+} sensing of this probe could be employed to design novel Fe^{2+} responsive **ABA** inducers that specifically control Fe^{2+}-induced cellular effects through **ABA** mediated protein dimerization (Figure 3.1).

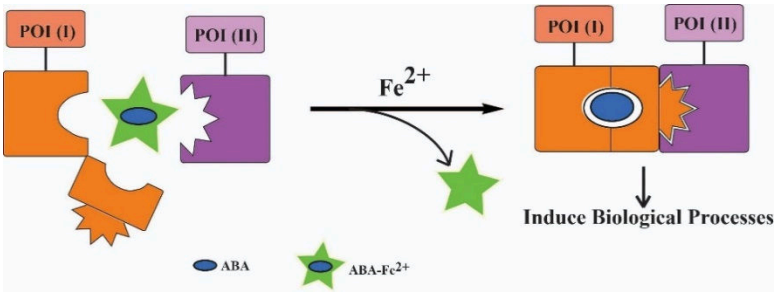

Figure 3.1 General process for Fe^{2+}-induced proximity to control biological processes.

3.2.1 Synthesis of ABA-FEs

Because free Fe^{2+} also exists in a normal cellular environment, caged inducers of this type must be stable under normal cellular Fe^{2+} concentrations and only become activated at abnormally high Fe^{2+} concentrations. To this end, we designed and synthesized a library of **ABA** derivatives (**ABA-FE**1 to 26) that contain differently substituted aniline, benzyl amine, and oxime derivatives conjugated to the carboxylate group of **ABA** through an O−N linkage (Figures 3.2-3.5). The aniline, benzylamine, and oxime moieties in these substances contain a variety of electron donating and withdrawing groups to enable tuning of the reactivity of the O−N linkage against Fe^{2+}. Bulky substituents (e.g., phenyl or tbutyl groups) were also introduced at the benzylic position of the benzyl amine and oxime groups to adjust the lability of the ester linkage caused by cellular esterases.

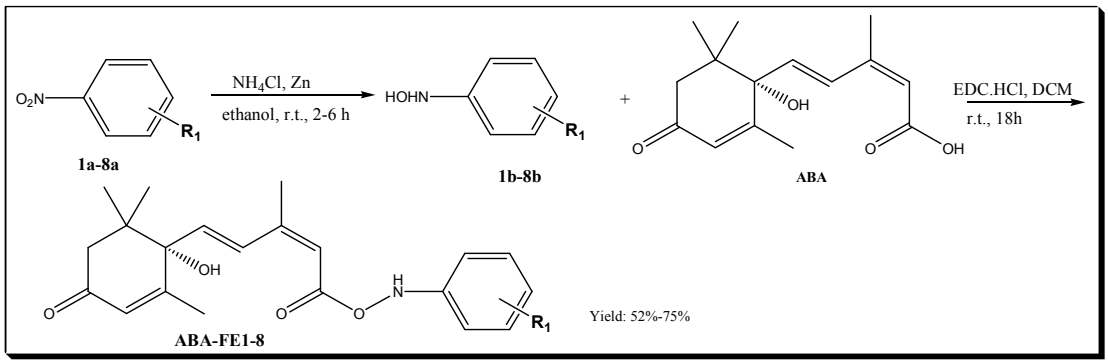

R_1 =	m-NO_2	o-NO_2	p-CN	p-CHO	o-Me	o-Cl	o-Br	o-I
	1	**2**	**3**	**4**	**5**	**6**	**7**	**8**

Figure 3.2 Synthesis of **ABA-FE**1-8.

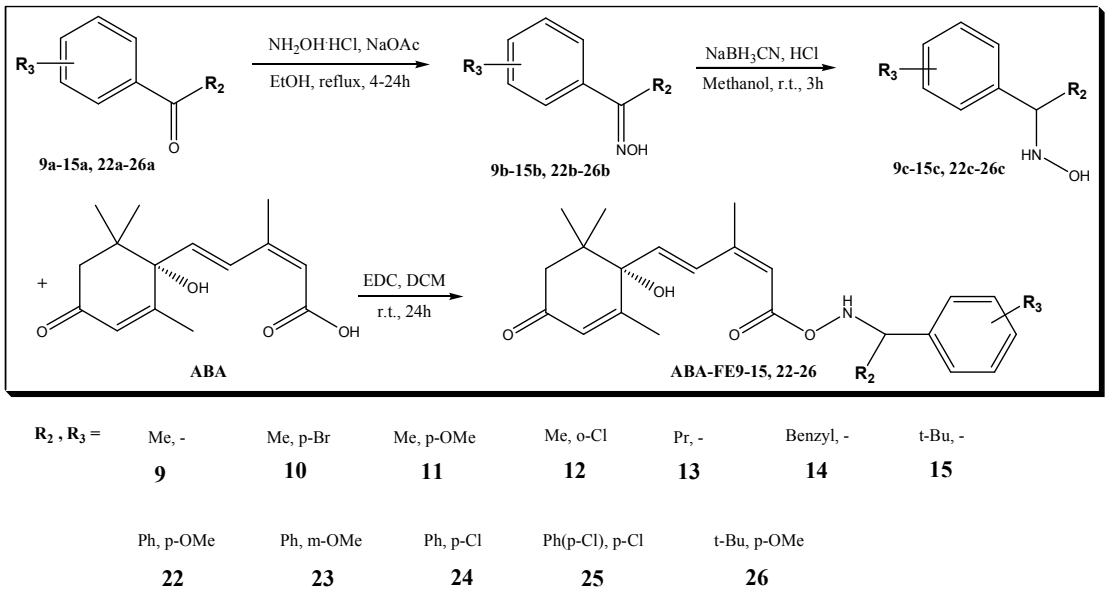

Figure 3.3 Synthesis of **ABA-FE9-15, 22-26**

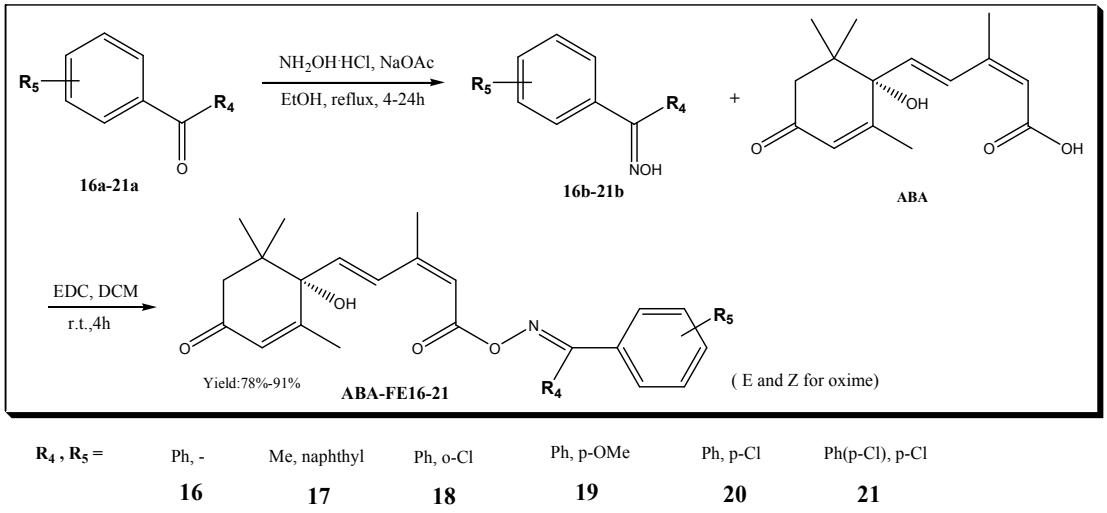

Figure 3.4 Synthesis of **ABA-FE16-21**

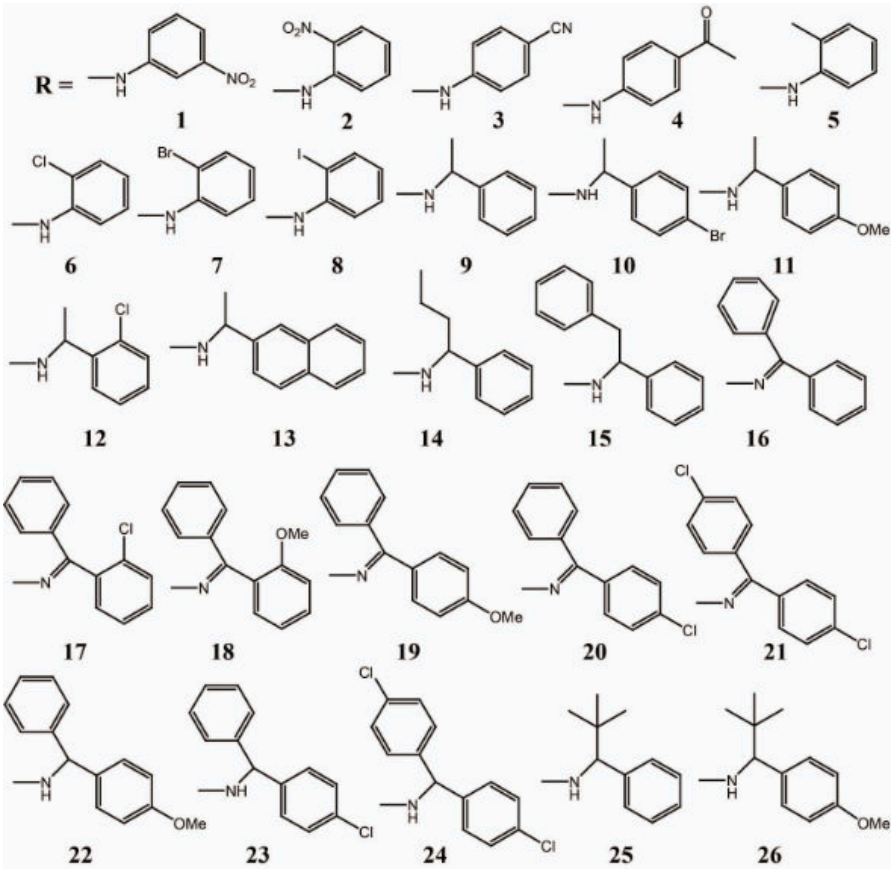

Figure 3.5 Structures of **ABA-FE**s

3.2.2 Screening of ABA-FEs

3.2.2.1 Screening of ABA-FEs with HPLC

To identify **ABA-FE**s that undergo Fe^{2+} specific bond cleavage and that are stable under cellular conditions (i.e., tolerating normal cellular levels of Fe^{2+} and other biomolecules), we probed the reactivity and selectivity of **ABA-FE**s using a series of assays. To check their chemical stability, **ABA-FE**s were incubated in the HEPES buffer at 37 °C for 1 h followed by HPLC analysis. The percentage of **ABA** generated

from each **ABA-FE** (indicating cleavage efficiency) was quantified. In the series, **ABA-FE**2 and **ABA-FE**8 are not stable under these conditions (Figure 3.6) and therefore eliminated from further studies.

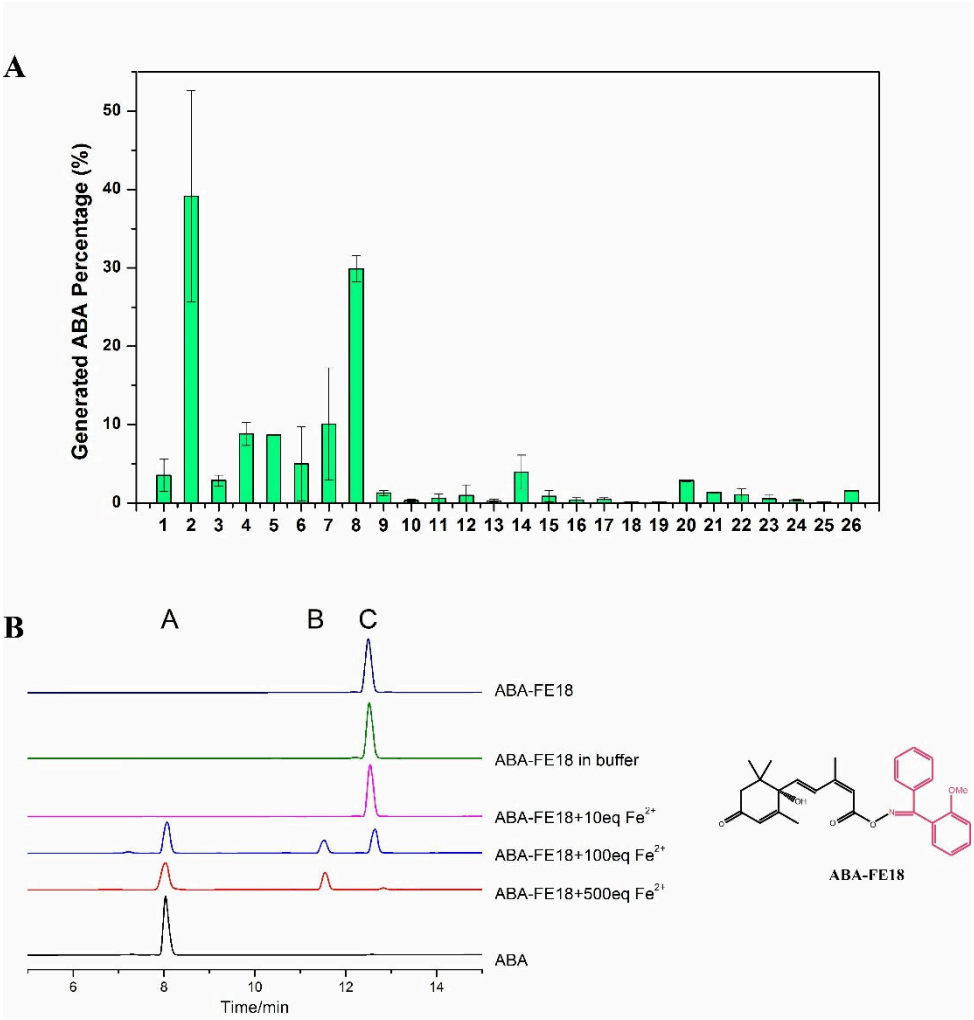

Figure 3.6 Stability of **ABA-FE**s. (**A**) Stability of **ABA-FEs** in HEPES/DMSO. 10 μM **ABA-FE** was incubated in 50% HEPES/DMSO (10 mM HEPES, pH 7.4) for 1 h at 37°C, followed by HPLC analysis. The results were quantified by integrating the peak area corresponding to the **ABA** peak over the total areas of **ABA** peak and caged **ABA**

peak to give the generated **ABA** percentage. The shown results were the average from 3 independent experiments. Error bars are SD (N=3). (**B**) Representative HPLC chromatograms of the analysis. Peak A is **ABA**, peak C is **ABA-FE18**, and peak B is the released byproduct. **ABA**% = area A/(area A + area C) x 100%.

To examine their relative Fe^{2+} promoted reactivity, 10 μM of **ABA-FE**s was incubated with 10 and 100 eq of Fe^{2+} for 1 h followed by HPLC analysis (Figure 3.7). Theresults show that **ABA-FE**5 and **ABA-FE**25 are not reactive even with the high level of Fe^{2+}. Many **ABA-FE**s displayed high reactivity in the presence of the lower level of Fe^{2+}. However, **ABA-FE**16 to 21, and **ABA-FE**26 have much lower reactivity at the low Fe^{2+} concentrations but reactive at high Fe^{2+} level. Most **ABA-FE**s have low reactivity toward Fe^{3+} (Figure 3.8).

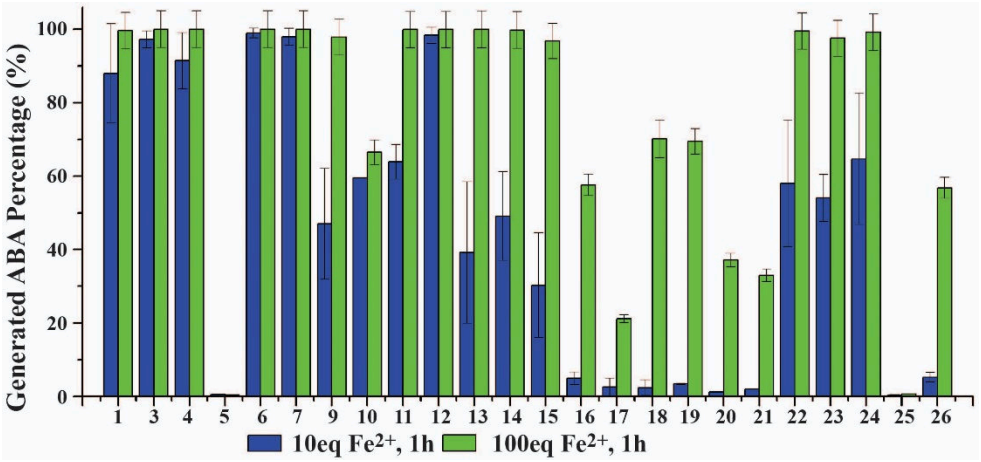

Figure 3.7 ABA-FEs (10 μM) treated with 10 eq and 100 eq Fe^{2+}, respectively, for 1 h and then quantified using HPLC analysis.

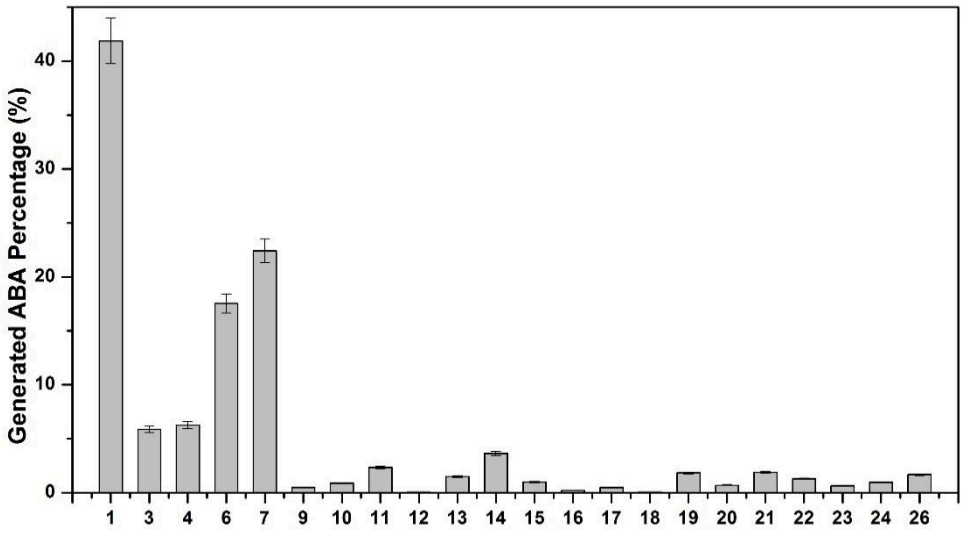

Figure 3.8 Reactivity of **ABA-FE**s towards Fe^{3+}**.** 10 μM **ABA-FE** was incubated with 100 μM Fe^{3+} in 50% HEPES/DMSO (10 mM HEPES, pH 7.4) for 1h at 37°C, followed by the HPLC analysis. The results were quantified by integrating the peak area corresponding to the **ABA** peak over the total areas of ABA peak and caged **ABA** peak to give the generated **ABA** percentage. The shown results were the average from 3 independent experiments. Error bars are SD (N=3).

Since **ABA-FE18** gave the most desired reactivity profile, we further tested its reactivity against various cellular molecules including metal ions (e.g., Cu^{2+}, Zn^{2+}, Mg^{2+}, Ca^{2+}, Na^{+}) and oxidizing or reducing species (e.g., H_2O_2, Na_2S, cysteine, ascorbate). The results show that **ABA-FE18** is selective and undergoes cleavage reaction to give **ABA** only in the presence of high concentrations of Fe^{2+} but not in the presence of the other tested molecules and ions (Figure 3.9).

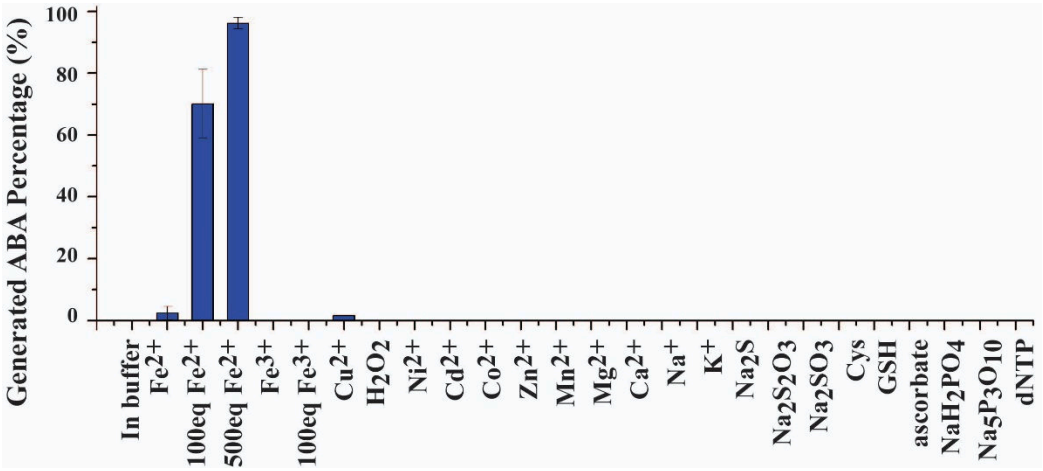

Figure 3.9 Stability test of **ABA-FE18** detecting with HPLC. **ABA-FE18** treated with indicated ions and molecules (10 eq for all unlabeled items) for 1 h and then quantified using HPLC analysis. The results were quantified by integrating the peak area corresponding to the **ABA** peak over the total areas of **ABA** peak and caged **ABA** peak to give the generated **ABA** percentage. The shown results were the average from 3 independent experiments. Error bars are SD (N=3). Error bars are SD (N = 3).

To further characterize **ABA-FE18**, the time course of **ABA-FE18** cleavage was tested by incubating it with 100 eq of Fe^{2+} for 5 min to 24 h. The cleavage of **ABA-FE18** occurred rapidly and was near completion at 1 h (Figure 3.10). In addition, the dosage response of **ABA-FE18** versus different concentrations of Fe^{2+} (1 to 500 equiv) was also studied. It required 100 eq or higher level of Fe^{2+} to achieve significant **ABA-FE18** cleavage, although less than 50 eq also gave low to moderate level of cleavage (Figure 3.11).

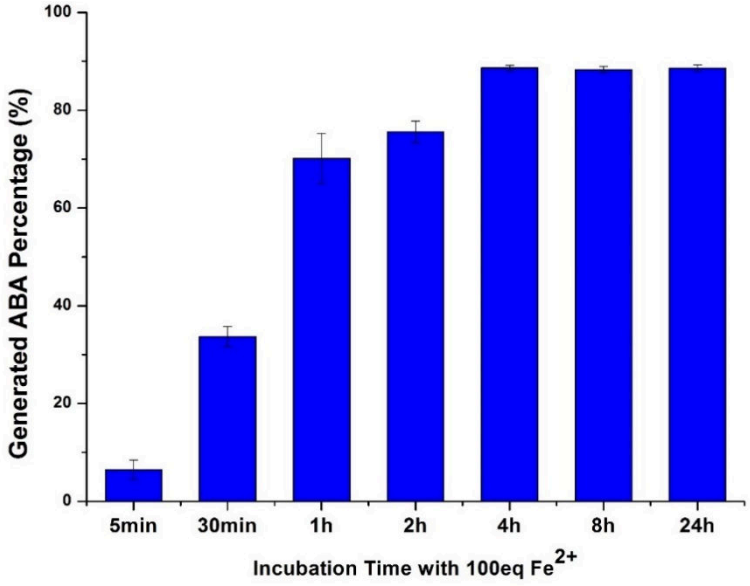

Figure 3.10 Time course of **ABA-FE18** cleavage by 100 eq of Fe^{2+}**.** 10 μM **ABA-FE18** was incubated with 100 eq of Fe^{2+} in 50% HEPES/DMSO (10mM HEPES, pH 7.4) for 5 min, 30 min, 1 h, 2 h, 4 h, 8 h and 24 h at 37˚C, followed by HPLC analysis. The results were quantified by integrating the peak area corresponding to the **ABA** peak over the total areas of **ABA** peak and caged **ABA** peak to give the generated **ABA** percentage. The shown results were the average from 3 independent experiments. Error bars are SD (N=3).

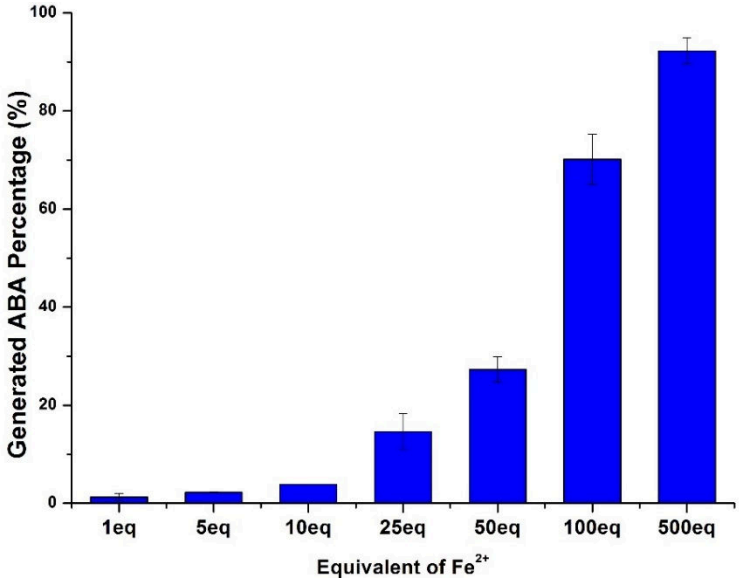

Figure 3.11 Dosage response of **ABA-FE18** versus different concentrations of Fe^{2+}**.** 10 μM **ABA-FE18** was incubated with 1 eq, 5 eq, 10 eq, 25 eq, 50 eq, 100 eq and 500 eq of Fe^{2+} in 50% HEPES/DMSO (10 mM HEPES, pH 7.4) for 1 h at 37˚C, followed by HPLC analysis. The results were quantified by integrating the peak area corresponding to the **ABA** peak over the total areas of **ABA** peak and caged **ABA** peak to give the generated **ABA** percentage. The shown results were the average from 3 independent experiments. Error bars are SD (N=3).

3.2.2.2 Screening of ABA-FEs in living cells

To determine the cellular stability and reactivity of **ABA-FE**s toward Fe^{2+} in cells, a HEK293T reporter cell line was used. This cell line contains **ABA**-response gene cassettes stably integrated in the genome that encode a split transcriptional activator (VP-PYL/GAL4DBD-ABI) and an inducible enhanced green fluorescent protein

(EGFP) with 5xUAS upstream (Figure 3.12).[15]

Figure 3.12 DNA constructs for **ABA**-inducible EGFP expression.

As a result, it produces EGFP in the presence of **ABA**. The cellular stability of **ABA-FE18** and other **ABA-FE**s was tested by incubating them (20 μM) with the reporter cells for 10 h. **ABA** and no drug treatment were used as positive and negative controls. The level of EGFP production, which indicates the degree of **ABA-FE** cleavage, was then determined using a fluorescence plate reader (Figure 3.13). Because the Fe^{2+} sensing units in **ABA-FE**s are linked to **ABA** through ester linkages, the endogenous cellular esterases can potentially affect the stability of **ABA-FE**s in cells. We expected that **ABA-FE**s containing bulky substituents close to the ester linkage (i.e., **ABA-FE**14−26) should have higher stability against esterases. Indeed, we observed several compounds in this group including **ABA-FE18** induced lower levels of EGFP expression (Figure 3.13). **ABA-EF**22−24 induced a much higher level of EGFP expression, which may be due to their higher sensitivity toward low levels of Fe^{2+} (Figure 3.7) or other molecules in cells.

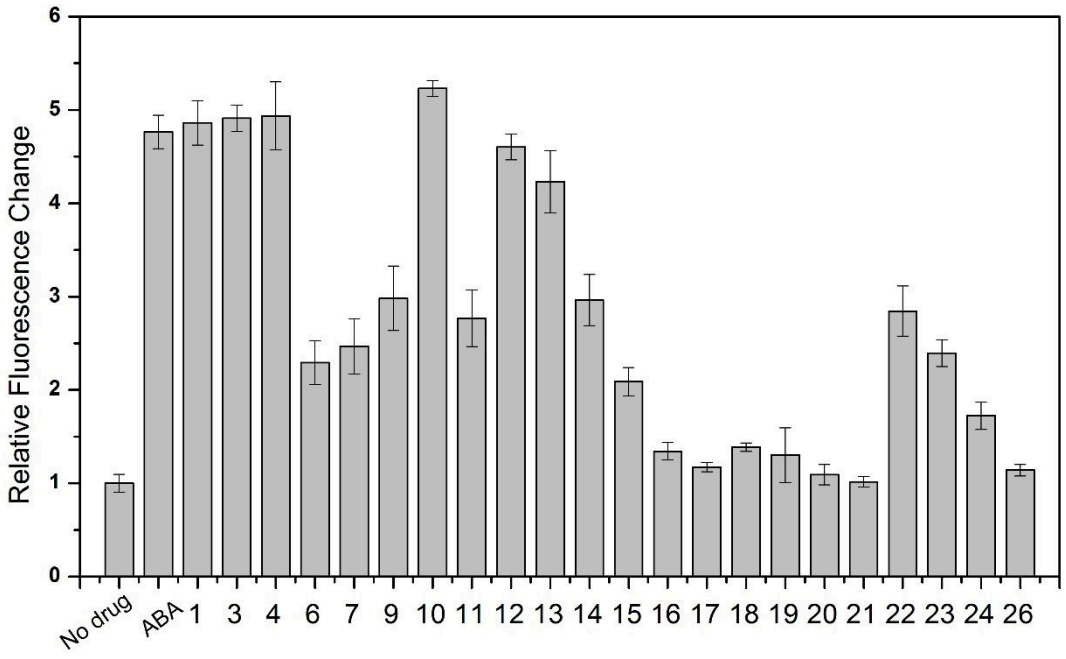

Figure 3.13 Cellular stability of **ABA-FEs.** 20 μM of **ABA-FE** (or with and without **ABA** as positive and negative controls) was incubated in the HEK293T EGFP reporter cell line for 10 h followed by the quantification of EGFP production using a fluorescence plate reader. The shown results were the average from 4 independent experiments. Error bars are SD (N = 4).

Considering its cellular stability, Fe^{2+}-responsive characteristics and selectivity for Fe^{2+}, **ABA-FE18** was subjected to further characterization. We incubated **ABA-FE18** with EGFP reporter cells for longer time periods (up to 24 h) and observed that it is relatively stable (Figure 3.14), although some low levels of EGFP expression had been observed that indicates further optimization will be needed for applications requiring long incubation times. To ensure the lack of EGFP expression in the above assay was due to the superior stability of **ABA-FE18** in cells instead of the complete degradation

of the compound, we also added 100 eq of Fe^{2+} in a separate experiment under the similar condition and showed that EGFP expression can be induced (Figure 3.14), which demonstrated that **ABA-FE18** was still functional to respond to Fe^{2+} and to generate **ABA**. We did not observe obvious cytotoxicity that can potentially be caused by the released Fe^{2+}-sensing unit.

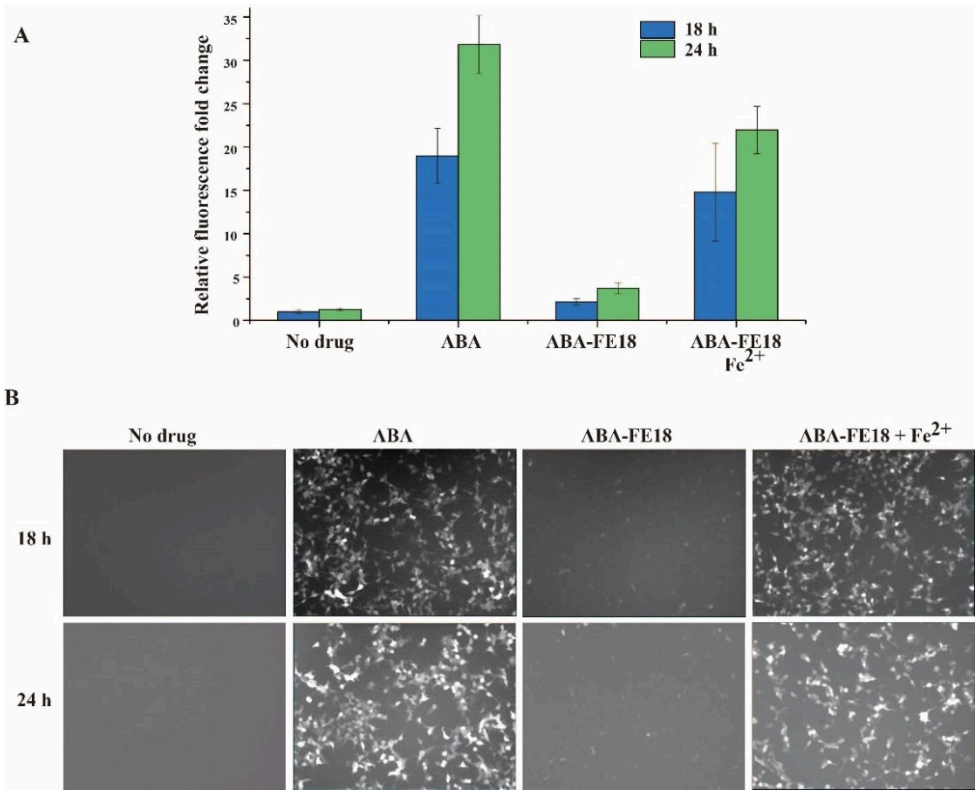

Figure 3.14 Cellular stability and reactivity of **ABA-FE18** over extended times. HEK293T EGFP reporter cells were treated with 20 μM **ABA**, **ABA-FE18**, or **ABA-FE18** plus 100 eq of Fe^{2+} for 18 and 24 h. (**A**) The production of EGFP was quantified using a fluorescence plate reader. The showed results were the average from 4

independent experiments. Error bars are SD (N = 4). (**B**) The representative image for each experimental condition.

To rule out the possibility that the uncaged byproduct of **ABA-FE18** can induce observed effects, we synthesized the Fe^{2+}-sensing unit released from **ABA-FE18** after cleavage and incubated it with EGFP reporter cells. We observed no EGFP expression was induced or obvious toxicity to cells (Figure 3.15).

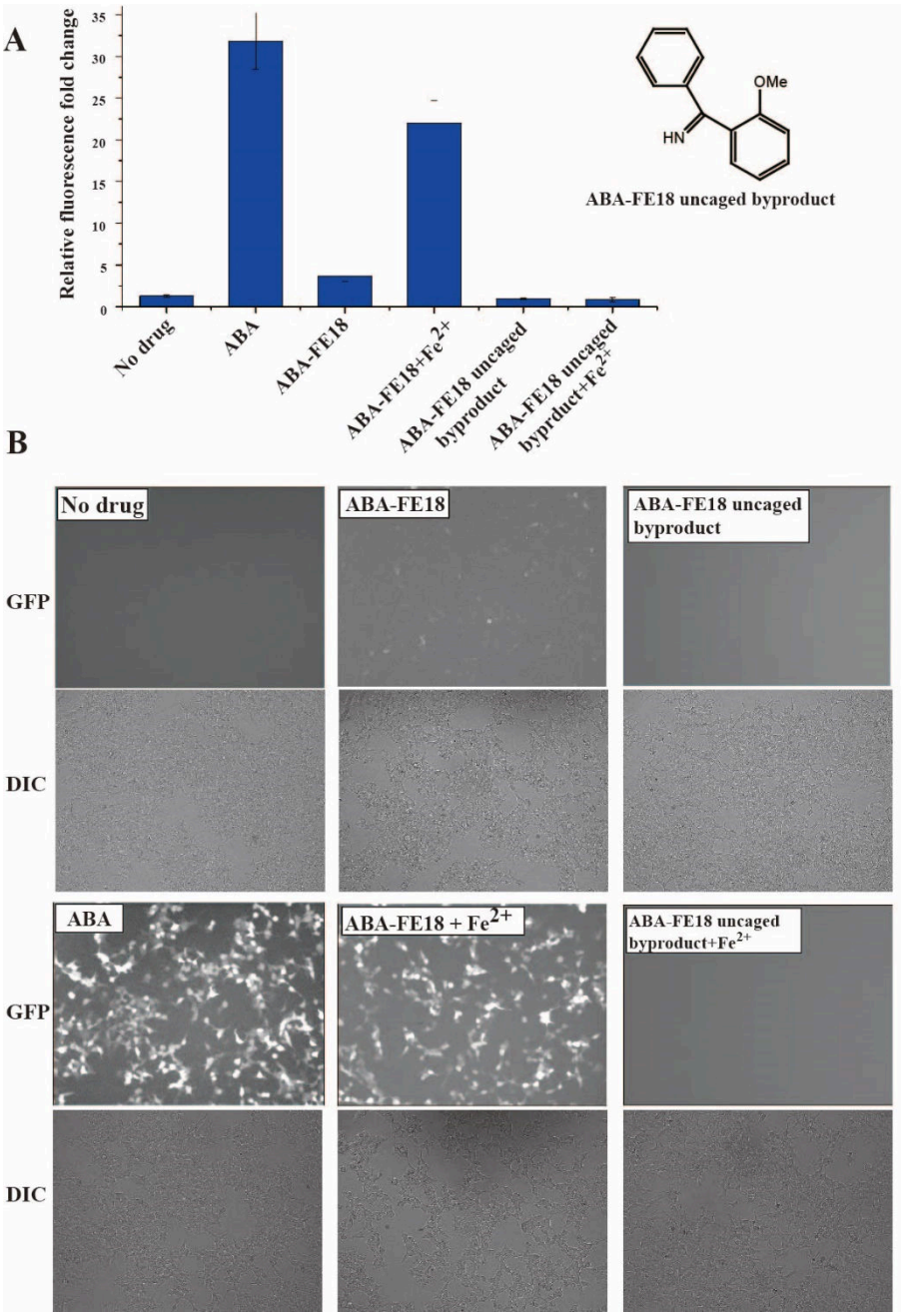

Figure 3.15 Testing effects of the uncaged byproduct from **ABA-FE18.** HEK293T EGFP reporter cells were treated with 20 μM **ABA**, **ABA-FE18** or the uncaged byproduct with or without 100 eq of Fe^{2+} for 24 h. (**A**) The production of EGFP was quantified using a fluorescence plate reader. The showed results were the average from

4 independent experiments. Error bars are SD (N = 4). (**B**) Representative images for each experimental condition.

3.3 Fe^{2+} induced biological processes in living cells

3.3.1 Fe^{2+} induced transcription activation in different living cells

The stability of **ABA-FE18** and its ability to connect Fe^{2+} to gene activation in mammalian cells were explored. For this purpose, HEK293T EGFP reporter cells, or cells (including HeLa, B35, and CHO cells) transfected with **ABA**-inducible EGFP reporter plasmids (Figure 3.12), were treated with 20 μM of **ABA-FE18** in the presence or absence of 100 eq of Fe^{2+} for 10 h. The induced EGFP expression was quantified in each condition using fluorescence plate reader and flow cytometer (Figure 3.16-3.18). **ABA-FE18** was found to be reasonably stable in all tested cell lines and it readily induced EGFP expression in response to the added high level of Fe^{2+}. On the basis of the combined observations described above, **ABA-FE18** was identified as the optimal **ABA-FE**-based Fe^{2+}- responding inducer.

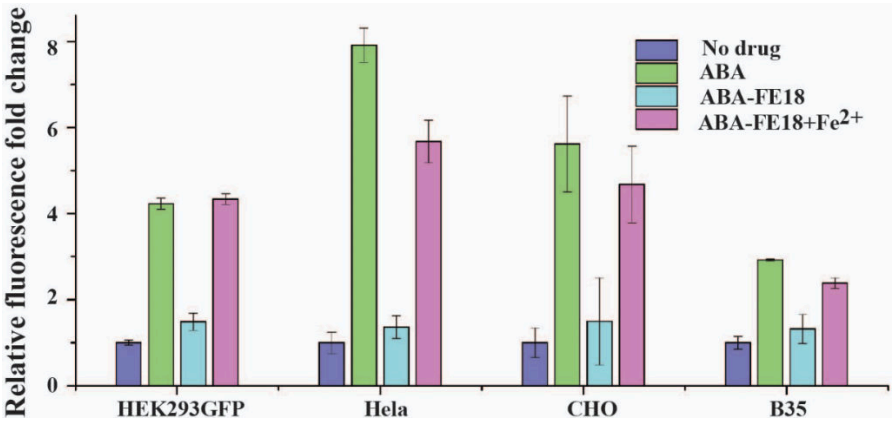

Figure 3.16 Induced EGFP expression by **ABA** or Fe^{2+} in different cell lines using micro plate reader. The fold changes are calculated based on "no drug" treatment samples.

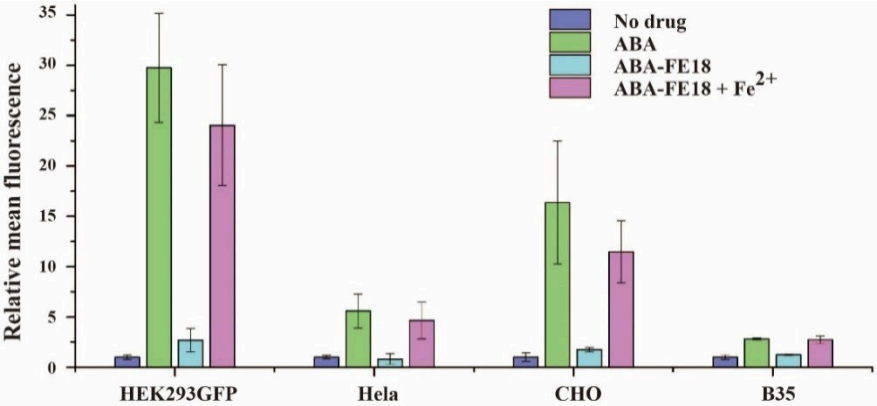

Figure 3.17 Induced EGFP expression by **ABA** or Fe^{2+} in different cell lines using flow cytometry. HEK293T EGFP reporter cells, and transfected CHO, HeLa and B35 cells were treated with 20 μM **ABA**, **ABA-FE18**, or **ABA-FE18** plus 100 eq of Fe^{2+}. After 10 h, cells were collected and analyzed by flow cytometry for EGFP expression. 10,000 cells were analyzed for each condition. Mean fluorescence intensity from analyzed cells under each condition was obtained and normalized to that of the non-treated cells. Error bars are SD (N = 3).

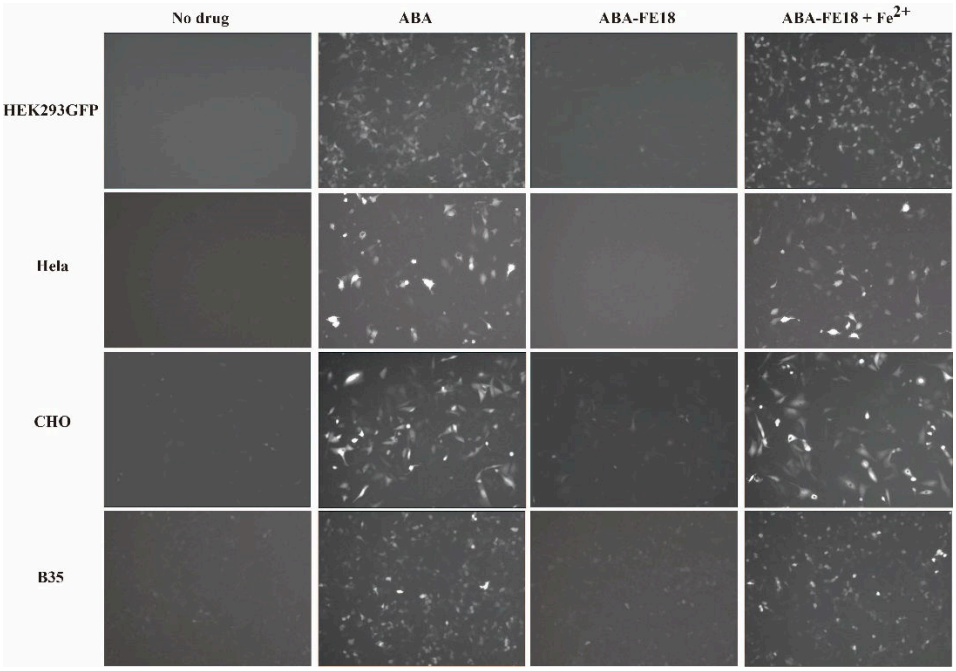

Figure 3.18 Representative images for each condition in **Figure 3.16 and 3.17.**

3.3.2 Fe^{2+} induced cytoskeletal remodeling in different living cells

In addition to directing an external Fe^{2+} signal to induce transcriptional activation, we wanted to explore whether artificial Fe^{2+} signaling can be constructed and integrated into an endogenous signaling circuit. For this purpose, we determined if Fe^{2+}-promoted release of **ABA** from **ABA-FE** can be used to induce cytoskeletal remodeling via activation of the Rac1 signaling pathway. Membrane translocation of Tiam1, a guanine exchange factor for Rac1, is sufficient to activate the Rac1 signaling pathway that leads to membrane ruffling.[30] CHO cells were transfected with DNA constructs (Figure 3.19) encoding membrane-localized ABI (myr-ABI) and cytoplasmic EGFP-PYL-fused Tiam1 (PYL-EGFP-Tiam1)[15] for 24 h. The cells were then treated either with 10 μM of

ABA, **ABA-FE18**, or **ABA-FE18** plus 100 eq of Fe^{2+} for 30 min. The membrane ruffling in all EGFP positive cells was then quantified through statistical analysis that quantified individual cell perimeters in each treated condition and compared them to that from cells transfected with EGFP-PYL (see Methods for details of analysis) using images taken by the fluorescence microscope. Obvious increases in ruffle formation were found to occur only when cells were treated with **ABA** or **ABA-FE18** plus 100 eq of Fe^{2+} (Figures 3.19 and 3.20).

Figure 3.19 DNA constructs for **ABA**-inducible Rac1 signaling/ruffle formation

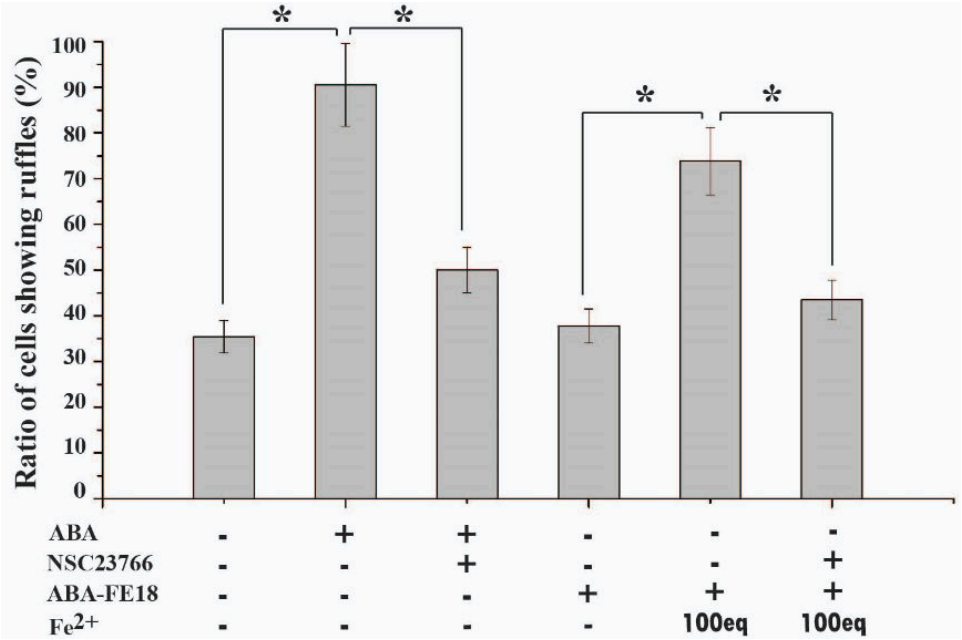

Figure 3.20 Ruffle formation of CHO cells. The ratio was calculated as described in the Methods section. Error bars are SD (SD = 4). *P value < 0.001

ABA-FE18 alone gave a similar background level of ruffling as the condition of no-drug treatment or cells transfected only with PYL-EGFP-Tiam1 (Figures 3.20 and 3.21). To confirm that ruffle formation is induced through activation of Rac1 signaling, transfected cells were pretreated for 1 h with 50 µM of NSC 23766, which is known to inhibit Rac1 signaling by blocking binding of Tiam1 to Rac1.[31] As expected, the presence of NSC 23766 led to a decrease in the percentage of ruffling in cells treated with **ABA** and **ABA-FE18** plus Fe^{2+} (Figure 3.20).

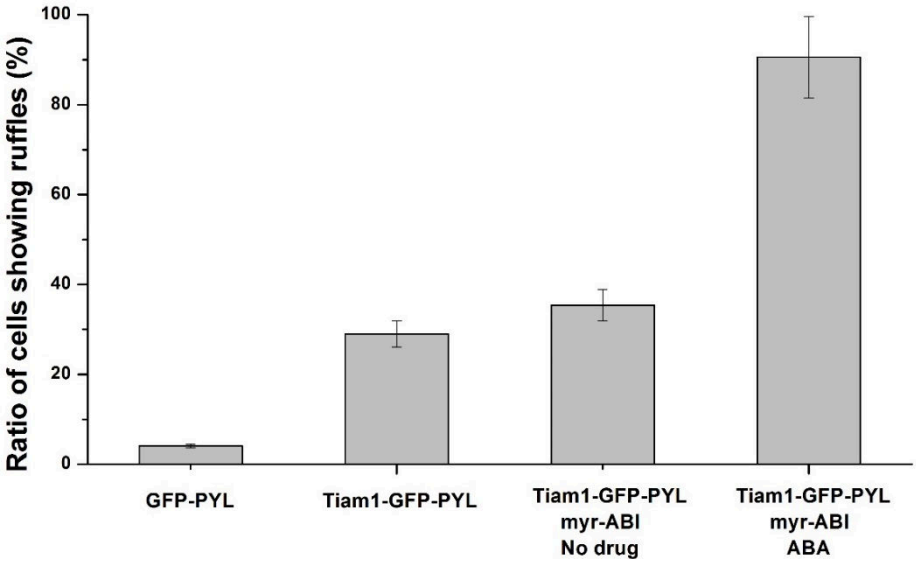

Figure 3.21 The ratio of cells showing ruffling in cells in negative and positive control conditions. CHO were seeded over glass coverslips in 24-well plates at 50,000/well for 24 h. Then cells were transfected with 0.3 µg EGFP-PYL only, or 0.3 µg PYL-EGFP-

Tiam1 only or 0.3 μg PYL-EGFP-Tiam1 and 0.3 μg myr-ABI DNA. After 24 h, cells were treated without addition, or with 10 μM **ABA**. Slides were prepared 30 min after adding **ABA** and images were then taken using a Zeiss fluorescence microscopy for statistical analysis.

3.4 Constructing of "AND" or "OR" Boolean logic to control the nuclear translocation of EGFP

To demonstrate that orthogonal signal-responsive caged CIP inducers can be incorporated to build artificial signaling networks, **ABA-FE18** and GA-HP[15] were used to construct two signaling networks that process different combinations of H_2O_2 and Fe^{2+} via "AND" or "OR" Boolean logic to control the nuclear translocation of EGFP. GA-HP is a H_2O_2-responsive caged compound containing gibberellic acid (**GA**),[15] which promotes the dimerization of GAI and GID1 fusion proteins.[32]

3.4.1 Constructing of "OR" Boolean logic to control the nuclear translocation of EGFP

To create an OR logic gate for protein translocation, DNA constructs encoding 4xNLS-ABI-GID1 and PYL-GAI-GFP fusion proteins (Figure 3.22) were made. In the presence of either **ABA** or GA, the EGFP fusion protein should be coupled to the nuclear localization signal (NLS) and lead to nuclear localization of EGFP (Figure 3.23).

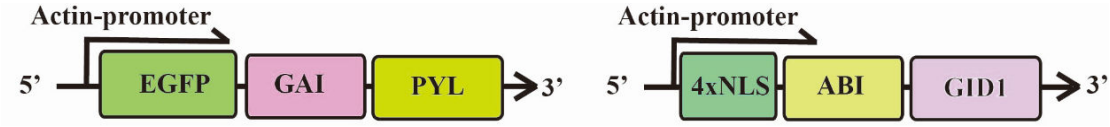

Figure 3.22 DNA constructs of OR logic gate for EGFP nuclear translocation.

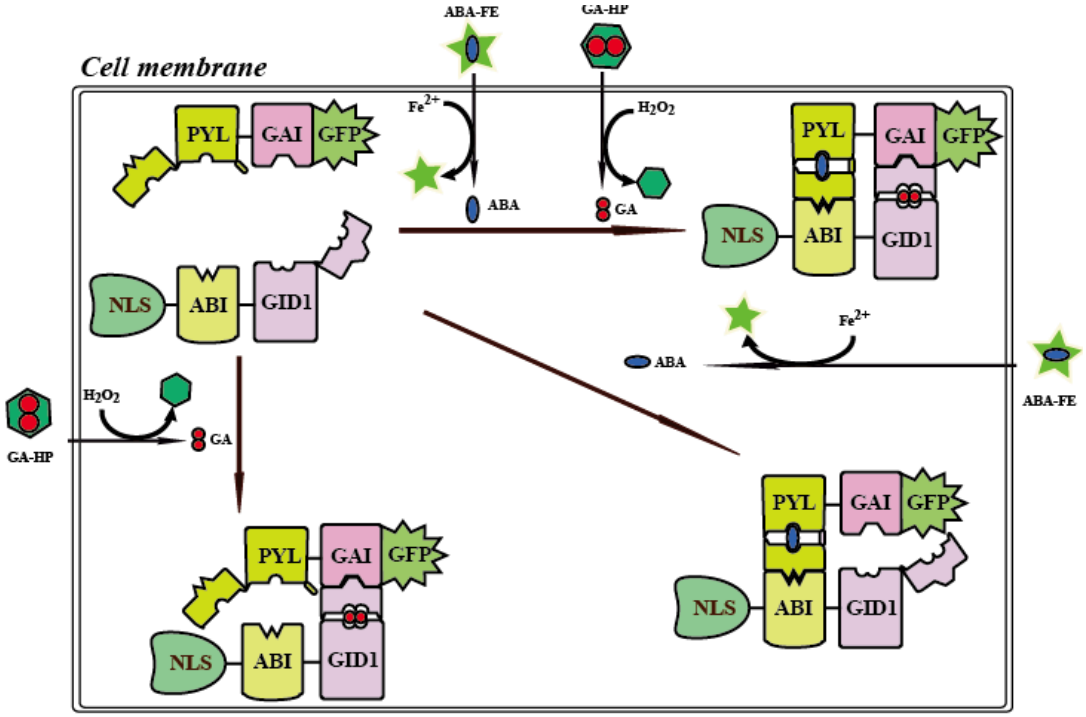

Figure 3.23 The design of the OR logical gate for EGFP nuclear translocation in response to stimuli.

To validate the OR logic gate, CHO cells were transfected with both plasmids for 24 h and then treated for 30 min with 20 μM **ABA**, 100 μM GA-AM (acetoxymethoxy ester of GA to facilitate cell permeability),[32] or both **ABA** and GA-AM. Nuclear localization of EGFP was then quantified through statistical analysis using images taken by the fluorescence microscope (Figure 3.24). The results show that, as designed, either

ABA or GA is sufficient to induce the EGFP translocation. To test if this logic gate system can be used to allow cells to respond to H_2O_2 and Fe^{2+}, the experiments were repeated using **ABA-FE18** and GAHP in the presence or absence of 100 μM H_2O_2 and/or 100 eq Fe^{2+}. As expected, the transfected cells responded to either or both H_2O_2 and Fe^{2+} to induce the translocation of EGFP. The cleavage of **ABA-FE18** by Fe^{2+} can occur both outside and inside the cells, and the generated **ABA** can freely diffuse across the cell membrane to induce effects. However, the observed effects induced by H_2O_2 should result from the cleavage of GA-HP in cells because free GA cannot pass the cell membrane.[32]

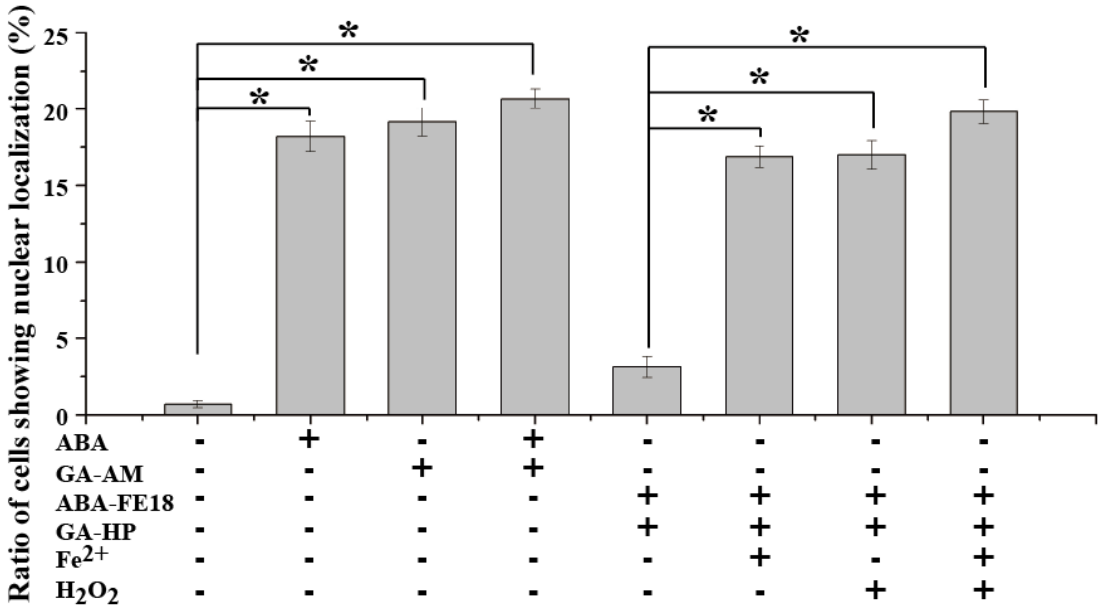

Figure 3.24 Ratio of transfected CHO cells (with plasmids in panel A) showing EGFP nuclear localization after treating with different inducing signals for 1 h. Error bars are SD (N = 4). *P-value < 0.001.

3.4.2 Constructing of "AND" Boolean logic to control the nuclear translocation of EGFP

To demonstrate that a different processing algorithm in response to detected signals can be engineered, we also created an AND logic gate for EGFP nuclear translocation using constructs encoding 4xNLS-GID1, GAI-ABI, and EGFP-PYL (Figures 3.25 and 3.26).

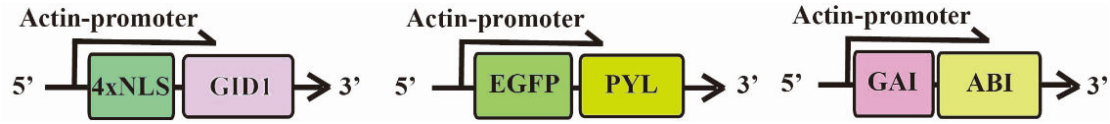

Figure 3.25 DNA constructs of AND logic gate for EGFP nuclear translocation.

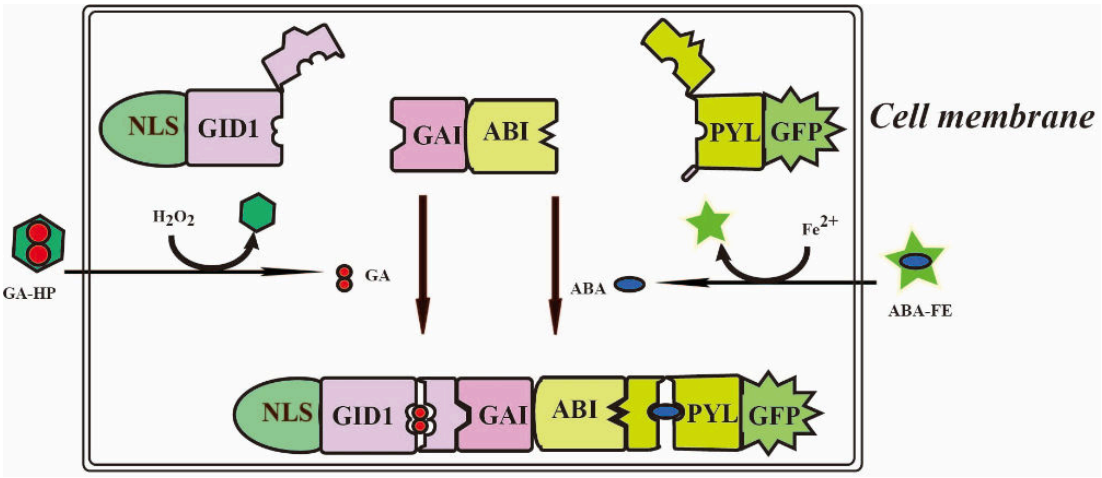

Figure 3.26 The design of the AND logical gate for EGFP nuclear translocation in response to stimuli.

Nuclear localization of EGFP was observed to take place in transfected CHO cells only when they were treated with both **ABA** and GA-AM (Figure 3.27). Similarly,

nuclear localization of EGFP in transfected cells that are treated with **ABA-FE18** and GA-HP occurred only when both Fe^{2+} and H_2O_2 were present. These observations demonstrate that the cells can be reprogrammed to respond to Fe^{2+} and/or H_2O_2 and produce different biological outputs following predefined signal processing rules.

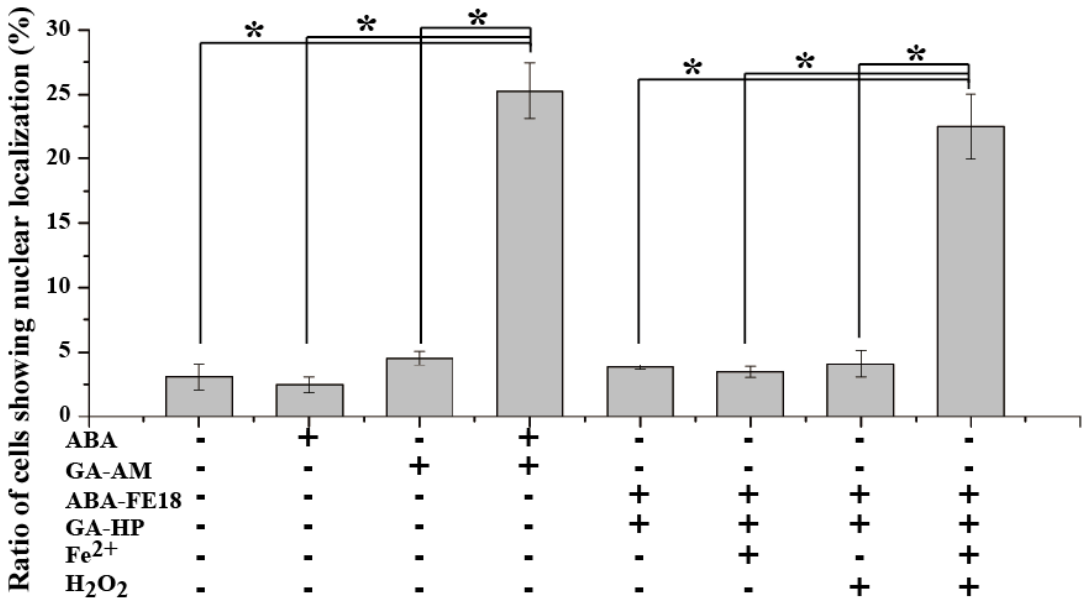

Figure 3.27 Percentage of transfected CHO cells (with plasmids in (A)) showing EGFP nuclear localization after being treated with different inducing signals for 1 h. Error bars are SD (N = 4). *P-value < 0.001.

3.5 Conclusion

In conclusion, in the investigation described above, we have developed Fe^{2+}-responsive **ABA** derivatives and identified **ABA-FE18** as an optimal Fe^{2+}-responsive inducer. We discovered that in general the oxime-based sensor units increased the stability of **ABA-FE**s against Fe^{2+} (e.g., **ABA-FE**19−21 vs 22−24) and electron-

withdrawing substituents decreased the reactivity toward Fe^{2+} within this group (e.g., **ABA-FE**17, 20, 21). We also demonstrated that adding bulky substituents near ester linkage can increase its stability in cells. Particularly, we identified oxime as a new, stable, and Fe^{2+} specific linkage (e.g., **ABA-FE18**). We believe that these observations can provide useful information for further optimization and future design of similar molecules. Our works present a unique strategy that specific sensor units can be integrated into orthogonal CIP inducers to build custom signaling pathways and logic gates responding to physiologically relevant signal cues. This new strategy should provide alternative approaches to engineer cellular signaling and responses in mammalian cells.

3.6 Materials and Methods

3.6.1 Primers

5’ GAI ATG SalI

CCGACAGTCGACGCCACCATGAAGAGAGATCATCATCATCAT

3’ GAI GS linker MluI

CCGACAACGCGTACCTGATCCACCTCCACCAGATCCAGGATTAAGGTCGGT GAGCA

5’ ABI MluI

CCGACAACGCGTGTGCCTTTGTATGGTTTTACT

3’ ABI MluI

CCGACAACGCGTCTTATCGTCATCGTCCTTGTA

5’ GAI GSGGGGSG AscI

CCGACAGGCGCGCCAGGATCTGGTGGAGGTGGATCAGGTAAGAGAGATCA
TCATCATCAT

3’ GAI GGSGGGAGGGGSGGGAGG AscI

CCGACAGGCGCGCCACCGCCAGCGCCTCCTCCGCTACCACCCCCTCCTGCC
CCCCCGCCGGATCCTCCAGGATTAAGGTCGGTGAGCAT

3.6.2 Chemical synthesis

General Information: All reactions were carried out in dried flasks. The reactions were monitored by TLC for completion. Commercially available reagents were used as received without further purification unless otherwise specified. Merck 60 silica gel was used for column chromatography, and Whatman silica gel plates with fluorescence F254 were used for thin-layer chromatography (TLC) analysis. ^{1}H and ^{13}C NMR spectra were recorded on Bruker Avance 300. Data for ^{1}H NMR are reported as follows:

chemical shift (ppm), and multiplicity (s = singlet, d = doublet, t = triplet, q = quartet, dd = double doublet, ddd = double double doublet, td = triple doublet, dt = double triplet, m = multiplet, bs = broad signal). Data for ^{13}C NMR are reported as ppm.

3.6.2.1 Synthesis of ABA-FE1-8

Substrates **1b-8b** were prepared according to literature procedure. To an ice cold solution of substitute nitrobenzenes **1a-8a** (8.00 mmol) in 95% ethanol (50 mL) was added zinc powder (12.0 mmol). Acetic acid (24 mmol) was then added dropwise and the reaction stirred for 2 h. The reaction was filtered to remove the zinc, avoiding over reduction to the amine. The ethanol was removed under reduced pressure, and the crude material was dissolved in methylene chloride, and directly absorbed onto silica gel by reduced pressure removal of the solvent. Flash column chromatography (ethyl acetate in hexanes as eluent) produced pure product.

Preparation of **ABA-FE1-8**: Compound **1b-8b** (0.01 mmol), EDCI (0.022 g, 0.12 mmol), **ABA** (0.026 g, 0.01 mmol) were suspended in DCM (15 mL) and stirred at room temperature for 18 h. The mixture was washed with H_2O and brine, dried over Na_2SO_4, and concentrated in vacuo. The residue was subjected to silica gel chromatography to afford the compounds **ABA-FE1-8**.

3.6.2.2 Synthesis of ABA-FE9-15, 22-26

The synthesis of the target compounds **ABA-FE9-15, 22-26** was accomplished in a convergent manner as shown in Schemes 1. Commercially available substituted acetophenones **9a-15a**, **22a-26a** were the starting materials for the synthesis of **ABA-FE9-15, 22-26**, respectively. Compounds **9a-15a**, **22a-26a** were each treated with hydroxylamine hydrochloride to give the corresponding oxime intermediates **9b-15b**, **22b-26b**, which was then *reduced* by $NaBH_3CN$ to afford **9c-15c**, **22c-26c** with hydroxylamine group. Finally, these hydroxylamines **9c-15c**, **22c-26c** coupled with **ABA** to afford the target compounds **ABA-FE9-15**, **22-26**.

Substrates **9b-15b**, **22b-26b** were prepared according to literature procedure.[33] A solution of phenome **9a-15a**, **22a-26a** (0.90 mmol), sodium acetate (0.90mol) and hydroxylamine hydrochloride (5.4 mmol) in hydrous ethanol (20 mL) was refluxed for 4-24 h at 80°C. The reaction mixture was allowed to cool to room temperature and evaporated to dryness in vacuo, and the residue was partitioned between water (10 mL) and CH_2Cl_2 (10 mL). The organic extract was washed with water (2-10 mL), and the aqueous layer was extracted with CH_2Cl_2 (2-10 mL). The combined organic extracts dried over anhydrous sodium sulfate and evaporated in vacuo gave the corresponding oximes **9b-15b**, **22b-26b** (85-97%).

Substrates **9c-15c, 22c-26c** were prepared according to literature procedure.[34] A solution of **9b-15b**, **22b-26b** (200 μmol, 1.0 equiv) in MeOH (10 mL) was treated with $NaBH_3CN$ (13.7 mg, 200 μmol, 1.0 equiv) and methyl orange (< 1 mg). The reaction

mixture was then kept at pH 3–4 by dropwise addition of aqueous HCl (1 N). After 2 h the reaction was basified to pH 10 (1 N NaOH), solid NaCl was added and the resulting mixture was extracted thrice with CH_2Cl_2 (20 mL). The combined organic layers were dried over Na_2SO_4 and concentrated to give a cude oil, which was purified by flash chromatography (hexanes/EtOAc 1:1) to give **9c-15c**, **22c-26c** (70-89%) as a colorless solid.

Preparation of **ABA-FE9-15**, **22-26**: Compound **9c-15c, 22c-26c** (0.01 mmol), EDCI (0.022 g, 0.12 mmol), **ABA** (0.026 g, 0.01 mmol) were suspended in DCM (15 mL) and stirred at room temperature for 18 h. The mixture was washed with H_2O and brine, dried over Na_2SO_4, and concentrated in vacuo. The residue was subjected to silica gel chromatography to afford the compounds **ABA-FE9-15**, **22-26**.

3.6.2.3 Synthesis of ABA-FE16-21

Preparation of **ABA-FE16-21**: Compound **16b-21b** (0.01 mmol), EDCI (0.022 g, 0.12 mmol), **ABA** (0.026 g, 0.01 mmol) were suspended in DCM (15 mL) and stirred at room temperature for 4 h. The mixture was washed with H_2O and brine, dried over Na_2SO_4, and concentrated in vacuo. The residue was subjected to silica gel chromatography to afford the compounds **ABA-FE16-21**.

3.6.2.4 NMR and mass data of ABA-FE1-26

(S)-4-hydroxy-3,5,5-trimethyl-4-((1E,3Z)-3-methyl-5-(3-nitrophenylaminooxy)-5-oxopenta-1,3-dienyl) cyclohex-2-enone (**ABA-FE1**)

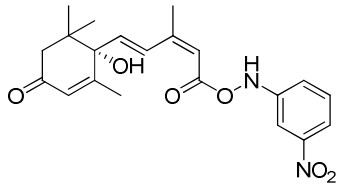

The title compound was obtained in 68% yield as yellow solid. ^{1}H NMR (300 MHz, $CDCl_3$) δ (ppm): 8.97 (s, 1H), 7.75-7.81 (m, 2H), 7.35-7.41 (m, 1H), 7.20-7.14 (m, 1H), 6.18 (d, J = 16.5 Hz, 1H), 5.84-5.87 (m, 2H), 2.23-2.45 (m, 2H), 2.05 (s, 3H), 1.97 (s, 1H), 1.83(s, 3H), 1.03(s, 3H), 0.94(s, 3H). TOF-HRMS (m/z) found (calcd.) for $C_{21}H_{24}N_2O_6$ (M): $[M+H]^+$, 401.1715 (401.1713); $[M+Na]^+$, 423.1511 (423.1532) and $[M+K]^+$, 439.1275 (439.1271).

(S)-4-hydroxy-3,5,5-trimethyl-4-((1E,3Z)-3-methyl-5-(2-nitrophenylaminooxy)-5-oxopenta-1,3-dienyl)cyclohex-2-enone (**ABA-FE2**)

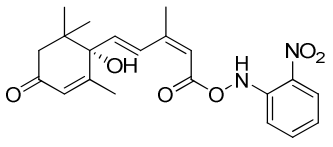

The title compound was obtained in 71% yield as yellow solid. ^{1}H NMR (300 MHz, $CDCl_3$) δ (ppm): 10.92 (s, 1H), 7.92(d, J = 15.9 Hz, 1H), 7.73 (dd, J = 1.2 Hz, 8.4 Hz, 1H), 7.55-7.60 (m, 1H), 7.30-7.33 (m, 1H), 7.01-7.06(m, 1H), 6.26 (d, J = 15.6

Hz, 1H), 5.93 (s, 2H), 2.27-2.50 (m, 2H), 2.08 (s, 3H), 2.04 (s, 1H), 1.90(s, 3H), 1.10(s, 3H), 1.00(s, 3H). TOF-HRMS (m/z) found (calcd.) for $C_{21}H_{24}N_2O_6$ (M): $[M+H]^+$, 401.1532 (401.1713); $[M+Na]^+$, 423.1537 (423.1532).

4-((2Z,4E)-5-((S)-1-hydroxy-2,6,6-trimethyl-4-oxocyclohex-2-enyl)-3-methylpenta-2,4-dienoyloxyamino)benzonitrile (**ABA-FE3**)

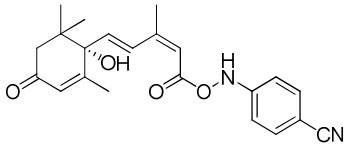

The title compound was obtained in 65% yield as white solid. ^{1}H NMR (300 MHz, $CDCl_3$) δ (ppm): 8.97 (s, 1H), 7.91(d, *J* = 15.9 Hz, 1H), 7.58 (d, *J* = 8.7 Hz, 2H), 7.05 (d, *J* = 8.7 Hz, 2H), 6.23 (d, *J* = 15.9 Hz, 1H), 5.87-5.94 (m, 2H), 2.26-2.49 (m, 3H), 2.10 (s, 3H), 1.89 (s, 3H), 1.10 (s, 3H), 1.01 (s, 3H). TOF-HRMS (m/z) found (calcd.) for $C_{22}H_{24}N_2O_4$ (M): $[M+H]^+$, 381.1826 (381.1814); $[M+Na]^+$, 403.1645 (403.1634) and $[M+K]^+$, 419.1390 (419.1373).

(S)-4-((1E,3Z)-5-(4-acetylphenylaminooxy)-3-methyl-5-oxopenta-1,3-dienyl)-4-hydroxy-3,5,5-trimethylcyclohex-2-enone (**ABA-FE4**)

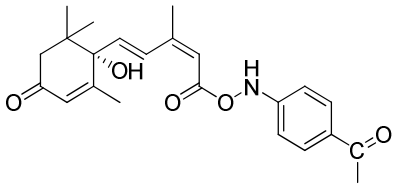

The title compound was obtained in 66% yield as white solid. ^{1}H NMR (300 MHz, $CDCl_3$) δ (ppm): 8.99 (s, 1H), 7.80-7.91(m, 3H), 7.03 (d, *J* = 8.7 Hz, 2H), 7.05 (d, *J* = 8.7 Hz, 2H), 6.22 (d, *J* = 15.9 Hz, 1H), 5.88-5.93 (m, 2H), 2.54 (s, 3H), 2.26-2.49 (m, 2H), 2.09 (s, 3H), 2.03 (s, 1H), 1.89 (s, 3H), 1.09 (s, 3H), 1.00 (s, 3H). TOF-HRMS (m/z) found (calcd.) for $C_{23}H_{27}NO_5$ (M): $[M+H]^+$, 398.1973 (398.1967); $[M+Na]^+$, 420.1778 (420.1787) and $[M+K]^+$, 436.1521 (436.1526).

(S)-4-hydroxy-4-((1E,3Z)-5-(2-iodophenylaminooxy)-3-methyl-5-oxopenta-1,3-dienyl)-3,5,5-trimethylcyclohex-2-enone (**ABA-FE5**)

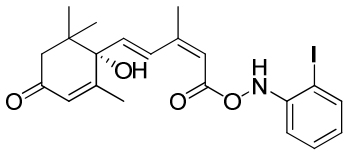

The title compound was obtained in 71% yield as white solid. ^{1}H NMR (300 MHz, $CDCl_3$) δ (ppm): 8.88 (s, 1H), 8.22 (dd, *J* = 1.2 Hz, 8.4 Hz, 1H), 7.86(d, *J* = 16.2 Hz, 1H), 7.26-7.32 (m, 1H), 7.06-7.09 (m, 1H), 6.74-6.79(m, 1H), 6.27 (d, *J* = 15.6 Hz, 1H), 5.88-5.93 (m, 2H), 2.33-2.45 (m, 2H), 2.08 (s, 3H), 2.03 (s, 1H), 1.90(s, 3H), 1.10(s, 3H), 1.00(s, 3H). TOF-HRMS (m/z) found (calcd.) for $C_{22}H_{27}NO_4$ (M): $[M+H]^+$,

370.2010 (370.2018); $[M+Na]^+$, 392.1830 (392.1838) and $[M+K]^+$, 408.1577 (408.1577).

(S)-4-((1E,3Z)-5-(((2-chlorophenyl)amino)oxy)-3-methyl-5-oxopenta-1,3-dien-1-yl)-4-hydroxy-3,5,5-trimethylcyclohex-2-enone (**ABA-FE6**)

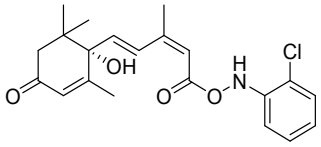

The title compound was obtained in 63% yield as yellow solid. ^{1}H NMR (300 MHz, $CDCl_3$) δ (ppm): 9.08 (s, 1H), 7.86-7.92 (m, 1H), 7.47-7.50 (m, 1H), 7.24-7.29 (m, 1H), 7.12-7.16(m, 1H), 6.88-6.93(m, 1H), 6.22 (d, *J* = 16.0 Hz, 1H), 5.93 (s, 1H), 5.88 (s, 1H), 2.27-2.50 (m, 2H), 2.08 (s, 3H), 2.04 (s, 1H), 1.90(s, 3H), 1.10(s, 3H), 1.00(s, 3H). TOF-HRMS (m/z) found (calcd.) for $C_{21}H_{24}ClNO_4$ (M): $[M+H]^+$, 390.1474 (390.172) and $[M+K]^+$, 428.1028 (428.1031).

(S)-4-((1E,3Z)-5-(((2-bromophenyl)amino)oxy)-3-methyl-5-oxopenta-1,3-dien-1-yl)-4-hydroxy-3,5,5-trimethylcyclohex-2-enone (**ABA-FE7**)

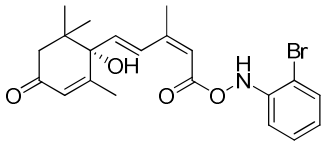

The title compound was obtained in 63% yield as yellow solid. ^{1}H NMR (300 MHz, $CDCl_3$) δ (ppm): 9.08 (s, 1H), 7.86-7.92 (m, 1H), 7.47-7.50 (m, 1H), 7.24-7.29 (m, 1H), 7.12-7.16(m, 1H), 6.88-6.93(m, 1H), 6.22 (d, *J* = 16.0 Hz, 1H), 5.93 (s, 1H), 5.88 (s, 1H), 2.27-2.50 (m, 2H), 2.08 (s, 3H), 2.04 (s, 1H), 1.90(s, 3H), 1.10(s, 3H), 1.00(s, 3H). TOF-HRMS (m/z) found (calcd.) for $C_{21}H_{24}BrNO_4$ (M): $[M+H]^+$, 434.0977 (434.0967); [M+Na]+, 456.0790 (456.0786) and [M+K]+, 472.0541 (472.0526).

(S)-4-hydroxy-3,5,5-trimethyl-4-((1E,3Z)-3-methyl-5-oxo-5-(o-tolylaminooxy) penta-1,3-dienyl) cyclohex-2-enone (**ABA-FE8**)

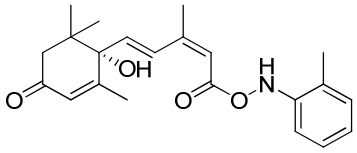

The title compound was obtained in 72% yield as white solid. ^{1}H NMR (300 MHz, $CDCl_3$) δ (ppm): 7.98(d, *J* = 15.9 Hz, 1H), 6.54-6.96 (m, 4H), 6.22 (d, *J* = 15.9 Hz, 1H), 5.90(s, 1H), 6.04 (s, 1H), 2.20-2.50(m, 4H), 2.03-2.12 (m, 5H), 1.89 (s, 3H), 1.10 (s, 3H), 1.00 (s, 3H). TOF-HRMS (m/z) found (calcd.) for $C_{21}H_{24}INO_4$ (M): $[M+H]^+$,

482.0817 (482.0828); $[M+Na]^+$, 504.0635 (504.0648) and $[M+K]^+$, 520.0383 (520.0387).

(4S)-4-hydroxy-3,5,5-trimethyl-4-((1E,3Z)-3-methyl-5-oxo-5-(1-phenylethylaminooxy) penta-1,3-dienyl) cyclohex-2-enone (**ABA-FE9**)

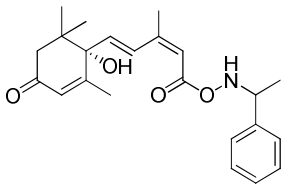

The title compound was obtained in 83% yield as white solid. ^{1}H NMR (300 MHz, $CDCl_3$) δ (ppm) 7.76-7.81 (m, 1H), 7.71 (s, 1H), 7.28-7.39 (m, 5H), 6.18 (d, J = 16.0 Hz, 1H), 5.93 (s, 1H), 5.67 (s, 1H), 4.13 (t, J = 7.2 Hz, 1H), 2.26-2.49 (m, 2H), 2.13 (s, 1H), 2.03(s, 3H), 1.90(s, 3H), 1.43(d, J = 6.0 Hz, 3H), 1.28(s, 3H), 1.23(s, 3H). TOF-HRMS (m/z) found (calcd.) for $C_{23}H_{29}NO_4$ (M): $[M+H]^+$, 384.2160 (384.2175); $[M+Na]^+$, 406.1985 (406.1994) and $[M+K]^+$, 422.1725 (422.1734).

(4S)-4-((1E,3Z)-5-(1-(4-bromophenyl)ethylaminooxy)-3-methyl-5-oxopenta-1,3-dienyl)-4-hydroxy-3,5,5-trimethylcyclohex-2-enone (**ABA-FE10**)

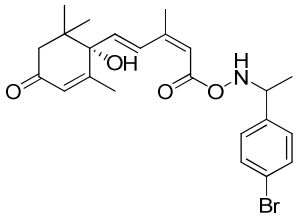

The title compound was obtained in 76% yield as yellow solid. ^{1}H NMR (300 MHz, $CDCl_3$) δ (ppm): 7.78-7.83 (m, 1H), 7.70 (s, 1H), 7.46-7.49 (m, 2H), 7.26-7.28 (m, 2H), 6.15 (d, J = 16.0 Hz, 1H), 5.95 (s, 1H), 5.66 (s, 1H), 4.14 (t, J = 7.2 Hz, 1H), 2.27-2.51 (m, 2H), 2.05 (s, 1H), 1.99(s, 3H), 1.91(t, J = 1.2 Hz, 3H), 1.43(d, J = 6.0 Hz, 3H), 1.12(s, 3H), 1.10(s, 3H). ^{13}C NMR (75.5 MHz, $CDCl_3$) δ (ppm): 197.4, 165.9, 161.9, 150.6, 140.5, 136.9, 131.4, 128.5, 127.7, 126.9, 121.3, 115.0, 79.4, 59.9, 49.5, 41.3, 24.1, 22.8, 21.0, 19.6, 18.7. TOF-HRMS (m/z) found (calcd.) for $C_{23}H_{28}BrNO_4$ (M): $[M+H]^+$, 462.1288 (462.1280); $[M+Na]^+$, 484.1101 (484.1099) and $[M+K]^+$, 500.0842 (500.0839).

(4S)-4-hydroxy-4-((1E,3Z)-5-(((1-(4-methoxyphenyl)ethyl)amino)oxy)-3-methyl-5-oxopenta-1,3-dien-1-yl)-3,5,5-trimethylcyclohex-2-enone (**ABA-FE11**)

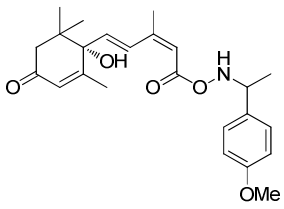

The title compound was obtained in 73% yield as white solid. ^{1}H NMR (300 MHz,

$CDCl_3$) δ (ppm): 7.79 (m, 1H), 7.70 (s, 1H), 7.27-7.29 (m, 2H), 6.88-6.92 (m, 2H), 6.15 (d, *J* = 16.0 Hz, 1H), 5.94 (s, 1H), 5.65 (s, 1H), 4.12 (d, *J* = 6.6 Hz, 1H), 2.27-2.51 (m, 2H), 2.03 (s, 1H), 1.99(s, 3H), 1.90(t, *J* = 1.2 Hz, 3H), 1.43(s, 3H), 1.12(s, 3H), 1.10(s, 3H). TOF-HRMS (m/z) found (calcd.) for $C_{24}H_{31}NO_5$ (M): $[M+H]^+$, 414.2278 (414.2280); $[M+Na]^+$, 436.2097 (436.2100) and $[M+K]^+$, 452.1848 (452.1839).

(4S)-4-((1E,3Z)-5-(((1-(2-chlorophenyl)ethyl)amino)oxy)-3-methyl-5-oxopenta-1,3-dien-1-yl)-4-hydroxy-3,5,5-trimethylcyclohex-2-enone (**ABA-FE12**)

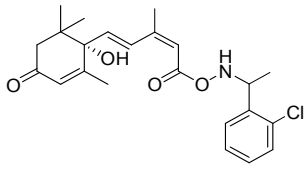

The title compound was obtained in 78% yield as yellow solid. ^1H NMR (300 MHz, $CDCl_3$) δ (ppm): 7.82 (s, 1H), 7.78 (s, 1H), 7.60-7.63 (m, 1H), 7.28-7.36 (m, 3H), 7.17-7.23(m, 1H), 6.13 (d, *J* = 16.0 Hz, 1H), 5.93 (s, 1H), 5.65 (s, 1H), 4.63 (s, 1H), 2.26-2.49 (m, 2H), 1.98(d, *J* = 1.2 Hz, 3H), 1.90(d, *J* = 1.2 Hz, 3H), 1.43(d, *J* = 6.0 Hz, 3H), 1.10(s, 3H), 0.99(s, 3H). TOF-HRMS (m/z) found (calcd.) for $C_{23}H_{28}ClNO_4$ (M): $[M+H]^+$, 418.1781 (418.1785); $[M+Na]^+$, 440.1593 (440.1605) and $[M+K]^+$, 456.1325 (456.1344).

(4S)-4-hydroxy-3,5,5-trimethyl-4-((1E,3Z)-3-methyl-5-(1-(naphthalen-1-yl)ethylaminooxy)-5-oxopenta-1,3-dienyl)cyclohex-2-enone (**ABA-FE13**)

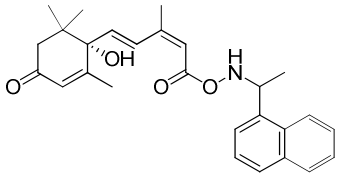

The title compound was obtained in 76% yield as white solid. ^{1}H NMR (300 MHz, $CDCl_3$) δ (ppm) 7.77-7.87 (m, 6H), 7.47-7.56 (m, 3H), 6.18 (d, *J* = 16.2 Hz, 1H), 5.94 (s, 1H), 5.67 (s, 1H), 4.38 (s, 1H), 2.27-2.50 (m, 2H), 2.06 (s, 1H), 1.98 (s, 3H), 1.88-1.90 (m, 6H), 1.53 (d, *J* = 6.6 Hz, 3H), 1.10 (s, 3H), 0.99 (d, *J* = 6.6 Hz, 3H). ^{13}C NMR (75.5 MHz, $CDCl_3$) δ (ppm): 197.4, 166.0, 162.0, 150.3, 138.9, 138.8, 136.7, 133.1, 132.8, 128.1, 127.7, 127.5, 126.9, 115.3, 79.4, 60.6, 53.2, 49.5, 41.3, 24.1, 22.8, 21.0, 19.9, 18.7. TOF-HRMS (m/z) found (calcd.) for $C_{27}H_{31}NO_4$ (M): $[M+H]^+$, 434.2333 (434.2331); $[M+Na]^+$, 456.2156 (456.2151) and $[M+K]^+$, 472.1885 (472.1890).

(4S)-4-hydroxy-3,5,5-trimethyl-4-((1E,3Z)-3-methyl-5-oxo-5-(1-phenylbutylaminooxy)penta-1,3-dienyl)cyclohex-2-enone (**ABA-FE14**)

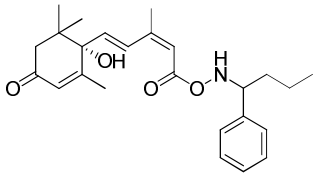

The title compound was obtained in 65% yield as white solid. ^{1}H NMR (300 MHz, $CDCl_3$) δ (ppm) 7.79 (s, 1H), 7.74 (s, 1H), 7.26-7.33 (m, 7H), 6.17 (d, *J* = 16.2 Hz, 1H), 5.92 (s, 1H), 5.63 (s, 1H), 3.96 (m, 1H), 2.25-2.48 (m, 2H), 2.03 (s, 1H), 1.97(s, 3H), 1.89(t, *J* = 1.2 Hz, 3H), 1.19-1.29(m, 4H), 1.09(s, 3H), 0.98(s, 3H), 0.85-0.90(m, 3H). ^{13}C NMR (75.5 MHz, $CDCl_3$) δ (ppm): 197.6, 166.0, 162.2, 150.2, 140.4, 136.8, 128.2, 127.7, 127.5, 127.3, 126.8, 115.3, 79.4, 66.8, 66.5, 49.5, 41.3, 35.8, 35.3, 24.1, 22.9, 21.0, 19.6, 18.7, 13.8. TOF-HRMS (m/z) found (calcd.) for $C_{25}H_{33}NO_4$ (M): $[M+H]^+$, 412.2494 (412.2488); $[M+Na]^+$, 434.2316 (434.2307) and $[M+K]^+$, 450.2051 (450.2047).

(4S)-4-((1E,3Z)-5-(((1,2-diphenylethyl)amino)oxy)-3-methyl-5-oxopenta-1,3-dien-1-yl)-4-hydroxy-3,5,5-trimethylcyclohex-2-enone. (**ABA-FE15**)

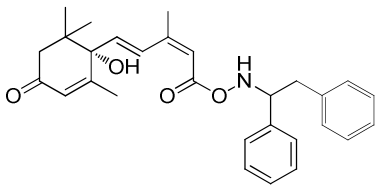

The title compound was obtained in 81% yield as white solid. ^{1}H NMR (300 MHz, $CDCl_3$) δ (ppm) 7.74-7.79 (m, 2H), 7.21-7.32 (m, 8H), 7.10-7.12(m, 2H), 6.13 (d, *J* = 16.2 Hz, 1H), 5.94 (s, 1H), 5.64 (s, 1H), 4.30 (s, 1H), 3.04-3.15(m, 2H), 2.28-2.50 (m, 2H), 2.06 (s, 1H), 1.98(s, 3H), 1.90(s, 3H), 1.11(s, 3H), 1.03(s, 3H). TOF-HRMS (m/z)

found (calcd.) for $C_{26}H_{35}NO_4$ (M): $[M+H]^+$, 426.2649 (426.2644); $[M+Na]^+$, 448.2466(448.2464) and $[M+K]^+$, 464.2211(464.2203). TOF-HRMS (m/z) found (calcd.) for $C_{29}H_{33}NO_4$ (M): $[M+H]^+$, 460.2490 (460.2488); $[M+Na]^+$, 482.2320 (482.2307) and $[M+K]^+$, 498.2050 (498.2047).

(4S)-4-((1E,3Z)-5-((phenyl)(phenyl)methylaminooxy)-3-methyl-5-oxopenta-1,3-dienyl)-4-hydroxy-3,5,5-trimethylcyclohex-2-enone (**ABA-FE16**)

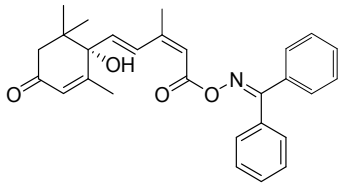

The title compound was obtained in 77% yield as white solid. ^{1}H NMR (300 MHz, $CDCl_3$) δ (ppm) 7.91-7.97 (m, 1H), 7.29-7.61 (m, 10H), 6.17 (d, *J* = 15.9 Hz, 1H), 5.93 (s, 1H), 5.62-5.66 (m, 1H), 5.21 (s, 1H), 3.04-3.15(m, 2H), 2.25-2.49 (m, 2H), 2.04 (s, 1H), 1.89-2.04 (m, 6H), 0.85-1.10(m, 6H).

(4S)-4-((1E,3Z)-5-((2-chlorophenyl)(phenyl)methylaminooxy)-3-methyl-5-oxopenta-1,3-dienyl)-4-hydroxy-3,5,5-trimethylcyclohex-2-enone (**ABA-FE17**)

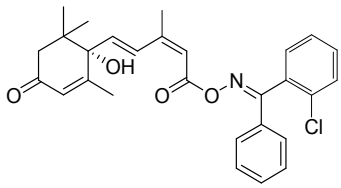

The title compound was obtained in 82% yield as yellow solid. ^{1}H NMR (300 MHz, $CDCl_3$) δ (ppm) 7.91-7.97 (m, 1H), 7.28-7.65 (m, 9H), 6.27 (dd, *J* = 16.8 Hz, 8.1 Hz, 1H), 5.95 (s, 1H), 5.58-5.79 (m, 1H), 2.27-2.52 (m, 2H), 1.93-2.07 (m, 7H), 1.03 (s, 3H), 0.85 (s, 3H). ^{13}C NMR (75.5 MHz, $CDCl_3$) δ (ppm): 197.6, 163.6, 163.5, 162.4, 157.9, 151.4, 137.0, 133.5, 131.4, 131.0, 129.3, 128.7, 127.9, 127.6, 126.8, 120.4, 115.6, 111.5, 79.3, 49.6, 41.3, 24.1, 22.8, 21.1, 18.7.

(4S)-4-((1E,3Z)-5-((2-methoxyphenyl)(phenyl)methylaminooxy)-3-methyl-5-oxopenta-1,3-dienyl)-4-hydroxy-3,5,5-trimethylcyclohex-2-enone (**ABA-FE18**)

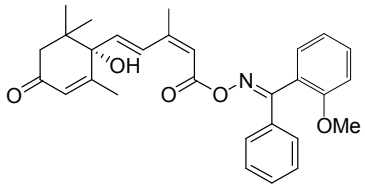

The title compound was obtained in 83% yield as white solid. ^{1}H NMR (300 MHz, $CDCl_3$) δ (ppm) 7.91-7.96 (m, 1H), 7.53 (d, *J* = 7.5 Hz, 1H), 7.40-7.45 (m, 6H), 7.03 (t, *J* = 7.2 Hz, 1H), 6.87 (d, *J* = 8.4 Hz, 1H), 6.19 (d, *J* = 16.2 Hz, 1H), 5.94 (s, 1H), 5.74 (s, 1H), 3.56 (s, 3H), 2.26-2.51 (m, 2H), 2.11 (s, 1H), 2.06 (s, 3H), 1.92 (s, 3H),

1.11 (s, 3H), 1.02 (s, 3H). ^{13}C NMR (75.5 MHz, $CDCl_3$) δ (ppm): 197.4, 163.5, 162.1, 157.9, 151.2, 136.8, 133.6, 131.3, 131.0, 129.3, 128.7, 128.1, 127.6, 126.9, 120.4, 115.7, 111.5, 79.4, 55.4, 49.6, 41.3, 24.1, 22.8, 21.1, 18.6. TOF-HRMS (m/z) found (calcd.) for $C_{29}H_{33}NO_5$ (M): $[M+Na]^+$, 498.2253 (498.2256).

(4S)-4-((1E,3Z)-5-((4-methoxyphenyl)(phenyl)methylaminooxy)-3-methyl-5-oxopenta-1,3-dienyl)-4-hydroxy-3,5,5-trimethylcyclohex-2-enone (**ABA-FE19**)

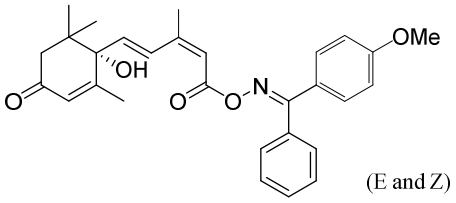

(E and Z)

The title compound was obtained in 81% yield as white solid. ^{1}H NMR (300 MHz, $CDCl_3$) δ (ppm) 7.94 (d, *J* = 16.2 Hz, 1H), 7.59-7.26 (m, 7H), 6.96 (d, *J* = 12.0 Hz, 2H for isomer 1), 6.86(d, *J* = 12.0 Hz, 2H for isomer 2), 6.20 (d, *J* = 16.2 Hz, H for isomer 1), 6.19 (d, *J* = 16.2 Hz, 2H for isomer 2), 5.92 (s, 1H), 5.68(s, 1H for isomer 1), 5.58 (s, 1H for isomer 2), 3.87 (s, 3H for isomer 1), 3.82 (s, 3H for isomer 2), 2.49-2.28 (m, 2H), 2.04 (s, 3H for isomer 2), 2.01 (s, 3H for isomer 1), 1.91 (s, 3H),1.10 (s, 3H), 1.00 (s, 3H). The ratio between isomer 1 and 2 is 2.1:1. ^{13}C NMR (75.5 MHz, $CDCl_3$) δ (ppm): 197.5, 164.1,163.4, 162.2,160.4,151.3,137.0, 135.3, 131.0, 130.5, 135.4, 129.2,

128.6, 128.1, 128.0, 127.0, 124.5, 115.7, 113.6, 113.3, 79.9, 55.2, 49.6, 41.4, 24.2, 22.9, 21.2, 18.7. TOF-HRMS (m/z) found (calcd.) for $C_{29}H_{31}NO_5$ (M): $[M+H]^+$, 474.2280 (474.2280); $[M+Na]^+$, 496.2100 (496.2100) and $[M+K]^+$, 512.1825 (512.1839).

(4S)-4-((1E,3Z)-5-((4-chlorophenyl)(phenyl)methylaminooxy)-3-methyl-5-oxopenta-1,3-dienyl)-4-hydroxy-3,5,5-trimethylcyclohex-2-enone (**ABA-FE20**)

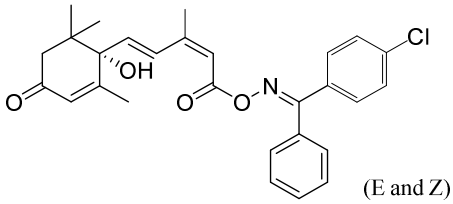

(E and Z)

The title compound was obtained in 78% yield as white solid. ^{1}H NMR (300 MHz, $CDCl_3$) δ (ppm) 7.92 (d, *J* = 16.2 Hz, 1H), 7.58-7.26 (m, 9H), 6.22 (d, *J* = 16.2 Hz, 1H for isomer 1),6.21 (d, *J* = 16.2 Hz, 1H for isomer 2), 5.90 (s, 1H), 5.30(s, 1H for isomer 1), 5.29 (s, 1H for isomer 2), 2.49-2.28 (m, 2H), 2.01 (s, 3H for isomer 2), 2.00 (s, 3H for isomer 1), 1.91 (s, 3H),1.10 (s, 3H), 1.00 (s, 3H). The ratio between isomer 1 and 2 is 1:1.2. ^{13}C NMR (75.5 MHz, $CDCl_3$) δ (ppm): 197.8, 163.5, 163.4, 162.2, 152.2, 137.2, 135.8, 134.6, 133.5, 132.3, 131.2, 130.5, 130.4, 129.9, 129.1, 129.0, 128.9, 128.8, 128.7, 128.6, 128.4, 128.2, 127.2, 115.5, 79.7, 49.9, 41.7, 24.4, 23.2, 21.4, 19.0. TOF-HRMS (m/z) found (calcd.) for $C_{28}H_{28}ClNO_4$ (M): $[M+H]^+$, 478.1778 (478.1785); $[M+Na]^+$, 496.2100 (496.2100) and $[M+K]^+$, 512.1825 (512.1839).

(S)-4-((1E,3Z)-5-(bis(4-chlorophenyl)methylaminooxy)-3-methyl-5-oxopenta-1,3-dienyl)-4-hydroxy-3,5,5-trimethylcyclohex-2-enone (**ABA-FE21**)

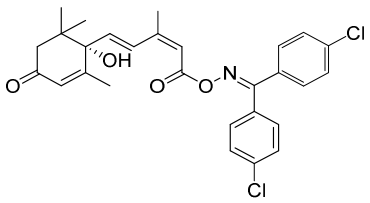

The title compound was obtained in 91% yield as yellow solid. ^{1}H NMR (300 MHz, $CDCl_3$) δ (ppm) 7.92 (d, *J* = 16.2 Hz, 1H), 7.56-7.24 (m, 8H), 6.24 (d, *J* = 16.2 Hz) 5.90 (s, 1H), 5.61 (s, 1H), , 2.50-2.30 (m, 2H), 2.03 (s, 3H for isomer 2), 1.92 (s, 3H for isomer 1), 1.91 (s, 3H),1.11 (s, 3H), 1.02 (s, 3H). ^{13}C NMR (75.5 MHz, $CDCl_3$) δ (ppm): 197.8, 163.2, 162.4, 152.5, 147.4, 137.7, 136.0, 133.1, 130.6, 130.4, 130.3, 129.1, 128.9, 128.1, 127.3, 115.2, 79.7, 49.8, 41.7, 24.4, 23.2, 21.5, 19.0. TOF-HRMS (m/z) found (calcd.) for $C_{28}H_{27}Cl_2NO_4$ (M): $[M+H]^+$, 512.1402 (512.1395); $[M+Na]^+$, 534.1239 (534.1215).

(4S)-4-hydroxy-4-((1E,3Z)-5-((4-methoxyphenyl)(phenyl)methylaminooxy)-3-methyl-5-oxopenta-1,3-dienyl)-3,5,5-trimethylcyclohex-2-enone (**ABA-FE22**)

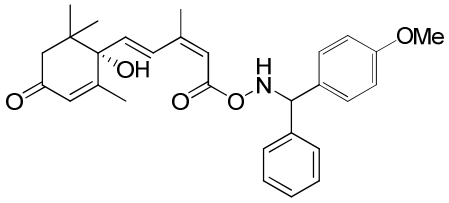

The title compound was obtained in 85% yield as white solid. ^{1}H NMR (300 MHz, $CDCl_3$) δ (ppm) 7.79-7.91 (m, 2H), 7.28-7.45 (m, 7H), 6.86 (d, J = 8.7 Hz, 2H), 6.15 (d, J = 16.2 Hz, 1H), 5.95 (s, 1H), 5.68 (s, 1H), 5.20 (s, 1H), 3.89 (s, 3H), 2.28-2.51 (m, 2H), 2.13 (s, 1H), 1.91-2.01 (m, 6H), 1.11 (s, 3H), 1.00 (s, 3H). ^{13}C NMR (75.5 MHz, $CDCl_3$) δ (ppm): 197.3, 166.2, 162.0, 159.2, 150.4, 136.9, 129.0, 128.5, 127.9, 127.6, 127.1, 115.6, 114.0, 79.5, 68.6, 55.2, 49.7, 41.4, 24.3, 23.0, 21.3, 18.7. TOF-HRMS (m/z) found (calcd.) for $C_{29}H_{33}NO_5$ (M): $[M+H]^+$, 476.2447 (476.2437); $[M+Na]^+$, 498.2260 (498.2256) and $[M+K]^+$, 514.2013 (514.1996).

(4S)-4-((1E,3Z)-5-((4-chlorophenyl)(phenyl)methylaminooxy)-3-methyl-5-oxopenta-1,3-dienyl)-4-hydroxy-3,5,5-trimethylcyclohex-2-enone (**ABA-FE23**)

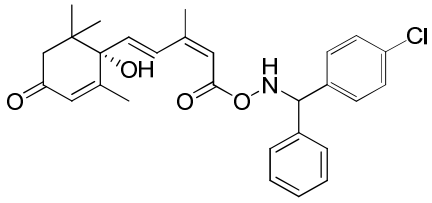

The title compound was obtained in 88% yield as yellow solid. ^{1}H NMR (300 MHz, $CDCl_3$) δ (ppm) 7.79-7.98 (m, 2H), 7.28-7.62 (m, 9H), 6.16 (d, J = 16.2 Hz, 1H),

5.96 (s, 1H), 5.67 (s, 1H), 5.29 (s, 1H), 2.28-2.51 (m, 2H), 1.92-2.06 (m, 7H), 1.13 (s, 3H), 1.01 (s, 3H). TOF-HRMS (m/z) found (calcd.) for $C_{28}H_{30}ClNO_4$ (M): $[M+H]^+$, 480.1925 (480.1942).

(S)-4-((1E,3Z)-5-(bis(4-chlorophenyl)methylaminooxy)-3-methyl-5-oxopenta-1,3-dienyl)-4-hydroxy-3,5,5-trimethylcyclohex-2-enone (**ABA-FE24**)

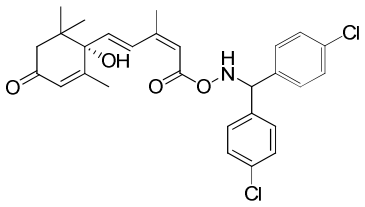

The title compound was obtained in 77% yield as yellow solid. ^{1}H NMR (300 MHz, $CDCl_3$) δ (ppm) 7.84-7.89 (m, 2H), 7.28-7.57 (m, 8H), 6.16-6.22 (m, 1H), 5.96 (s, 1H), 5.67 (s, 1H), 5.17 (s, 1H), 2.29-2.51 (m, 2H), 1.92-2.07 (m, 7H), 1.13 (s, 3H), 1.01 (s, 3H). ^{13}C NMR (75.5 MHz, $CDCl_3$) δ (ppm): 197.4, 166.0, 162.0, 150.6, 136.9, 130.5, 129.2, 128.7, 127.7, 127.5, 126.9, 115.1, 79.4, 68.1, 49.5, 41.3, 24.1, 22.8, 21.1, 18.7. TOF-HRMS (m/z) found (calcd.) for $C_{28}H_{29}Cl_2NO_4$ (M): $[M+Na]^+$, 536.1348 (536.1371).

(4S)-4-((1E,3Z)-5-(((2,2-dimethyl-1-phenylpropyl)amino)oxy)-3-methyl-5-oxopenta-1,3-dien-1-yl)-4-hydroxy-3,5,5-trimethylcyclohex-2-enone (**ABA-FE25**)

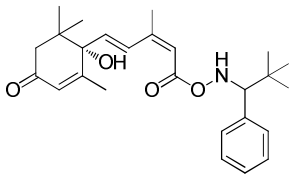

The title compound was obtained in 65% yield as white solid. ^{1}H NMR (300 MHz, $CDCl_3$) δ (ppm) 7.46-7.48 (m, 2H), 7.29-7.32 (m, 3H), 7.04-7.17(m, 1H), 6.18 (dd, *J* = 6.6 Hz, 12.0 Hz, 1H), 5.86 (s, 1H), 5.90 (s, 1H), 4.64 (s, 1H), 2.22-2.40 (m, 2H), 2.04 (s, 1H), 1.98(s, 3H), 1.82(d, *J* = 12.0 Hz, 3H), 1.04-1.07(m, 12H), 0.91(d, *J* = 12.0 Hz, 3H). TOF-HRMS (m/z) found (calcd.) for $C_{26}H_{35}NO_4$ (M): $[M+H]^+$, 426.2649 (426.2644); $[M+Na]^+$, 448.2466 (448.2464) and $[M+K]^+$, 464.2211 (464.2203).

4S)-4-hydroxy-4-((1E,3Z)-5-(1-(4-methoxyphenyl)-2,2-dimethylpropylaminooxy)-3-methyl-5-oxopenta-1,3-dienyl)-3,5,5-trimethylcyclohex-2-enone (**ABA-FE26**)

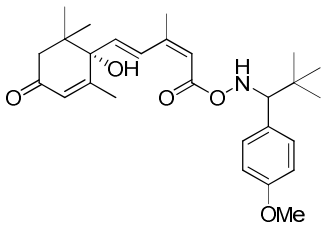

The title compound was obtained in 79% yield as white solid. ^{1}H NMR (300 MHz, $CDCl_3$) δ (ppm) 8.25 (s, 1H), 7.73-7.81 (m, 1H), 7.25-7.38 (m, 2H), 6.86-6.91 (m, 2H), 6.16 (d, *J* = 16.2 Hz, 1H), 5.94 (s, 1H), 5.58 (s, 1H), 3.82 (s, 3H), 3.76 (s, 1H), 2.28-2.50 (m, 2H), 1.87-2.06 (m, 7H), 1.13 (s, 3H), 0.99 (s, 12H), 0.91 (s, 3H). ^{13}C NMR

(75.5 MHz, $CDCl_3$) δ (ppm): 197.5, 166.3, 162.2, 158.7, 149.8, 136.7, 131.2, 129.7, 129.5, 127.8, 127.0, 115.7, 113.2, 112.9, 79.5, 73.2, 55.1, 49.7, 41.4, 34.3, 33.9, 27.2, 24.1, 23.0, 21.1, 18.8. TOF-HRMS (m/z) found (calcd.) for $C_{27}H_{37}NO_5$ (M): $[M+H]^+$, 456.2744 (456.2750); $[M+Na]^+$, 478.2566 (478.2569) and $[M+K]^+$, 494.2298 (494.2309). TOF-HRMS (m/z) found (calcd.) for $C_{27}H_{37}NO_5$ (M): $[M+H]^+$,456.2744 (456.2750); $[M+Na]^+$, 478.2566 (478.2569) and $[M+K]^+$, 494.2298 (494.2309).

3.7 References

1. Lienert, F.; Lohmueller, J. J.; Garg, A.; Silver, P. A., Synthetic biology in mammalian cells: next generation research tools and therapeutics. *Nat Rev Mol Cell Bio* **2014,** *15* (2), 95-107.

2. Bashor, C. J.; Horwitz, A. A.; Peisajovich, S. G.; Lim, W. A., Rewiring cells: synthetic biology as a tool to interrogate the organizational principles of living systems. *Annual review of biophysics* **2010,** *39*, 515-37.

3. Wang, Y. H.; Wei, K. Y.; Smolke, C. D., Synthetic Biology: Advancing the Design of Diverse Genetic Systems. *Annu Rev Chem Biomol* **2013,** *4*, 69-102.

4. Aubel, D.; Fussenegger, M., Mammalian synthetic biology - from tools to therapies. *Bioessays* **2010,** *32* (4), 332-345.

5. Ruder, W. C.; Lu, T.; Collins, J. J., Synthetic Biology Moving into the Clinic. *Science* **2011,** *333* (6047), 1248-1252.

6. Rogers, J. K.; Taylor, N. D.; Church, G. M., Biosensor-based engineering of biosynthetic pathways. *Current opinion in biotechnology* **2016,** *42*, 84-91.

7. Nandagopal, N.; Elowitz, M. B., Synthetic Biology: Integrated Gene Circuits. *Science* **2011,** *333* (6047), 1244-1248.

8. Brophy, J. A. N.; Voigt, C. A., Principles of genetic circuit design. *Nature methods* **2014,** *11* (5), 508-520.

9. Miyamoto, T.; Razavi, S.; DeRose, R.; Inoue, T., Synthesizing Biomolecule-Based Boolean Logic Gates. *ACS synthetic biology* **2013,** *2* (2), 72-82.

10. Slusarczyk, A. L.; Lin, A.; Weiss, R., Foundations for the design and implementation of synthetic genetic circuits. *Nat Rev Genet* **2012,** *13* (6), 406-420.

11. DeRose, R.; Miyamoto, T.; Inoue, T., Manipulating signaling at will: chemically-inducible dimerization (CID) techniques resolve problems in cell biology. *Pflugers Archiv : European journal of physiology* **2013,** *465* (3), 409-17.

12. Fegan, A.; White, B.; Carlson, J. C.; Wagner, C. R., Chemically controlled protein assembly: techniques and applications. *Chemical reviews* **2010,** *110* (6), 3315-36.

13. Gestwicki, J. E.; Marinec, P. S., Chemical control over protein-protein interactions: beyond inhibitors. *Combinatorial chemistry & high throughput screening* **2007,** *10* (8), 667-75.

14. Chan, J.; Dodani, S. C.; Chang, C. J., Reaction-based small-molecule fluorescent probes for chemoselective bioimaging. *Nat Chem* **2012,** *4* (12), 973-984.

15. Zeng, G.; Zhang, R.; Xuan, W.; Wang, W.; Liang, F. S., Constructing de novo H2O2 signaling via induced protein proximity. *ACS chemical biology* **2015,** *10* (6), 1404-10.

16. Wright, C. W.; Guo, Z. F.; Liang, F. S., Light Control of Cellular Processes by Using Photocaged Abscisic Acid. *Chembiochem : a European journal of chemical biology* **2015,** *16* (2), 254-261.

17. Liang, F. S.; Ho, W. Q.; Crabtree, G. R., Engineering the **ABA** plant stress pathway for regulation of induced proximity. *Science signaling* **2011,** *4* (164), rs2.

18. Theil, E. C.; Goss, D. J., Living with iron (and oxygen): questions and answers about iron homeostasis. *Chemical reviews* **2009,** *109* (10), 4568-79.

19. Breuer, W.; Shvartsman, M.; Cabantchik, Z. I., Intracellular labile iron. *The international journal of biochemistry & cell biology* **2008,** *40* (3), 350-4.

20. Oshiro, S.; Morioka, M. S.; Kikuchi, M., Dysregulation of iron metabolism in Alzheimer's disease, Parkinson's disease, and amyotrophic lateral sclerosis. *Advances*

in pharmacological sciences **2011,** *2011*, 378278.

21. Jenner, P., Oxidative stress in Parkinson's disease. *Annals of neurology* **2003,** *53 Suppl 3*, S26-36; discussion S36-8.

22. Dixon, S. J.; Stockwell, B. R., The role of iron and reactive oxygen species in cell death. *Nature chemical biology* **2014,** *10* (1), 9-17.

23. Mercer, A. E.; Maggs, J. L.; Sun, X. M.; Cohen, G. M.; Chadwick, J.; O'Neill, P. M.; Park, B. K., Evidence for the involvement of carbon-centered radicals in the induction of apoptotic cell death by artemisinin compounds. *The Journal of biological chemistry* **2007,** *282* (13), 9372-82.

24. Au-Yeung, H. Y.; Chan, J.; Chantarojsiri, T.; Chang, C. J., Molecular imaging of labile iron(II) pools in living cells with a turn-on fluorescent probe. *Journal of the American Chemical Society* **2013,** *135* (40), 15165-73.

25. Hirayama, T.; Okuda, K.; Nagasawa, H., A highly selective turn-on fluorescent probe for iron(II) to visualize labile iron in living cells. *Chem Sci* **2013,** *4* (3), 1250-1256.

26. Li, P.; Fang, L. B.; Zhou, H.; Zhang, W.; Wang, X.; Li, N.; Zhong, H. B.; Tang, B., A New Ratiometric Fluorescent Probe for Detection of Fe2+ with High Sensitivity and Its Intracellular Imaging Applications. *Chem-Eur J* **2011,** *17* (38), 10520-10523.

27. Niwa, M.; Hirayama, T.; Okuda, K.; Nagasawa, H., A new class of high-contrast Fe(II) selective fluorescent probes based on spirocyclized scaffolds for visualization of intracellular labile iron delivered by transferrin. *Organic & biomolecular chemistry* **2014,** *12* (34), 6590-6597.

28. Spangler, B.; Morgan, C. W.; Fontaine, S. D.; Vander Wal, M. N.; Chang, C. J.; Wells, J. A.; Renslo, A. R., A reactivity-based probe of the intracellular labile ferrous iron pool. *Nature chemical biology* **2016,** *12* (9), 680-+.

29. Xuan, W.; Pan, R.; Wei, Y.; Cao, Y.; Li, H.; Liang, F. S.; Liu, K. J.; Wang, W., Reaction-Based "Off-On" Fluorescent Probe Enabling Detection of Endogenous Labile Fe(2+) and Imaging of Zn(2+)-induced Fe(2+) Flux in Living Cells and Elevated Fe(2+) in Ischemic Stroke. *Bioconjugate chemistry* **2016,** *27* (2), 302-8.

30. Michiels, F.; Habets, G. G. M.; Stam, J. C.; Vanderkammen, R. A.; Collard, J. G., A Role for Rac in Tiam1-Induced Membrane Ruffling and Invasion. *Nature* **1995,** *375* (6529), 338-340.

31. Gao, Y.; Dickerson, J. B.; Guo, F.; Zheng, J.; Zheng, Y., Rational design and characterization of a Rac GTPase-specific small molecule inhibitor. *Proceedings of the National Academy of Sciences of the United States of America* **2004,** *101* (20), 7618-7623.

32. Miyamoto, T.; DeRose, R.; Suarez, A.; Ueno, T.; Chen, M.; Sun, T. P.; Wolfgang, M. J.; Mukherjee, C.; Meyers, D. J.; Inoue, T., Rapid and orthogonal logic gating with a gibberellin-induced dimerization system. *Nature chemical biology* **2012,** *8* (5), 465-470.

33. Zhang, G. F.; Wen, X.; Wang, Y.; Mo, W. M.; Ding, C. R., Sodium Nitrite Catalyzed Aerobic Oxidative Deoximation under Mild Conditions. *J Org Chem* **2011,** *76* (11), 4665-4668.

34. Pusterla, I.; Bode, J. W., The mechanism of the alpha-ketoacid-hydroxylamine amide-forming ligation. *Angew Chem Int Ed Engl* **2012,** *51* (2), 513-6.

Chapter 4

A Self-Reporting Chemically Induced Protein Proximity System Based on a Malachite Green Derivative and the L5** Fluorogen Activating Protein

(This chapter is based on a manuscript in preparation)

4.1 Introduction

The chemically induced proximity (CIP), or chemically induced dimerization (CID), method uses a small molecule inducer that homo- or hetero-dimerizes two unique inducer-binding protein domains fused individually to any two proteins of interest (POIs). Depending on the choice of linked POIs, a variety of downstream cellular events can be triggered temporally by the chemical inducer.[1-4] Several CIP systems have been engineered that each uses a unique chemical inducer to dimerize a corresponding pair of inducer-binding proteins.[5-14] These orthogonal CIP systems allow multiple biological events to be controlled simultaneously and independently in the same cell and the construction of sophisticated bio-computation systems.[15] Recently, several studies have shown that these CIP inducers can be chemically modified to become activatable by artificial or endogenous cellular signals that greatly expands the utility of CIP

methods in synthetic biology.[16-21] One limitation of existing CIP systems is that the inducer-triggered dimerization cannot be directly monitored, therefore, the kinetics of dimerization and that between dimerization and the induced downstream effects is difficult to follow.

Fluorogen activating proteins (FAPs) derived from single chain antibodies (scFv) induce fluorescent signals upon binding from certain organic dyes (fluorogens) which are otherwise non-fluorescent when free in solution.[22-28] Structural studies of the malachite green (MG-based FAP system revealed that MG forms a 1:2 ligand:protein complex with two L5** proteins, the V_L domain of an antibody, which leads to the activation of intense fluorescence.[29] Importantly, these L5** protein domains do not self-dimerize in the absence of dye, and association is induced in the presence of fluorogenic dye. We reason that by linking two POIs individually to each L5** protein, a new MG inducible CIP system can be built that can trigger downstream effects through MG-induced VL-POI dimerization and also self-report the dimerization by activation of MG fluorescent signals upon dimerization, producing a self-reporting chemically induced proximity system (**Figure** 4.1).

Figure 4.1 MG-based chemically induced proximity method to control biological processes.

4.2 MG-based fluorogenic CIP system to induce transcriptional activation

To create an MG-based fluorogenic CIP system, we first constructed an MG inducible transcriptional activation system based on L5**-fusion proteins (**Figure** 4.2). We generated DNA plasmids encoding the MG-inducible gene expression cassette including a yeast Gal4 DNA binding domain (Gal4DBD)-L5** and a herpes simplex virusVP16 transactivation domain (VP16AD)-L5** fusion proteins. A reporter construct with five copies of the upstream activation sequence (UAS) that Gal4DBD recognizes inserted upstream of a luciferase gene was used to test the transcriptional activation. In this system, luciferase expression can be turned on only when MG induces hetero-dimerization of GAL4DBD-L5** and L5**-VP16AD. Furthermore, fluorescence will be observed only when MG forms a complex with two L5** fusion proteins. Although the homo-dimerization of two identical L5** fusion proteins can also induce MG fluorescence, we expect that any activated fluorescence will report

combined occurring dimerization events from both hetero- and homo-dimerizations and provide the information regarding the dimerization kinetics.

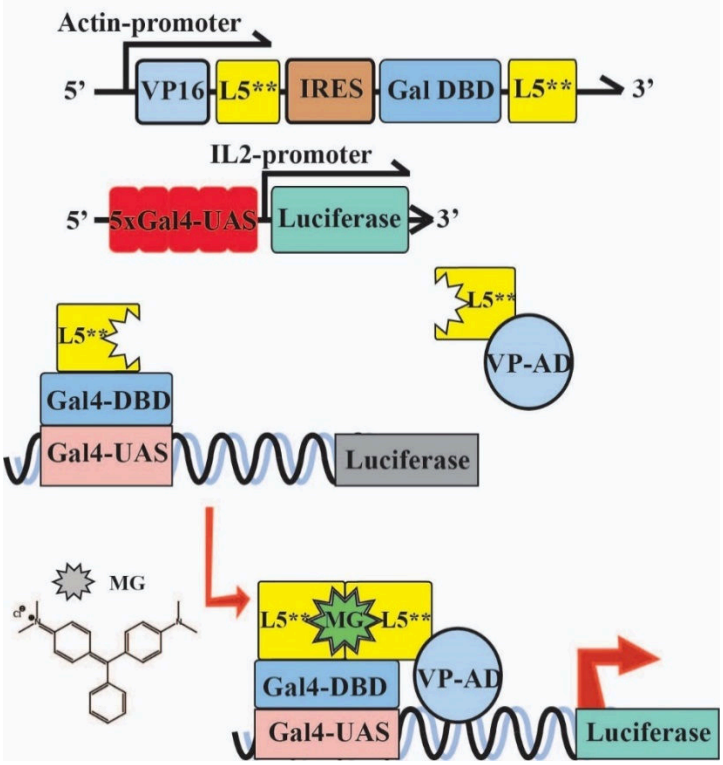

Figure 4.2 Scheme and constructs of MG-induced luciferase expression system.

To test this system, we co-transfected HEK293T cells with the MG-inducible gene expression cassette and the UAS-luciferase reporter (**Figure** 4.2) for 24 h and then treated cells with 500 nM MG and two MG derivatives, a cell-permeant MGnBu[30] and cell-excluded MG-B-Tau,[31] (**Figure** 4.3) for another 24 h. Under these conditions, the cell excluded MG-B-Tau would be expected to stimulate no protein proximity, while the cell permeant analogs MG and MGnBu could induce protein interactions and drive reporter expression.

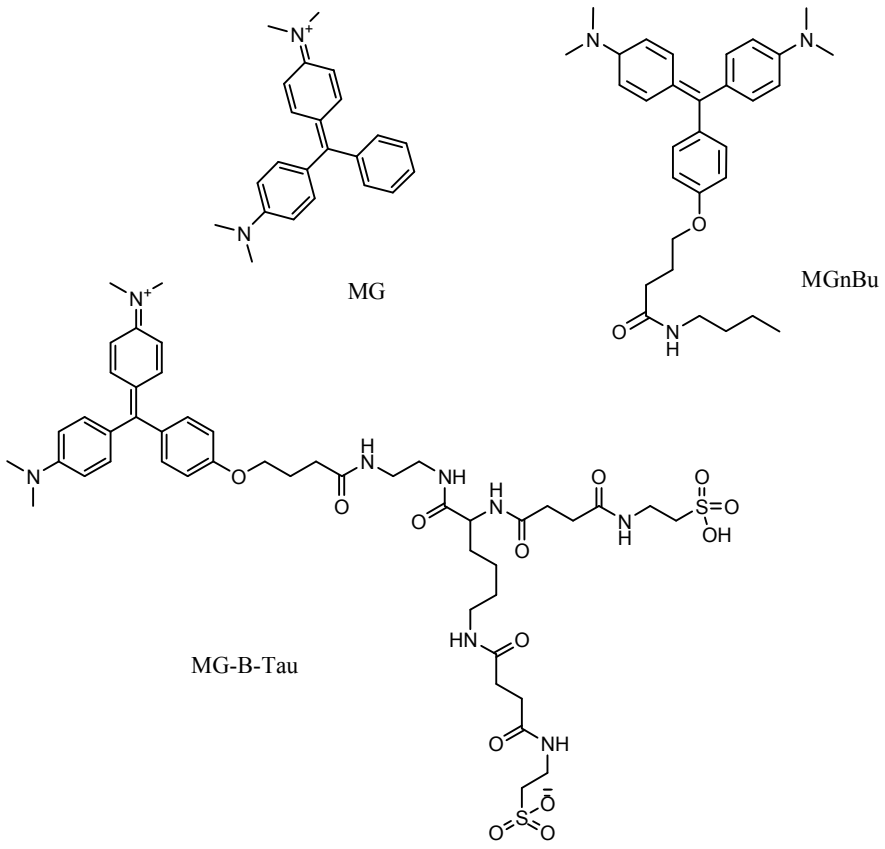

Figure 4.3 Structures of MG, MGnBu and MG-B-Tau

Resulting cells were washed and analysed under a fluorescence plate reader to detect the activated MG fluorescence (excitation 640 nm/ emission 670 nm), or lysed for luciferase assays. A 30-fold (for MG-B-Tau) to 250-fold (for MGnBu) fluorescence increase from activated MG fluorescence can be observed (**Figure** 4.4), as well as a 3-fold increase in luciferase expression in the case of MGnBu induction (**Figure** 4.5). This study showed that an MG-based fluorogenic CIP system can be established and the observed activated MG fluorescence is correlated with the observed induced luciferase expression. The low induction

fold in luciferase expression is likely a result of the competition between the hetero- and homo-dimerization of GAL4DBD-L5** and L5**-VP16AD. Since MGnBu gave the highest fluorescent signal upon dimerization and induced the highest level of luciferase expression, we focused on MGnBu as the inducer for the following studies.

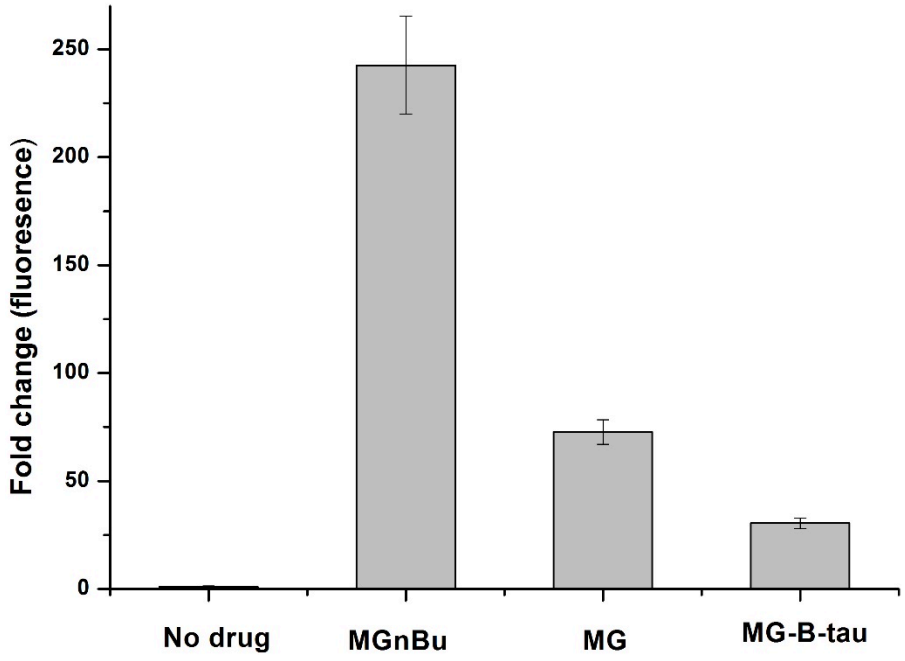

Figure 4.4 Activated MG fluorescence fold changes in HEK293T cells by MG, MGnBu and MG-B-Tau. The cells were transfected with the constructs shown in Figure 4.2 for 24 h before addition of 500 nM MG or MGnBu or MG-B-Tau for another 24 h. Cells were washed and analyzed by fluorescence plate reader. The induced fold change was calculated by comparison to the values of ethanol-treated samples. Independent experiments were repeated five or more times. Errors bars are SD (N=5).

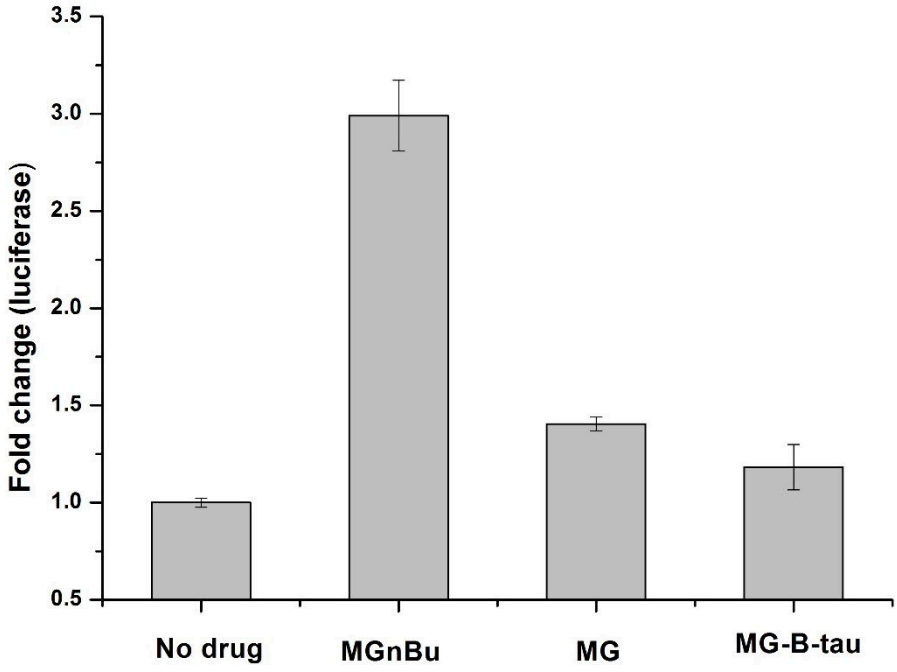

Figure 4.5 Induced luciferase expression in HEK293T cells by MG, MGnBu and MG-B-Tau. The cells were transfected with the constructs shown in Figure 4.2 for 24 h before addition of 500 nM MG or MGnBu or MG-B-Tau for another 24 h. Cells were washed and analyzed by luciferase assays. The induced fold change was calculated by comparison to the values of ethanol-treated samples. Independent experiments were repeated five or more times. Errors bars are SD (N=5).

We next tested if there is dosage dependence in this new MG-based CIP system as seen in other CIP systems. We transfected HEK293T cells with the MG-inducible gene expression cassette and the UAS-luciferase reporter for 24 h, and then treated cells with MGnBu (from 0 to 1000 nM) for another 24 h. We observed that activated MGnBu fluorescence showed a dosage-dependent increase and gave the highest signal at 500 nM (**Figure** 4.6). A similar dosage-dependent increase was observed in luciferase

induction, which also reached the highest expression at 500 nM (**Figure** 4.7).

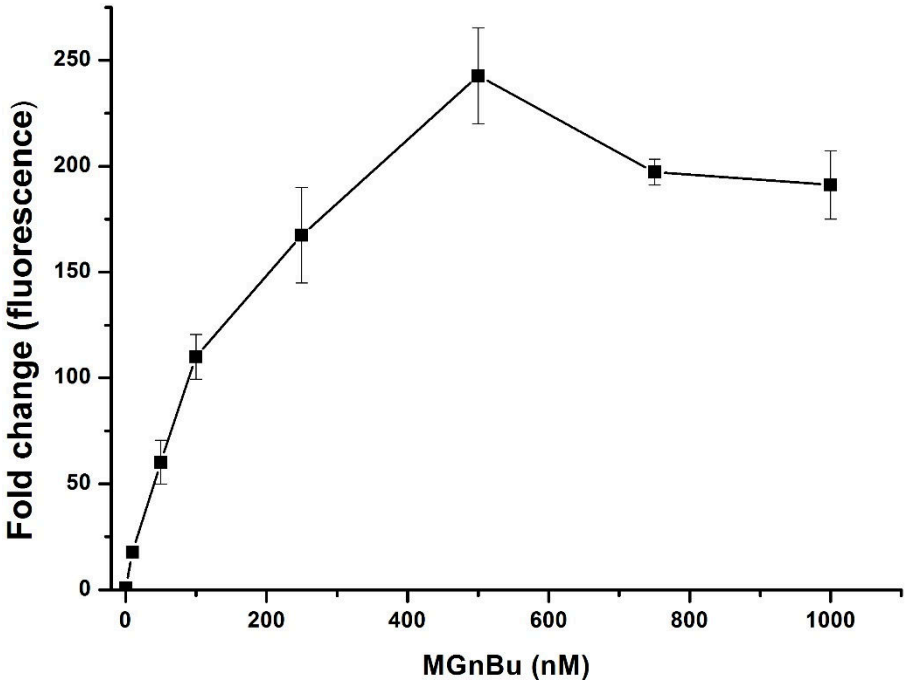

Figure 4.6 Dosage response of activated MGnBu fluorescence fold change in HEK293T cells. The cells were transfected with the constructs shown in Figure 4.2 for 24 h before addition of 0-1000 nM of MGnBu for another 24 h. Cells were washed and analyzed by fluorescence plate reader. The induced fold change was calculated by comparison to the values of ethanol-treated samples. Independent experiments were repeated five or more times. Errors bars are SD (N=5).

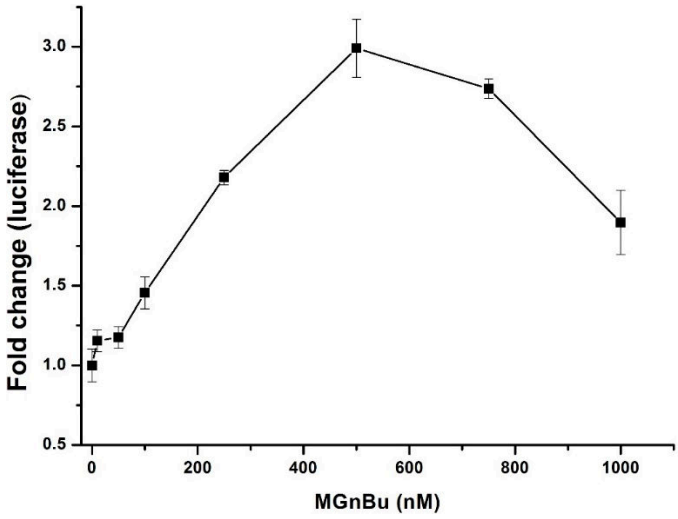

Figure 4.7 Dosage response of induced luciferase expression in HEK293T cells. The cells were transfected with the constructs shown in Figure 4.2 for 24 h before addition of 0-1000 nM of MGnBu for another 24 h. Cells were washed and analyzed by luciferase assays. For The induced fold change was calculated by comparison to the values of ethanol-treated samples. Independent experiments were repeated five or more times. Errors bars are SD (N=5).

4.3 MG-based fluorogenic CIP system to control protein translocation

Next, we tested if the MG-induced CIP system can be used to control protein translocation. We constructed DNA plasmids encoding the nuclear export sequence-tagged L5** (NES-L5**) and the EYFP-L5** fusion proteins (**Figure** 4.8).

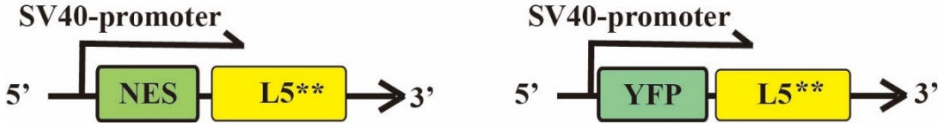

Figure 4.8 DNA constructs for EYFP translocation experiments.

We transfected CHO cells with both constructs for 24 h and followed by treating cells with 500 nM MGnBu (or ethanol as a negative control). Cells were then collected at different time points after MGnBu addition for analysis of MGnBu fluorescence activation and EYFP-L5** translocation. We quantified the fold changes of activated MGnBu fluorescence due to dimerization with a fluorescence plate reader. We observed a rapid and significant increase in fluorescence of MGnBu within 5 min, which continued to increase during the observation time period up to 4 h (**Figure** 4.9).

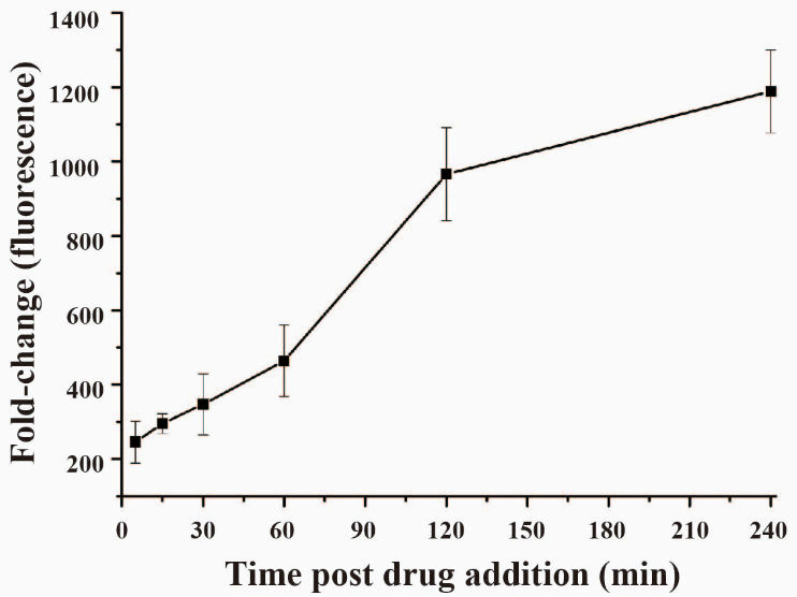

Figure 4.9 Time course (0 to 4 h) of activated MGnBu fluorescence fold change. Cells were transfected with the constructs in Figure 4.8 for 24 h before treating with 500 nM MGnBu for indicated time periods. Then cells were washed and collected for analysis by fluorescence plate reader.

Meanwhile, the subcellular distribution of EYFP-L5** proteins was monitored

under a fluorescence microscope. When expressed in the cell, EYFP-L5** proteins were found to freely cross the nuclear envelope, and distributed throughout the cell although a preferential nuclear localization was observed (**Figure** 4.10-i). In the presence of MGnBu, the dimerization between of EYFP-L5** and NES-L5** led to an obvious translocation of EYFP-L5** out of the nucleus (**Figure** 4.10-ii). Such nuclear exclusion is due to the association of EYFP with NES after MGnBu heterodimerization between EYFP-L5** and NES-L5** instead of the increased size of the homodimerized EYFP-L5** because the same EYFP translocation was not observed when cells were transfected only with EYFP-L5** and treated with MGnBu (**Figure** 4.11).

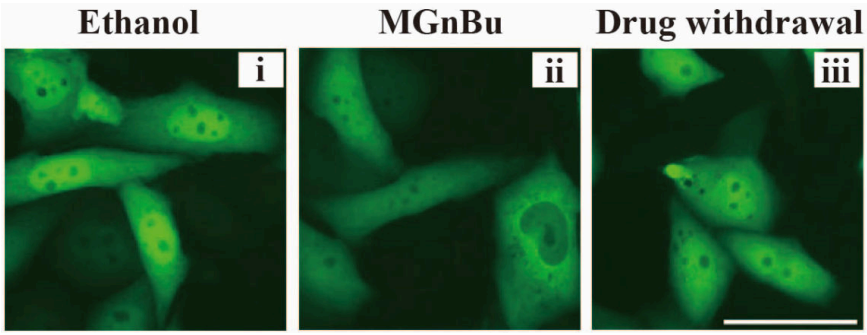

Figure 4.10 Representative EYFP images of transfected CHO cells without MGnBu (i), with 500 nM MGnBu (ii), or removal of MGnBu after treatment (iii). Scale bar is 50 μm.

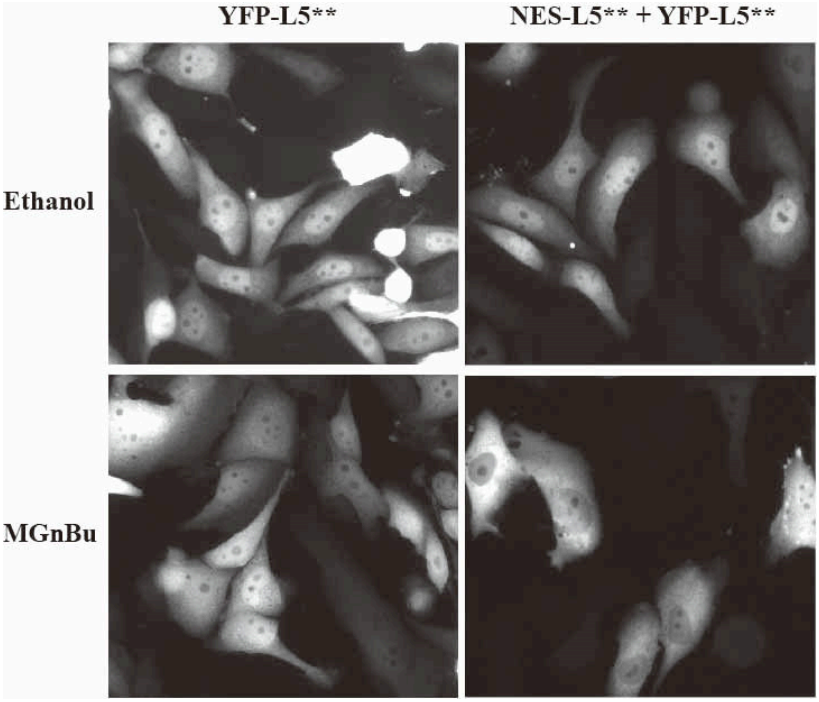

Figure 4.11 Representative images for: CHO cells were transfected with 0.2 μg SV40-EYFP-L5** only or with 0.4 μg SV40-NES-L5** for another 24 hours. Cell were treated with ethanol or with 500 nM of MGnBu for 24 hours.

We quantified the degree of MGnBu-induced EYFP-L5** translocation by first calculating an EYFP-L5** nuclear-distribution ratio defined by the EYFP fluorescence intensity inside versus outside the nucleus in non-MGnBu-treated cells (100 – 200 random cells counted along the diagonal of each field of view from 5 fields total). After MGnBu treatment, the same EYFP-L5** nuclear-distribution ratio value was determined for each cell (100 – 200 random cells counted in each condition), and the number of cells showing a lower nuclear-distribution ratio value (defined as nuclear exported or translocated) was calculated and the percentage of translocated cells over

the total counted cells was determined at each indicated time point after MGnBu addition. We observed a rapid translocation of EYFP-L5** into cytoplasm (**Figure** 4.12) and the kinetics of the activated MGnBu fluorescence is well correlated with the kinetics of induced protein translocation.

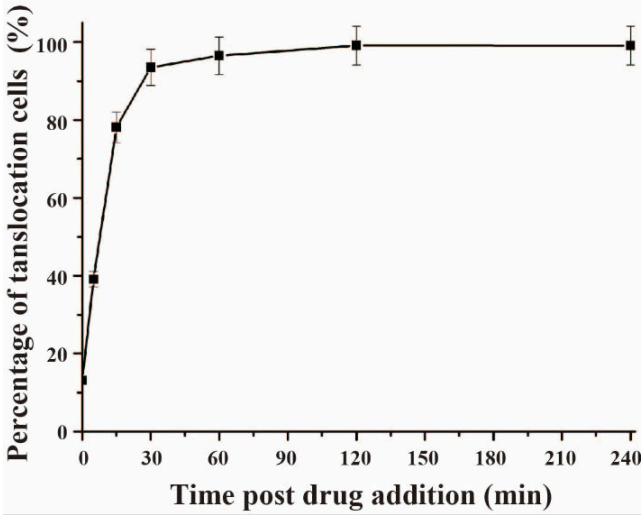

Figure 4.12 The percentage of cells showing induced EYFP translocation in transfected CHO cells treated with MGnBu (0 to 4 h). Cells were transfected with the constructs in Figure 4.8 for 24 h before treating with 500 nM MGnBu for indicated time periods. Then cells were observed under a fluorescence microscope. The statistical data were obtained by counting cells showing EYFP translocation over the total EYFP positive cells to give the percentage of translocated cells. Cells were counted from three separate experiments, and 100-200 cells were counted for each sample. Error bars are SD (N = 3).

To investigate whether the MG-induced CIP system is reversible, after CHO cells

were transfected with EYFP-L5** and NES-L5** constructs and treated with MGnBu for 4 h, cells were washed with fresh media (without MGnBu) for 3 times and collected for analysis at different time points after the withdrawal of MGnBu. The activated MGnBu fluorescence fold change and the percentage of cells showing cytoplasmic translocation were quantified as described above. We observed that both the activated MGnBu fluorescence and the induced EFYP-L5** translocation was readily reversible and well-correlated with each other (**Figures** 4.13 and 4.14).

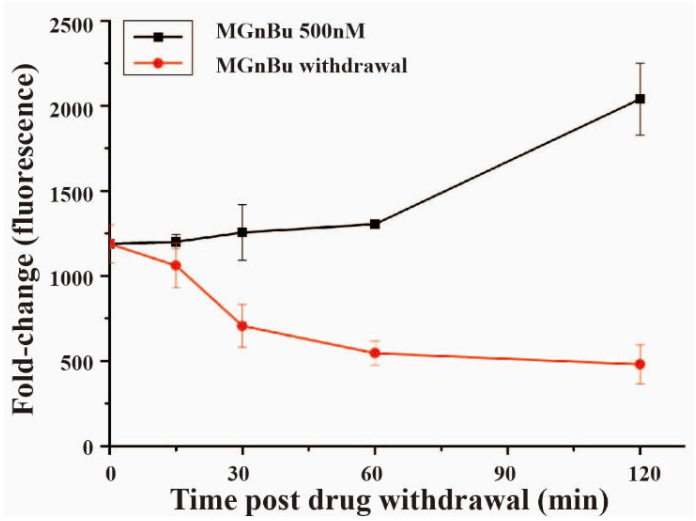

Figure 4.13 Time course (0 to 4 h) of activated MGnBu fluorescence fold change after MGnBu withdrawal in transfected CHO cells originally treated with MGnBu. After indicated time, cells were washed and collected for analysis by fluorescence plate reader.

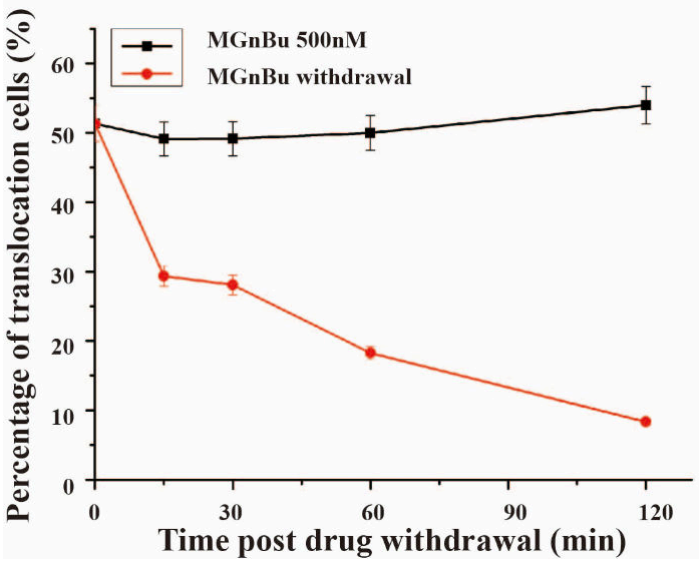

Figure 4.14 Time course (0 to 4 h) of the percentage of cells showing induced EYFP translocation after MGnBu withdrawal in transfected CHO cells originally treated with MGnBu. The statistical data were obtained by counting cells showing EYFP translocation over the total EYFP positive cells to give the percentage of translocated cells. Cells were counted from three separate experiments, and 100-200 cells were counted for each sample. Error bars are SD (N = 3).

4.4 orthogonal test to other existing CIP systems

Finally, we tested whether this new MG-based CIP system is orthogonal to other existing CIP systems including abscisic acid (**ABA**)-based system that dimerizes ABI/PYL fusion proteins,[13] gibberellin acid (GA)-based system that dimerizes GAI/GID1 fusion proteins,[14] and rapamycin (Rap)-based system that dimerize FRB/FKBP fusion proteins.[5] We constructed a new plasmid encoding GA-inducible transcriptional activation cassette (**Figure** 4.15-iii) and used the MG, **ABA** and Rap

inducible constructs that were developed in this study or previously (**Figure** 4.15).

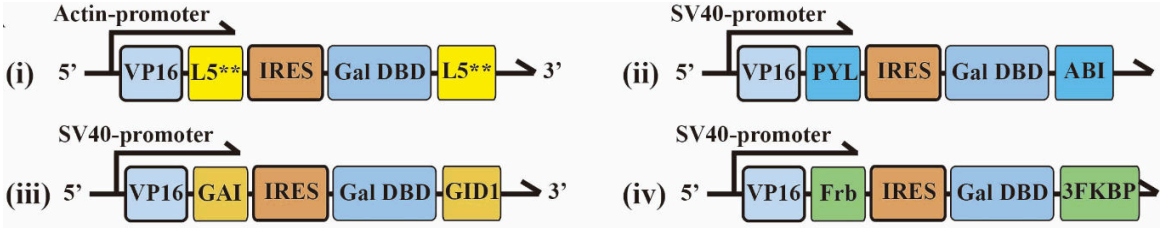

Figure 4.15 DNA constructs for inducible gene expression induced by (i) MGnBu, (ii) **ABA**, (iii) GA, (iv) Rap.

We co-transfected CHO cells with a UAS luciferase reporter and individually with each of these inducible transcriptional activation cassettes for 24 h. MGnBu, GA-AM, **ABA**, Rap or ethanol (negative control) was then separately added to each transfected condition for another 24 h. Afterwards, cells were collected and analysed by a fluorescence plate reader for activated inducer fluorescence or by luciferase assays for induced luciferase expression. We observed that only cells transfected with the MG-inducible cassette and treated with MGnBu gave detectable fluorescence signals (**Figure** 4.16). We also confirmed that these four tested CIP systems are orthogonal in that only the corresponding inducer can dimerize the matching fusion protein pairs to induce luciferase expression (**Figure** 4.17). The MGnBu induced CIP system is the only method that allows direct monitoring the induced dimerization and also triggering downstream cellular effects.

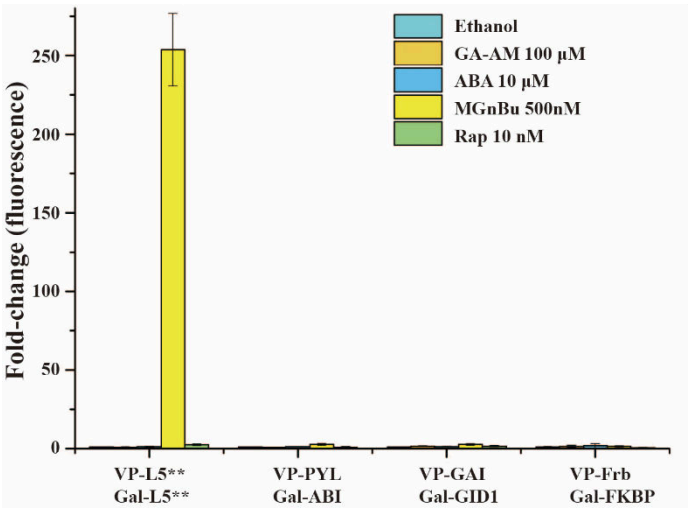

Figure 4.16 Activated inducer fluorescence fold change after transfected HEK293T cells were treated by different CIP inducers for 24 h. For all experiments, the induction fold change was calculated relative to the values of non-induced (i.e. ethanol treated) samples. Independent experiments were repeated five or more times. Errors bars are SD (N=5).

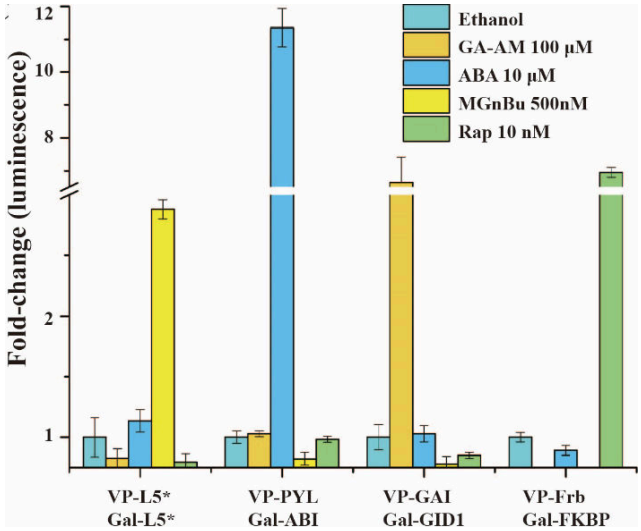

Figure 4.17 Induced luciferase expression after transfected HEK293T cells were treated by different CIP inducers for 24 h. For all experiments, the induction fold change was calculated relative to the values of non-induced (i.e. ethanol treated) samples. Independent experiments were repeated five or more times. Errors bars are SD (N=5).

4.5 Conclusions

In summary, we developed a unique new fluorogenic CIP system that uses an MG derivative (MG-nBu) as an inducer that is able to trigger specific downstream cellular events through the dimerization of two L5** fusion proteins and also generates fluorescence signal upon forming the ternary. This is the first CIP system that is able to achieve direct reporting of dimerization. Although the induced effects are not as high as other CIP systems that dimerize two non-identical inducer-binding proteins, we expect that new FAP-based MG binding proteins can be engineered to offer new and improved fluorogenic CIP systems with specific heterodimerization. In addition to the range of MG-analog binding FAP proteins, a variety of additional fluorogens with cognate fluorogen activating proteins, several of which have been found to form ternary complexes sandwiching a single ligand suggests that a range of additional CIP systems could be derived from FAP-fluorogen pairs.[27, 32]

4.6 Methods

4.6.1 Cloning and plasmid construction

All DNA fragments were amplified by PCR (Polymerase chain reaction) from other intermediate constructs with the enzyme of Phusion DNA Polymerase (New England Biolabs) under S1000 thermal cycler with Dual 48/48 Fast Reaction Module (Bio-Rad). All the restriction enzymes used below are purchased from New England Biolabs. All the constructs with L5** were amplified using pcDNA3.1-KozATG-dL5-2XG4S-mCer3 (plasmid #73207 from Addgene) as the template.

Actin-VP-L5**-ires-Gal-L5** was derived from SV40-VP-PYL-ires-Gal-ABI by replacing PYL to L5** using AscI and BamHI sites (amplified by primers CCGACAGGCGCGCCACAGGCCGTCGTTACCCAAGAA and CCGACAGGATC CTCAAGCGTAATCTGGAACATCGTATGGGTAGGACAGAACCGTCAGTTGTG T), replacing ABI to L5** using MluI and NotI sites (amplified by primers CCGACAACGCGTCAGGCTGTGGTGACTCAGGAG and CCGACAGCGGCCG CTTCACTTGTCGTCATCGTCTTTGTAGTCGGAGAGGACGGTCAGCTGGGT), and then replacing SV40 to Actin using SpeI and EcoRI sites (insert restricted from Actin-EGFP-PYL [2i]).

SV40-NES-L5** was generated from SV40-VP-PYL-ires-Gal-ABI by replacing VP-PYL-ires-Gal-ABI to NES-L5** using EcoRI and NotI sites (amplified by primers

CCGACAGAATTCGCCACCATGCTTCCTCCACTAGAACGTCTGACTCTGGAT GGATCCCAGGCTGTGGTGACTCAGGAG and CCGACAGCGGCCGCTTCACT TGTCGTCATCGTCTTTGTAGTCGGAGAGGACGGTCAGCTGGGT).

SV40-EYFP-L5** was generated from SV40-VP-PYL-ires-Gal-ABI by replacing ABI to L5** using MluI and NotI sites (amplified primers are the same as the ones when making Actin-VP-L5**-ires-Gal-L5**), and replacing VP-PYL-ires-Gal to EYFP using EcoRI and MluI sites (amplified by primers CCGACAGAATTCATGGTGAGCAAGGGCGAGGAGCTG and CCGACAACGC GTCTTGTACAGCTCGTCCATGCC, template YFP-GID1 from Addgene #37305).

SV40-VP-GAI-ires-Gal-GID1 was generated from SV40-VP-PYL-ires-Gal-ABI by replacing PYL to GAI using AcsI and BamHI sites (amplified by primers CCGACAGGCGCGCCAGGATCTGGTGGAAAGAGAGATCATCATCATCAT and CCGACAGGA TCCTCAAGGATTAAGGTCGGTGAGCAT), and replacing ABI to GID1 using MluI and NotI sites (amplified by primers CCGACAACGCGTGGATCTGGTGGAGCTGCGAGCGATGAAGTTAAT and CCGACAGCGGCCGCTCAACATTCCGCGTTTACAAACGC). Templates were Actin-4XNLS-GID1 and Actin-GAI-ABI [4b].

4.6.2 Mammalian cell culture and transfection

All cells were cultured in DMEM medium (Gibco) supplemented with 10% FBS,

2 mM GlutaMAX (life technologies), 100 U/ml penicillin (life technologies) and 100 μg/ml streptomycin (life technologies) at 37℃ in a humidified atmosphere containing 5% CO_2.

Fluorescence micro plate reader quantification and luciferase activity quantification. (1) For compounds screening and dosage dependent experiments, HEK293T cells were seeded in 24-well plate at 100,000/well for 24 hours and then transfected with 0.4 μg of Actin-VP-L5**-ires-Gal-L5** & 0.2 μg of 5XUAS-luciferase and waited for another 24 hours. Then, cells were treated with ethanol or 500 nM of MG or MGnBu or MG-B-Tau, or treated with 0 nM to 1000 nM of MGnBu. After 24 hours, cells were harvested and washed with PBS twice, and resulting cells were re-suspended in 100 μL of PBS and fluorescence was quantified by fluorescent plate reader (ex/em 640 nm/670 nm). Meanwhile, cells samples with the same conditions were harvested and quantified with the luciferase activity. (2) For experiments testing orthogonality with different CIP systems, HEK293T cells were seeded in 24-well plate at 100,000/well for 24 hours and then transfected with 0.2 μg of 5XUAS-luciferase together with 0.4 μg of Actin-VP-L5**-ires-Gal-L5**, or SV40-VP-PYL-ires-Gal-ABI, or SV40-VP-GAI-ires-Gal-GID1, or SV40-VP-Frb-ires-Gal-3FKBP, for another 24 hours. And then cells treated with ethanol, or 500 nM MGnBu, or 10 μM **ABA**, 100 μM GA-AM, 10 nM rap. After 24 hours, cells were harvested and washed with PBS twice, and resulting cells were re-suspended in 100 μL of PBS and

fluorescence was quantified by fluorescent plate reader. Meanwhile, cells samples with the same conditions were harvested and quantified the luciferase activity. All cellular experiments were conducted 3 to 4 independent times and each time with triplicate or quadruplicate.

Protein translocation. CHO were seeded over glass coverslips in 24-well plates at 50,000/well for 24 hours. Then cells were transfected with 0.2 μg SV40-EYFP-L5** and 0.4 μg SV40-NES-L5** for another 24 hours. Cell were treated with ethanol or with 500 nM of MGnBu for 5 min, 15 min, 30 min, 1 hour, 2 hours and 4 hours. After indicated time, cells were fixed with 4% paraformaldehyde and mounted on a glass slide with Vectashield (VWR) mounting media and images of cells were then taken by using a fluorescence microscope. For drug withdrawal experiments, after treatment with 500 nM of MGnBu for 4 hours, cells were washed with warm and fresh medium for three times (5 mins for between each wash) and then incubated with 15 min, 30 min, 1 hour and 2 hours. After indicated time, cells were fixed to make the cover slides and images were taken by using a fluorescence microscope. For all conditions, in the meanwhile of making the coverslips, cells samples with the same conditions were harvested and fluorescence was quantified by fluorescent plate reader (ex/em 640 nm/670 nm). All cellular experiments were conducted 3 to 4 independent times and each time with triplicate or quadruplicate.

4.6.3 Fluorescence microscopy

Zeiss Axio Observer. D1 outfitted with HBO 100 microscopy illumination system (excitation 470/40 and emission 525/50) was used for Ruffle formation experiments. Fluorescent channels in all experiments were adjusted to the same intensity ranges. Acquisition times ranged from 50 to 500 ms.

4.6.4 Statistical analysis of cell population

To determine the translocation of EYFP upon the drug treatment, first we measured the fluorescence intensity ratio of nucleus/cytoplasm for the cells without drug treatment, to get the ratio range (mean initial±SD). After treatment with MGnBu for indicated time, we measured the fluorescence intensity ratio of nucleus/cytoplasm for the cells, and identified the cells with translocation when the fluorescence intensity ratio of nucleus/cytoplasm was lower than the lowest ratio (mean initial-SD). And percentage of the cells with EYFP translocation was calculate by numbers of translocation cells over total cells number.

In a similar way, we quantified the reversibility of the EYFP translocation process. First, we measured the fluorescence intensity ratio of nucleus/cytoplasm for the cells before the drug withdrawal, to get the ratio range (mean treatment±SD). After wash with medium and incubated with different time, we measured the fluorescence intensity ratio of nucleus/cytoplasm for the cells, and identified the cells with translocation reversible when the fluorescence intensity ratio of nucleus/cytoplasm was higher than

the highest ratio (mean treatment + SD).

Cell images were collected from 5 different areas (4 quarters and center) in each of the 3 independent experiments. For each condition, 110 to 200 cells were analyzed along the diagonal lines. Mean fluorescence of nucleus and cytoplasm were analyzed by using Image J and get the ratio of these two for each analyzed cell.

4.7 references

1. Fegan, A.; White, B.; Carlson, J. C.; Wagner, C. R., Chemically controlled protein assembly: techniques and applications. *Chemical reviews* **2010,** *110* (6), 3315-36.

2. Gestwicki, J. E.; Marinec, P. S., Chemical control over protein-protein interactions: beyond inhibitors. *Combinatorial chemistry & high throughput screening* **2007,** *10* (8), 667-75.

3. DeRose, R.; Miyamoto, T.; Inoue, T., Manipulating signaling at will: chemically-inducible dimerization (CID) techniques resolve problems in cell biology. *Pflugers Archiv : European journal of physiology* **2013,** *465* (3), 409-17.

4. Voss, S.; Klewer, L.; Wu, Y. W., Chemically induced dimerization: reversible and spatiotemporal control of protein function in cells. *Current opinion in chemical biology* **2015,** *28*, 194-201.

5. Spencer, D. M.; Wandless, T. J.; Schreiber, S. L.; Crabtree, G. R., Controlling signal transduction with synthetic ligands. *Science* **1993,** *262* (5136), 1019-24.

6. Ho, S. N.; Biggar, S. R.; Spencer, D. M.; Schreiber, S. L.; Crabtree, G. R., Dimeric

ligands define a role for transcriptional activation domains in reinitiation. *Nature* **1996,** *382* (6594), 822-6.

7. Lin, H. N.; Abida, W. M.; Sauer, R. T.; Cornish, V. W., Dexamethasone-methotrexate: An efficient chemical inducer of protein dimerization in vivo. *Journal of the American Chemical Society* **2000,** *122* (17), 4247-4248.

8. Clemons, P. A.; Gladstone, B. G.; Seth, A.; Chao, E. D.; Foley, M. A.; Schreiber, S. L., Synthesis of calcineurin-resistant derivatives of FK506 and selection of compensatory receptors. *Chem Biol* **2002,** *9* (1), 49-61.

9. Bayle, J. H.; Grimley, J. S.; Stankunas, K.; Gestwicki, J. E.; Wandless, T. J.; Crabtree, G. R., Rapamycin analogs with differential binding specificity permit orthogonal control of protein activity. *Chem Biol* **2006,** *13* (1), 99-107.

10. Czlapinski, J. L.; Schelle, M. W.; Miller, L. W.; Laughlin, S. T.; Kohler, J. J.; Cornish, V. W.; Bertozzi, C. R., Conditional glycosylation in eukaryotic cells using a biocompatible chemical inducer of dimerization. *Journal of the American Chemical Society* **2008,** *130* (40), 13186-13187.

11. Skwarczynska, M.; Molzan, M.; Ottmann, C., Activation of NF-kappaB signalling by fusicoccin-induced dimerization. *Proceedings of the National Academy of Sciences of the United States of America* **2013,** *110* (5), E377-86.

12. Erhart, D.; Zimmermann, M.; Jacques, O.; Wittwer, M. B.; Ernst, B.; Constable, E.; Zvelebil, M.; Beaufils, F.; Wymann, M. P., Chemical development of intracellular protein heterodimerizers. *Chem Biol* **2013,** *20* (4), 549-57.

13. Liang, F. S.; Ho, W. Q.; Crabtree, G. R., Engineering the ABA plant stress pathway for regulation of induced proximity. *Science signaling* **2011,** *4* (164), rs2.

14. Miyamoto, T.; DeRose, R.; Suarez, A.; Ueno, T.; Chen, M.; Sun, T. P.; Wolfgang, M. J.; Mukherjee, C.; Meyers, D. J.; Inoue, T., Rapid and orthogonal logic gating with a gibberellin-induced dimerization system. *Nature chemical biology* **2012,** *8* (5), 465-70.

15. Miyamoto, T.; Razavi, S.; DeRose, R.; Inoue, T., Synthesizing biomolecule-based Boolean logic gates. *ACS synthetic biology* **2013,** *2* (2), 72-82.

16. Zeng, G.; Zhang, R.; Xuan, W.; Wang, W.; Liang, F. S., Constructing de novo H2O2 signaling via induced protein proximity. *ACS chemical biology* **2015,** *10* (6), 1404-10.

17. Zeng, G.; Li, H.; Wei, Y.; Xuan, W.; Zhang, R.; Breden, L. E.; Wang, W.; Liang, F. S., Engineering Iron Responses in Mammalian Cells by Signal-Induced Protein Proximity. *ACS synthetic biology* **2017,** *6* (6), 921-927.

18. Wright, C. W.; Guo, Z. F.; Liang, F. S., Light Control of Cellular Processes by Using Photocaged Abscisic Acid. *Chembiochem : a European journal of chemical biology* **2015,** *16* (2), 254-261.

19. Karginov, A. V.; Zou, Y.; Shirvanyants, D.; Kota, P.; Dokholyan, N. V.; Young, D. D.; Hahn, K. M.; Deiters, A., Light Regulation of Protein Dimerization and Kinase Activity in Living Cells Using Photocaged Rapamycin and Engineered FKBP. *Journal of the American Chemical Society* **2011,** *133* (3), 420-423.

20. Umeda, N.; Ueno, T.; Pohlmeyer, C.; Nagano, T.; Inoue, T., A Photocleavable

Rapamycin Conjugate for Spatiotemporal Control of Small GTPase Activity. *Journal of the American Chemical Society* **2011,** *133* (1), 12-14.

21. Brown, K. A.; Zou, Y.; Shirvanyants, D.; Zhang, J.; Samanta, S.; Mantravadi, P. K.; Dokholyan, N. V.; Deiters, A., Light-cleavable rapamycin dimer as an optical trigger for protein dimerization. *Chem Commun* **2015,** *51* (26), 5702-5705.

22. Feldhaus, M. J.; Siegel, R. W.; Opresko, L. K.; Coleman, J. R.; Feldhaus, J. M.; Yeung, Y. A.; Cochran, J. R.; Heinzelman, P.; Colby, D.; Swers, J.; Graff, C.; Wiley, H. S.; Wittrup, K. D., Flow-cytometric isolation of human antibodies from a nonimmune Saccharomyces cerevisiae surface display library. *Nature biotechnology* **2003,** *21* (2), 163-70.

23. Fisher, G. W.; Adler, S. A.; Fuhrman, M. H.; Waggoner, A. S.; Bruchez, M. P.; Jarvik, J. W., Detection and quantification of beta2AR internalization in living cells using FAP-based biosensor technology. *Journal of biomolecular screening* **2010,** *15* (6), 703-9.

24. Szent-Gyorgyi, C.; Schmidt, B. F.; Creeger, Y.; Fisher, G. W.; Zakel, K. L.; Adler, S.; Fitzpatrick, J. A.; Woolford, C. A.; Yan, Q.; Vasilev, K. V.; Berget, P. B.; Bruchez, M. P.; Jarvik, J. W.; Waggoner, A., Fluorogen-activating single-chain antibodies for imaging cell surface proteins. *Nature biotechnology* **2008,** *26* (2), 235-40.

25. Ozhalici-Unal, H.; Pow, C. L.; Marks, S. A.; Jesper, L. D.; Silva, G. L.; Shank, N. I.; Jones, E. W.; Burnette, J. M., 3rd; Berget, P. B.; Armitage, B. A., A rainbow of fluoromodules: a promiscuous scFv protein binds to and activates a diverse set of

fluorogenic cyanine dyes. *Journal of the American Chemical Society* **2008,** *130* (38), 12620-1.

26. Szent-Gyorgyi, C.; Schmidt, B. F.; Fitzpatrick, J. A. J.; Bruchez, M. P., Fluorogenic Dendrons with Multiple Donor Chromophores as Bright Genetically Targeted and Activated Probes. *Journal of the American Chemical Society* **2010,** *132* (32), 11103-11109.

27. Zanotti, K. J.; Silva, G. L.; Creeger, Y.; Robertson, K. L.; Waggoner, A. S.; Berget, P. B.; Armitage, B. A., Blue fluorescent dye-protein complexes based on fluorogenic cyanine dyes and single chain antibody fragments. *Organic & biomolecular chemistry* **2011,** *9* (4), 1012-1020.

28. Telmer, C. A.; Verma, R.; Teng, H.; Andreko, S.; Law, L.; Bruchez, M. P., Rapid, specific, no-wash, far-red fluorogen activation in subcellular compartments by targeted fluorogen activating proteins. *ACS chemical biology* **2015,** *10* (5), 1239-46.

29. Szent-Gyorgyi, C.; Stanfield, R. L.; Andreko, S.; Dempsey, A.; Ahmed, M.; Capek, S.; Waggoner, A. S.; Wilson, I. A.; Bruchez, M. P., Malachite green mediates homodimerization of antibody VL domains to form a fluorescent ternary complex with singular symmetric interfaces. *Journal of molecular biology* **2013,** *425* (22), 4595-613.

30. Lydia A. Perkins, G. W. F., Matharishwan Naganbabu, Brigitte F. Schmidt, Frederick Mun, Marcel P. Bruchez, High-content Surface and Total Expression siRNA Kinase Library Screen with VX-809 Treatment Reveals Synergistic Kinase Targets that Enhance F508del-CFTR Rescue. *Molecular Pharmaceutics* **2017**, submited.

31. Yan, Q.; Schmidt, B. F.; Perkins, L. A.; Naganbabu, M.; Saurabh, S.; Andreko, S. K.; Bruchez, M. P., Near-Instant Surface-Selective Fluorogenic Protein Quantification Using Sulfonated Triarylmethane Dyes and Fluorogen Activating Proteins. *Organic & biomolecular chemistry* **2015,** *13* (7), 2078-86.

32. Senutovitch, N.; Stanfield, R. L.; Bhattacharyya, S.; Rule, G. S.; Wilson, I. A.; Armitage, B. A.; Waggoner, A. S.; Berget, P. B., A Variable Light Domain Fluorogen Activating Protein Homodimerizes To Activate Dimethylindole Red. *Biochemistry* **2012,** *51* (12), 2471-2485.